Evolution of Proton Exchange Membrane Fuel Cell Technology for Aviation Applications: A Review

Yifan Xue, Mohammad Alnajideen,* and Rukshan Navaratne

Cite This: https://doi.org/10.1021/acs.energyfuels.5c03463

Read Online

ACCESS | Metrics & More | Article Recommendations

ABSTRACT: This review provides a comprehensive analysis of recent advancements in proton exchange membrane fuel cell (PEMFC) technology, with a specific focus on aviation applications. Each component of the PEMFC (bipolar plates, gas flow fields, gas diffusion layers, catalyst layers, and membranes) is critically examined in the context of aerospace requirements, including high specific power, lightweight construction, and operation under varying pressure, temperature, and humidity. Key aviation-specific challenges, such as water management in microgravity-aligned configurations, oxygen transport under low ambient pressures, and thermal cycling resilience, are discussed. Material innovations such as corrosion-resistant metallic bipolar plates, nanostructured Pt-alloy catalysts, hydrophobically tuned gas diffusion layers, reinforced composite membranes, and integrated flow field—diffusion interfaces are highlighted for their relevance to flight-ready systems. System-level trade-offs—balancing durability, efficiency, and safety—are also reviewed based on recent demonstrator platforms. The review concludes by identifying critical research directions to advance PEMFC deployment in short- and medium-range aircraft with particular emphasis on improving specific power, durability under load cycling, and component multifunctionality.
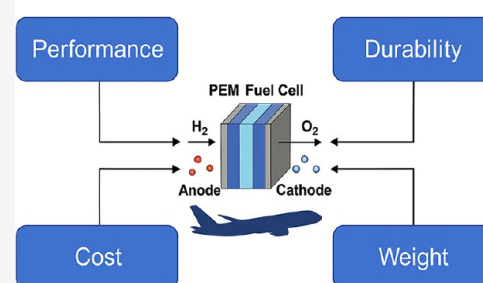
1. INTRODUCTION

Aviation serves as a critical pillar of modern transportation, facilitating rapid and efficient travel over long distances and playing a vital role in global connectivity and economic development. However, the sector also exerts a disproportionately large impact on the climate system. Approximately one-third of aviation-induced radiative forcing is attributable to carbon dioxide (CO_2) emissions, while the remaining two-thirds result primarily from non-CO_2 effects, including nitrogen oxides (NO_x), water vapor, and the formation of contrail-induced cirrus clouds 1. The aviation sector emitted about 1.03 $GtCO_2$ in 2019, representing 3.1% of global CO_2 emissions from fossil-fuel combustion, and approximately 1.7 $GtCO_2$-equivalent (CO_2e) when non-CO_2 effects are considered 2. Although emissions fell by nearly 40% in 2020 due to worldwide lockdown as a result of the COVID-19 pandemic, air-travel demand is projected to continue rising.[1] By 2023, emissions had rebounded to ~950 Mt CO_2,[2] and without mitigation could reach 1.9 Gt CO_2 by 2050—around 2.6 times 2021 levels, or 3.4 Gt CO_2e including non-CO_2 effects.[3] Air-travel demand correlates strongly with affluence, with wealthier regions contributing disproportionately,[4] drawing criticism from climate activists who highlight the inconsistency between frequent flying and calls for emission cuts.[1,5] Although aviation emits less total CO_2 than road transport, its climate impact is intensified by the difficulty of decarbonization, the rapid growth in demand, and high-altitude radiative-forcing effects

such as contrails and water vapor.[6] Consequently, aviation has become a key target in global decarbonization efforts.

In recent years, sustainable aviation fuels (SAFs) have been proposed as an alternative to conventional jet fuels.[7] However, SAF production, which is largely reliant on waste oils and biomass residues, faces significant challenges related to scalability and resource availability. Therefore, a more robust and long-term solution is urgently required.[2] On the other hand, hydrogen has been recognized as a clean energy vector with high energy density and zero carbon emissions when burned.[8] Its utility in aviation can be realized through two main approaches: direct combustion or conversion via fuel cells. While hydrogen combustion engines offer fast response and high power output, they face technical hurdles related to combustion control, safety, storage, and NO_x emissions.[9,10] In contrast, fuel cells enable the direct conversion of hydrogen's chemical energy into electricity, offering higher efficiency and better controllability.[11] Compared with hydrogen internal combustion engines, the fuel cell has a simpler structure,

A

Table 1. Representative Review Articles on PEMFCs and Hydrogen Propulsion Relevant to Aviation Applications

Year	ref	Focus of study	Scope and limitations	How this work differs
2025	43	Broad hydrogen for aviation (concepts, storage, propulsion options, policy)	High-level aviation survey; not a PEMFC component review; limited stack-level quantification	Delivers a component-level PEMFC roadmap with aviation constraints, quantitative targets, test matrix, manufacturability, and certification hooks.
2025	44	Sustainable, biobased PEMs (materials chemistry and performance)	Materials-centric; not aviation-specific; sparse low-RH/altitude data	Quantify 30–50% RH conductivity, H_2 crossover, and puncture/tear strength for thin membranes (20–40 μm) and tie them to aviation pass/fail criteria.
2024	45	Hybrid/composite PEMs: conductivity and stability	No flight-representative pressure/RH or vibration; little on certification	Extends to low-pressure/low-RH operation; reinforcement strategies linked to a standardized flight test matrix and certification evidence.
2024	46	Ohmic/charge-transfer resistances; diagnostics	General PEMFC; no aviation boundary conditions; no mass/volume or BP manufacturability view	Connects resistance management to BP coating/ICR drift, orientation-dependent GDL drainage, and power-to-weight/volume targets.
2023	15	Comparative review of FC types for electrified commercial aviation	Concept-level comparison; limited component-scale, low-RH/low-p data	Provides component-level PEMFC roadmap with numeric targets.
2023	47	Hydrogen-powered aircraft—fundamentals, technologies, environmental impacts	Airframe/propulsion concepts at high level; not a PEMFC component review	Links materials/manufacturing (BP coatings, membranes, CL) to flight-rep. validation and certification artifacts.
2022	48	GDL/MPL architecture and materials (review and outlook)	Not aviation-specific; very limited altitude/low-p, orientation or Mach/Re coupling	Ties GDL/MPL and flow fields to aerodynamic boundary conditions; proposes wind-tunnel/rotating-platform validation.
2022	49	Degradation models for PEMFCs: effects of BPs, seals, contaminants	Broad stationary/auto data sets; little on pressure cycling/vibration	Maps degradation pathways to your proposed flight ASTs (pressure/RH/vibration) and aviation durability targets.
2022	50	Integrated thermal management systems in PEMFC vehicles	Automotive context; no flight-representative low-p/RH or weight-critical constraints	Translates thermal management insights to aircraft mass/volume limits and altitude-RH operation for aviation PEMFC stacks.
2019	51	Fuel-cell-based propulsion systems for UAVs	UAV focus; limited stack-internal physics under altitude/RH/vibration	Extends to crewed aircraft constraints; quantifies O_2/saturation distribution under aerodynamic loads and low-p operation.
2019	17	Hydrogen and fuel cell technology in aviation/aerospace (high-level survey)	System-level overview; minimal stack/component quantification; not cantered on low-RH/low-pressure PEM operation	Drills down to BP/flow field—GDL/CL/membrane with quantitative aviation targets and pass/fail protocols.
2018	24	SOFC-APU systems for aircraft	SOFC/APU-focused; not a PEMFC component review; limited airworthiness/testing linkage	SOFC/APU-focused; not a PEMFC component review; limited airworthiness/testing linkage.
2017	52	PEMFC for aeronautic applications—durability aspects	Early aeronautic perspective; largely qualitative; lacks modern low-RH/low-p quantification or vibration coupling	Provide quantitative conductivity/crossover/mechanics for thin membranes and combined electro-mechanical ASTs.

B

resembling that of a conventional battery.[12] When hydrogen is used as a fuel, its principle is equivalent to the reverse reaction of water decomposition.[13]

Fuel cells are primarily classified according to the type of electrolyte they employ, which determines key characteristics, such as operating temperature, efficiency, and suitable applications. The main types are proton exchange membrane fuel cell (PEMFC, also known as polymer electrolyte membrane), solid oxide fuel cell (SOFC), phosphoric acid fuel cell (PAFC), alkaline fuel cell (AFC), direct methanol fuel cell (DMFC), and molten carbonate fuel cell (MCFC).[14] However, not all fuel cell types are suitable for the rigorous demands of flight. The fuel cells most commonly recommended and studied for aviation are PEMFC and SOFC.[15−21] SOFCs operate at high temperatures (600−1000 °C) and can utilize a wide range of fuels, including hydrogen and hydrocarbons.[20] While they offer fuel flexibility and improved tolerance to impurities, their long start-up time, slow dynamics, and heavyweight make them unsuitable as the primary power source for electric aircraft.[20−22] Instead, SOFCs are more appropriate for stationary airport power or as part of a hybrid propulsion system that recycles engine waste heat.[21,23,24] In contrast, PEMFCs operate at lower temperatures, offer faster start-up, and demonstrate high efficiency, making them well suited for aviation applications.[16,25] Major aerospace companies such as Boeing and Airbus have already launched development programs for PEMFC-powered aircraft.[26,27] Organizations including NASA and Rolls-Royce are also actively investing in this technology.[28−32] Significant progress has been made, particularly in unmanned aerial vehicles (UAVs) applications where PEMFCs have enabled extended flight duration.[33−38] More recently, successful test flights of PEMFC-powered small passenger aircraft have been reported.[39−42]

While numerous reviews cover general PEMFC science and systems, there is still no focused synthesis that translates component-level advances into flight-relevant requirements. Unlike automotive or stationary settings, aircraft imposes stringent constraints on power-to-weight and volumetric efficiency, operation at low pressure/low humidity, mechanical vibration, and strict safety/certification. This Perspective addresses that gap with a component-level assessment of PEMFC technology under flight-representative conditions. We examine the design requirements, material innovations, and performance trade-offs of the five core stack elements (bipolar plates, flow fields, gas diffusion layers, catalyst layers, and proton exchange membranes) and evaluate their suitability for integration into next-generation electric aircraft. We also link materials and architecture choices to manufacturability, representational validation, and certification evidence.

To situate this contribution within the literature, Table 1 benchmarks representative review papers published between 2018 and 2025, summarizing their focus, coverage, and scope limitations. Most prior work emphasizes automotive PEMFCs, broad hydrogen-aviation concepts, or demonstrator case studies, with limited quantitative treatment of low-pressure/ low-RH operation, aero-hydrodynamic coupling, combined electro-mechanical durability, or manufacturability/certification. The present review integrates these dimensions to provide a cohesive roadmap from laboratory R&D to airworthiness-ready PEMFC technology for aviation. A summary schematic of the review structure and the interactions among PEMFC stack components under aviation constraints is shown in Figure 1.
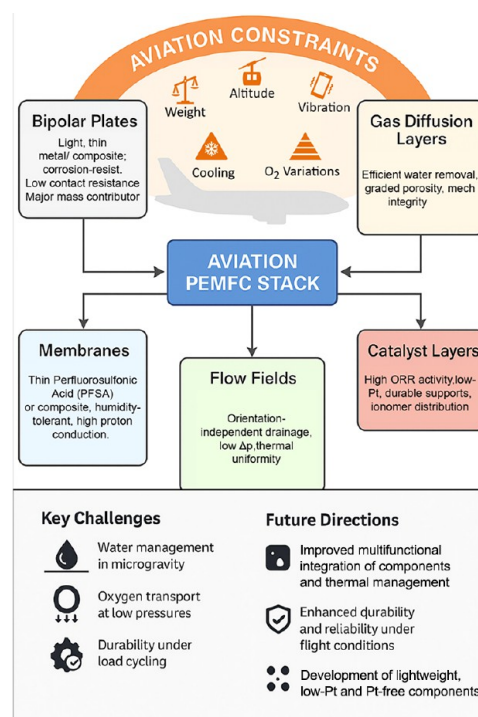

Figure 1. Schematic overview of PEMFC stack components and their interrelations under flight-relevant constraints.

2. OVERVIEW OF PEMFCS

PEMFCs are electrochemical devices that convert the chemical energy of hydrogen and oxygen directly into electrical energy through redox reactions, with water and heat as the only byproducts. Owing to their high efficiency, low operating temperature, rapid start-up capability, and clean emissions, PEMFCs are considered a leading technology for mobile electrification, particularly in aviation applications.[16] A single PEMFC unit consists of five fundamental components: bipolar plates (BPs), gas flow channels (GFCs), gas diffusion layers (GDLs), catalyst layers (CLs), and a proton-conducting polymer electrolyte membrane. The GDL, CL, and membrane together form the membrane electrode assembly (MEA), which is the electrochemically active core of the system. Figure 2 schematically illustrates the structure and working principle of a single PEMFC.

Hydrogen is introduced at the anode side, where it dissociates into protons (H^+) and electrons (e^-) in the presence of a platinum-based catalyst. The protons migrate through the PEM to the cathode, while the electrons travel through an external circuit, providing usable electric power. At the cathode, the protons and electrons recombine with oxygen to form water. As long as hydrogen and oxygen are supplied, the PEMFC can continuously generate electricity.[21] The key advantages of PEMFCs—zero emissions, low noise, modularity, and scalability—make them attractive for aviation.[16,17,19] However, achieving practical implementation in crewed aircraft requires overcoming several engineering and material challenges including improvements in power density, system compactness, durability, and weight reduction. The following sections present a detailed review of the major components of
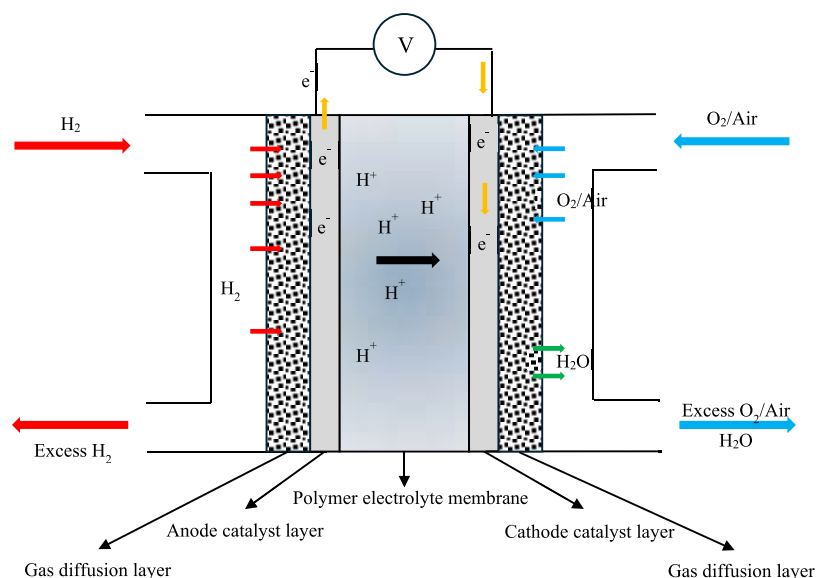
Figure 2. Schematic diagram of a single PEMFC.

PEMFCs and analyze the latest research trends and design innovations aimed at meeting the rigorous demands of aerospace applications.

3. BIPOLAR PLATES (BPS)

Bipolar plates (BPs) are critical structural and functional components in PEMFC stacks positioned between adjacent membrane electrode assemblies (MEAs). Their primary role is to electrically connect individual cells in series while simultaneously performing a range of essential functions. These include: (i) supplying and distributing reactant gases through integrated flow fields,[53] (ii) removing product water and excess gases, (iii) conducting electrons between cells, (iv) dissipating heat, and (v) providing mechanical support for the stack structure.[53−55] A typical BP features separate GFCs for the anode and cathode sides, often integrated into both faces of the plate. Plates located at the terminal ends of a stack are termed end plates and feature only a single flow field. Figure 3 illustrates the configuration of a PEMFC stack and the positioning of BPs within the system.[56]

In aviation applications, BP design becomes significantly more constrained due to strict power-to-weight and volumetric efficiency requirements.[57] BPs can account for up to 80% of the total stack mass.[58,59] Therefore, lightweight, corrosion-resistant, and high-conductivity materials are critical to achieving the specific power thresholds (W/kg) required for airborne propulsion.[60] For instance, Airbus and ZeroAvia have identified BPs as a major design bottleneck in scaling PEMFC stacks for crewed aviation, with current efforts focusing on ultrathin, coated metallic plates and carbon-polymer composites.[47,61] The aviation environment, characterized by vibrations, pressure fluctuations, and extended duty cycles—also imposes stringent demands on mechanical robustness and thermal conductivity. BPs must not only provide structural integrity under dynamic flight loads but also ensure uniform heat dissipation to prevent local hot spots, which can degrade membrane and catalyst performance at altitude.[62,63]

3.1. BP Materials. Conventional BP materials include graphite, metals (e.g., stainless steel, titanium, aluminum), and carbon-based polymer composites.[63,64] Each type of material
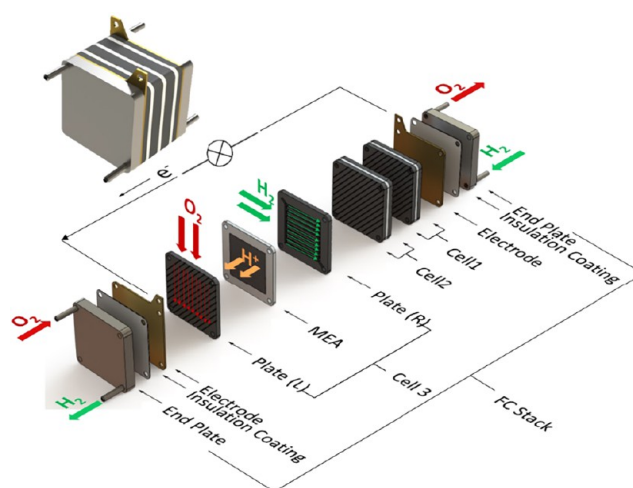

Figure 3. Configuration of PEMFC stack.[56] Reprinted with permission from ref 56. Copyright 2017 Elsevier.

offers distinct advantages and limitations, and its selection often involves trade-offs among conductivity, durability, manufacturability, and weight.

Graphite has traditionally been used in PEMFCs due to its high electrical and thermal conductivity, chemical inertness, and corrosion resistance. However, its inherent brittleness requires thicker plates for mechanical strength, increasing volume, and weight. Moreover, graphite's porosity raises concerns regarding gas permeability.[65−67] Metals like stainless steel, aluminum, titanium, and nickel are widely studied as alternatives to graphite for their mechanical strength, thin-form factor, and ease of mass production. However, exposure to the acidic and humid PEMFC environment accelerates corrosion and leads to the formation of oxide layers. These layers increase interfacial contact resistance, thereby reducing the overall power output of the PEMFC.[68,69] To mitigate this, various surface coatings are applied.[70−73]

Coated metals coating with materials such as titanium diboride (TiB_2), zirconium nitride (ZrN), chromium nitride (CrN), and amorphous carbon have shown promise in

Table 2. Materials Used for Bipolar Plates in PEMFCs. [65,67,69,86−88]

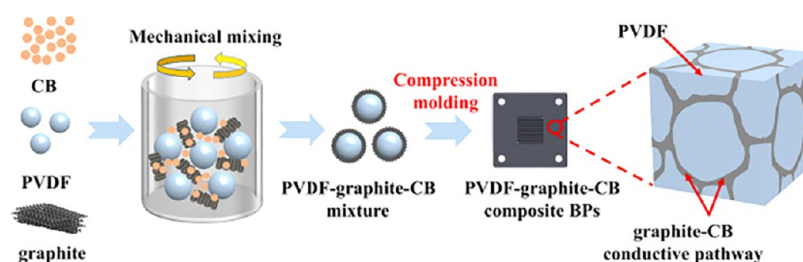| Types			Materials	Description	Relevance to aviation applications
Graphite			Nonporous, pure graphite	High conductivity, corrosion resistance; brittle and bulky	Limited use in aviation due to high density, thickness, and mechanical fragility under vibration and impact
Metallic	Base		Stainless steel	Excellent mechanical strength and conductivity; prone to corrosion in acidic environments	Favored in aviation when thinned and coated; supports high power density and lightweight stack designs
			Aluminum		
			Titanium		
			Nickel		
	Surface coating		Graphite	Applied to improve corrosion resistance and reduce interfacial contact resistance	Essential in aerospace to maintain performance under temperature swings, humidity, and long-term flight cycles
			Conductive polymer		
			Noble metals		
			Carbides		
			Nitrides		
Composite	Metal-based	Base plate	Stainless steel	Combine metal strength with carbon flow paths; complexity in assembly and contact resistance	Potential for structural reinforcement, though weight penalties limit suitability unless optimized
			Aluminum		
			Titanium		
			Nickel		
		Flow field plate	Graphite		
	Carbon-based	Thermosetting resin	Epoxy	Low density, good corrosion resistance; electrical conductivity enhanced by fillers	Highly relevant for aviation—lightweight, chemically stable, and tailorable for mechanical and thermal resilience
			Phenolic		
			Vinyl ester		
			Furan		
		Thermoplastic	Polypropylene		
			Polyvinylidene fluoride		
			Polyphenylene sulfide		
			Polyethylene		
		Filler	Graphite		
			Expanded graphite & Graphite nanoplatelet		
			Carbon black		
			Carbon fiber		
			Carbon nanotubes		

Figure 4. Typical fabrication process of a carbon-based composite bipolar plate. Reprinted with permission from ref 101. Copyright 2022 Elsevier.

enhancing corrosion resistance and electrical conductivity. For instance, TiB$_2$ coatings on 304 stainless steel improved both corrosion resistance and open circuit voltage stability,[74] while ZrN coatings on 306L stainless steel achieved optimal performance at a thickness of 1 μm.[75] Aluminum BPs coated with NiCrBSi have demonstrated enhanced corrosion resistance.[72] Nanocomposite carbon coatings and diamond-like carbon films have also demonstrated excellent chemical stability and reduced contact resistance.[76−78] Despite the excellent performance of coated metallic BPs, their high cost and the need for precision machining remain significant limitations.[79−81] Composite plates combine the advantages of metals and carbon-based materials. Metal-based composites typically feature metal substrates combined with carbon flow field plates, but they suffer from increased contact resistance and assembly complexity.[82,83] Polymer-based composites— especially those using carbon-filled thermosetting or thermoplastic resins—offer lightweight and good corrosion resistance. These materials can be engineered with conductive fillers such as graphite nanoplatelets, carbon nanotubes, or carbon fibers to enhance electrical and thermal conductivity.[84,85] Table 2 presents a summary of materials commonly employed for BPs in PEMFCs and their suitability for aviation.

In aviation, graphite—despite its corrosion resistance—has limited suitability due to bulk and brittleness, leading to undesirable stack volume and fragility under mechanical shock.[86−88] Metallic BPs, particularly thin titanium or stainless steel sheets with corrosion-resistant coatings (e.g., TiN, CrN, or carbon films), offer a better balance of mechanical strength, conductivity, and low thickness, making them more attractive for aerospace use.[63] Recent aerospace PEMFC demonstrators (e.g., H2FLY HY4, ZeroAvia Dornier 228, Airbus ZEROe) have employed lightweight metallic BPs with protective coatings, prioritizing weight reduction, manufacturability, and durability under high-altitude conditions.[89−98] In parallel, carbon-polymer composites incorporating materials such as carbon nanotubes or graphite nanoplatelets are emerging as strong candidates for aviation PEMFCs. These materials offer high conductivity, reduced mass, and tailorable properties.[63,99] NASA's recent work on high-specific-power PEMFCs for aircraft propulsion highlights these composites as essential for future kilowatt-scale lightweight stacks.[100]

3.2. BP Fabrication. Carbon-based composite BPs have attracted significant interest due to their lightweight nature and corrosion resistance. A typical fabrication process involves blending conductive fillers with polymer matrices, followed by molding or compression, as illustrated in Figure 4.[101] Optimization focuses on maximizing conductivity while maintaining mechanical strength and minimizing filler content.[84,85]

Rigail-Cedeño et al.[102] investigated the impact of varying amounts of carbon black and graphite nanosheets as secondary fillers on the performance of expanded graphite/epoxy resin composite BP. Experimental results revealed that an optimal filler concentration of 1 wt % yielded the highest in-plane electrical conductivity. Interestingly, when carbon black was used as the secondary filler, the conductivity reached 50 S/cm, attributed to the formation of effective electron-conducting pathways throughout the composite.

Darıcık et al.[103] achieved a significantly higher in-plane conductivity of 120.05 S/cm by filling 1.25 wt % multiwalled carbon nanotubes (MWCNTs) into a carbon fiber/epoxy resin composite. The resulting plate not only exhibited electrical performance comparable to that of 3106 aluminum alloy but also offered substantial weight reduction. Furthermore, the addition of MWCNTs enhanced both longitudinal and transverse flexural strengths by 40%, underscoring their contribution to the composite's mechanical reinforcement.

Hu et al.[104] prepared a composite BP using polyvinylidene fluoride (PVDF) as the polymer matrix, with 35 wt % graphite and 5 wt % MWCNTs serving as primary and secondary conductive fillers. Morphological analysis revealed the formation of cooperative, segregated, conductive networks at the filler−resin interface. This architecture enabled the plate to achieve a high in-plane conductivity of 161.57 S/cm, a low area-specific resistance of 7.55 mΩ·cm^2, and a flexural strength of 42.65 MPa. Furthermore, the plate demonstrated excellent corrosion resistance and hydrophobicity. In a follow-up study, Hu et al.[101] replaced the MWCNTs with carbon black as the secondary filler in the graphite/PVDF composite. At low filler loadings, this modified plate attained an even higher in-plane conductivity of 177.87 S/cm. Although the area-specific resistance increased slightly to 9.30 mΩ·cm^2, the overall power density improved, reaching 646.08 mW/cm^2.

Yao et al.[105] explored the effects of surface oxidation treatment on graphite/epoxy resin composite BPs. Their results indicated that introducing oxygen-containing functional groups significantly enhanced the interfacial bonding between graphite and the resin, leading to improvements in both mechanical strength and electrical conductivity. They suggested that surface oxidation presents a promising avenue for the future development of high-performance composite BPs.

In aerospace applications, BP fabrication methods must prioritize not only performance metrics (e.g., conductivity and corrosion resistance) but also scalability, geometric precision, and surface finish quality, which affect sealing, leakage, and thermal cycling durability.[49,106] Fabrication methods like compression molding of composite plates, precision coating of metallic BPs, and additive manufacturing (3D printing) are under active investigation to meet aerospace PEMFC
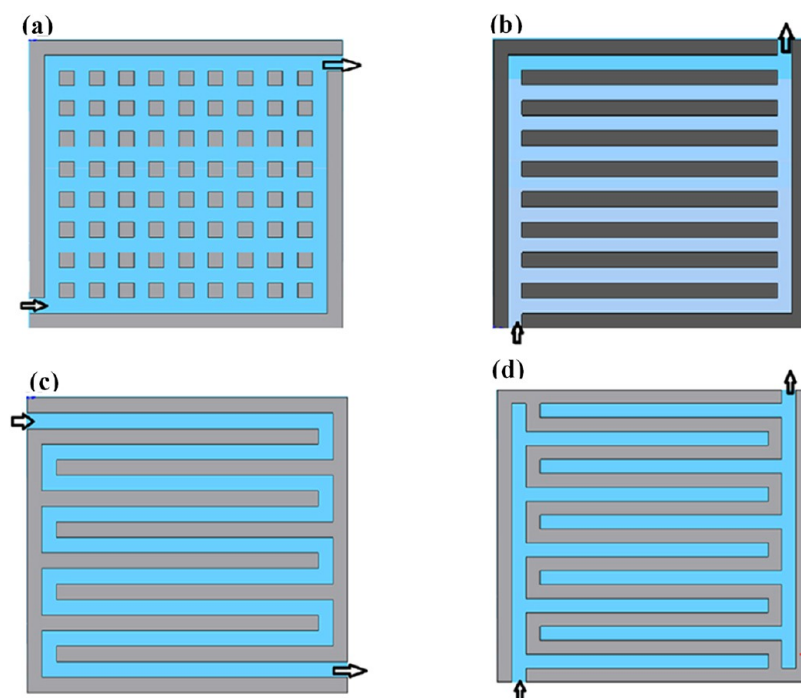
Figure 5. Common design types of gas flow field of (a) pin-type, (b) parallel-type, (c) serpentine-type, and (d) interdigitated-type. Reproduced from ref 116. Available under a CC-BY license. Copyright 2014 Liu, Li, Juarez-Robles, Wang and Hernandez-Guerrero. Front. Energy Res. 2:2.

needs.[63,107,108] Diamond-like carbon (DLC) and amorphous carbon coatings have been successfully used to protect metal BPs in PEMFC flight demonstrators, offering excellent corrosion resistance with minimal increase in weight or contact resistance.[90,109−111]

4. GAS FLOW FIELD AND CHANNELS

The gas flow field functions as the "vascular system" of a PEMFC, directing the supply of reactant gases (hydrogen and oxygen/air) and the removal of product water.[112] It is embedded within the BPs and plays a pivotal role in ensuring uniform current distribution, effective water management, and thermal regulation.[113] Consequently, the design of the flow field has a direct influence on fuel cell performance, particularly in mitigating localized flooding or membrane dehydration, which degrades efficiency and durability.

In aviation applications, the design of gas flow fields must accommodate unique constraints such as variable-pressure conditions, dynamic power demands, orientation changes, and limited space for reactant delivery systems.[16] As aircraft operate across a wide range of altitudes and ambient temperatures, the flow field architecture must be optimized for stable operation under low ambient pressure, passive water removal, and minimal pressure drop to reduce parasitic losses and compressor size. The integration of PEMFCs into aircraft also demands modular, compact stack geometries, where gas distribution systems can be aligned with aircraft aerodynamics and cooling airflow, especially for wing-embedded or fuselage-integrated systems.[32,114,115] The development of low-pressure drop, high-reactant-utilization flow fields is critical for enabling passive or fan-assisted cathode systems in aviation.

4.1. Field Flow Design Strategies. Current research on field flow optimization is primarily focused on improving geometric configurations to enhance the distribution of reactants and facilitate effective water and heat removal.[54]

Four conventional flow field types, pin-type, parallel-type, serpentine-type, and interdigitated-type, form the foundation of design efforts, as illustrated in Figure 5. While these have been extensively studied in terrestrial PEMFCs, their suitability in aviation depends on trade-offs among water management, pressure loss, and stack compactness.

4.1.1. Pin-Type Flow Field. The pin-type flow field is one of the most common and straightforward configurations. It consists of uniformly distributed pins of various shapes, offering multiple flow paths that promote a low pressure drop. The pin-type field is useful for UAVs or aircraft with passive airflow cathode systems. However, uneven gas distribution often arises due to preferential flow along paths of least resistance, which can lead to flooding or uneven current density.[54]

Guo et al.[117] compared conventional and optimized pin-type designs (Figure 6a,b) using simulations and found that the optimized version mitigated reactant flow imbalance and water accumulation. Atyabi et al.[118] proposed a hexagonal honey-comb pin-type configuration (Figure 6c,d), which achieved superior performance in terms of oxygen distribution, thermal uniformity, and water drainage performance of multichannel serpentine fields.

4.1.2. Parallel-Type Flow Field. In the parallel-type flow field, pins are aligned to form straight parallel channels. This design also offers a low-pressure drop but is susceptible to localized flooding. Once water accumulates in a channel, it disrupts airflow and accelerates further water buildup due to uneven flow distribution.[54] To address this, Ghasabehi et al.[119] introduced an innovative parallel-type layout that achieved more uniform oxygen and current density distributions through multiphysics simulations, as shown in Figure 7a,b. Similarly, Atyabi and Afshari[120] designed a sinusoidal wave-form parallel flow field, which improved reactant distribution and water removal at the cost of increased pressure drop. Parallel-type fields are prone to flooding at altitude unless
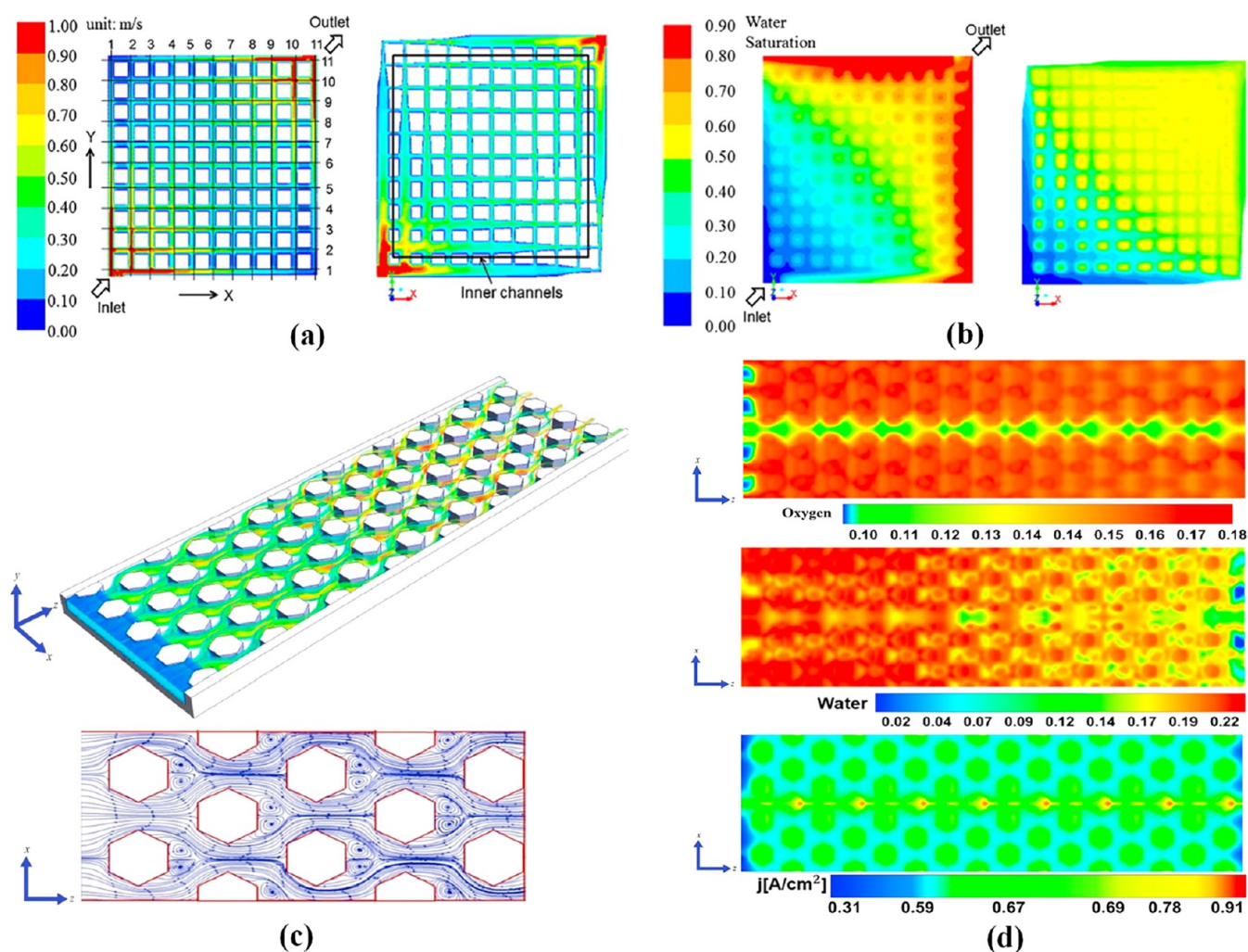
Figure 6. Flow velocity distribution and water saturation in the cathode GDL for (a) conventional and (b) optimized pin-type flow field, adapted from ref 117; (c) honeycomb pin-type flow field design and (d) corresponding distributions of oxygen mass fraction, water mass fraction, and local current density distribution at cathode GDL/CL interface using proposed honeycomb design; adapted from ref 118. Reprinted with permission from ref 117. Copyright 2013 Elsevier. Reprinted with permission from ref 118. Copyright 2019 Elsevier.

integrated with hydrophobically treated GDLs or grooved interfaces to facilitate drainage in microgravity or varying g-load conditions.[121,122]

4.1.3. Serpentine-Type Flow Field. The serpentine-type design forces gases through a winding, single-path channel, enhancing water removal through shear and promoting effective reactant utilization. However, it can induce high pressure drops and localized oxygen depletion near bends, especially at the outlet. Despite higher pressure drops, serpentine-type fields have shown robust performance under aircraft-like transient loads, with effective water removal and oxygen utilization, making them favored in high-altitude or tilt-sensitive configurations.[16,123] Velisala et al.[124] proposed an asymmetric serpentine design with gradually narrowing channels to reduce pressure gradients, achieving uniform gas and water distribution and improving peak power density. Rostami et al.[125] introduced a V-ribbed structure at corners to balance pressure and flow, thereby enhancing the electrochemical performance of PEMFCs, as shown in Figure 8.

Liu et al.[126] proposed a multiserpentine configuration, dividing the field into several zones. While it improved the airflow, it suffered from uneven distribution. Abdulla et al.[127] refined Liu et al.[126] design by reorienting the subchannels (see

Figure 9), resulting in improved oxygen delivery, lower pressure losses, and enhanced current density.

4.1.4. Interdigitated-Type Flow Field. Unlike the previous types, interdigitated flow fields feature dead-end inlet or outlet channels, forcing gas to flow laterally through the porous gas diffusion layer (GDL) via convection. This design significantly enhances oxygen transport and water removal, especially under high current densities. However, this requires elevated inlet pressure, which increases parasitic power consumption and potential structural stress. Whiteley et al.[128] combined parallel-type and interdigitated-type flow fields and proposed micro-hole arrays with a dead-end structure, significantly improving high-humidity and high-current performance while reducing pressure drop. Limjeerajarus and Santiprasertkul[129] designed a serpentine–interdigitated hybrid that reduced pressure drop by 90% and improved oxygen, current, and water distribution, extending PEMFC durability. Figure 10 illustrates these innovative gas flow field configurations.

4.1.5. Bioinspired and Unconventional Designs. Recent efforts in bioinspired channel geometries (e.g., nautilus-, leaf-, and lung-shaped) offer promising avenues for aviation. These architectures provide uniform reactant distribution, even under low air density, and enable directional drainage by capillary
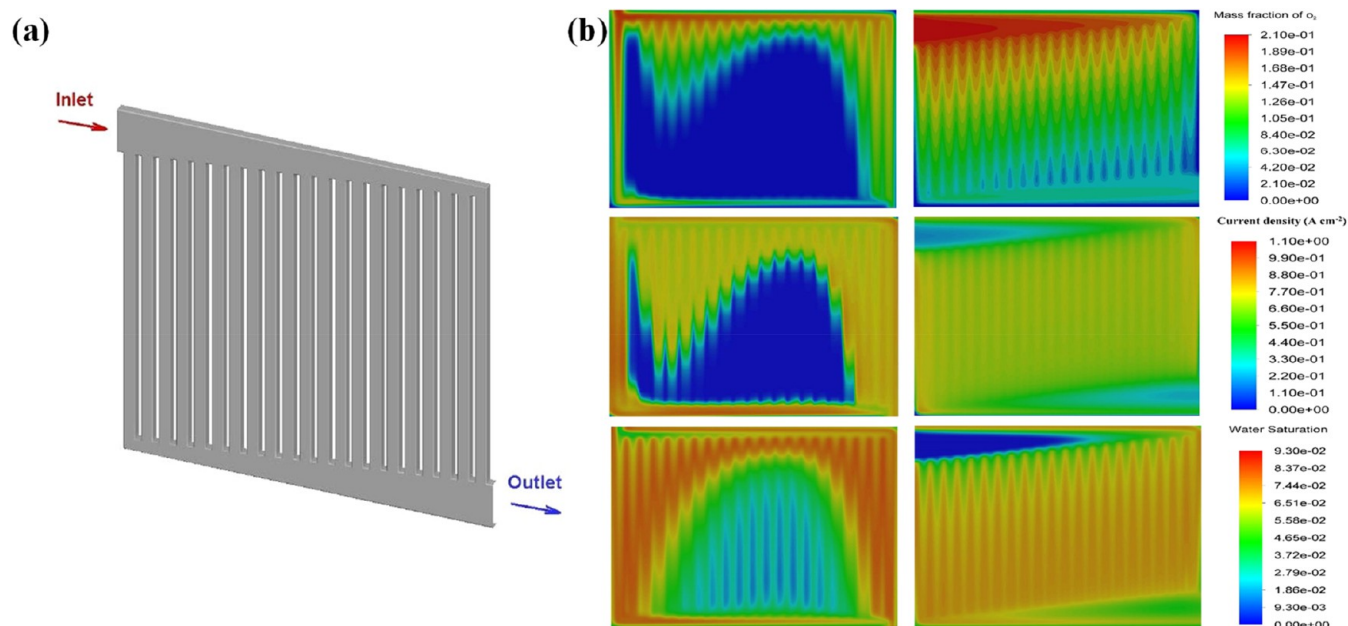
Figure 7. (a) Schematic design of the flow field and (b) distribution of oxygen mass fraction, current density, and water saturation at the cathode GDL/CL interface for conventional parallel-type flow field; adapted from ref 119. Reprinted with permission from ref 119. Copyright 2021 Elsevier.
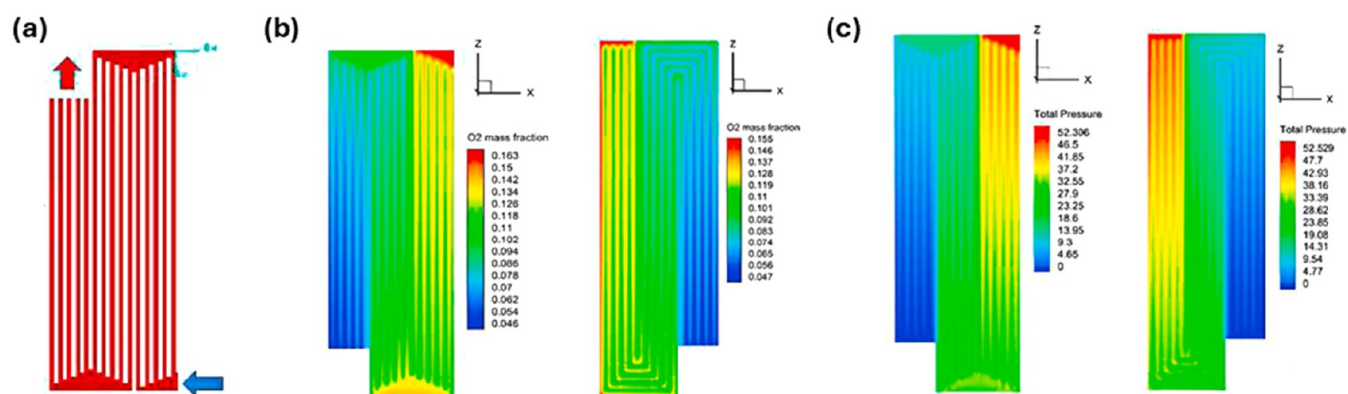

Figure 8. (a) V-Ribbed serpentine-type flow field configuration introduced and (b, c) comparison of oxygen mass fraction and pressure distribution at cathode side GDL/CL interface by Rostami et al.[125] Reprinted with permission from ref 125. Copyright 2022 Elsevier.
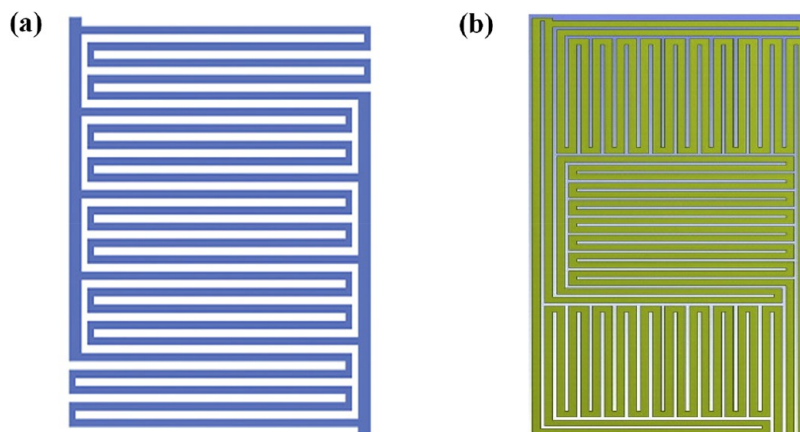

Figure 9. Geometric designs of enhanced serpentine-type flow fields: (a) configuration proposed by Liu et al.[126] and (b) configuration refined by Abdulla et al.[127] Reprinted with permission from ref 126. Copyright 2018 John Wiley and Sons. Reprinted with permission from ref 127. Copyright 2020 Elsevier.

action, especially beneficial for fuel cell stacks integrated into tilted or nonhorizontal orientations in aircraft fuselage or wings. Several biomimetic and novel configurations have been reported in the literature, as illustrated in Figure 11. Li et al.[130]
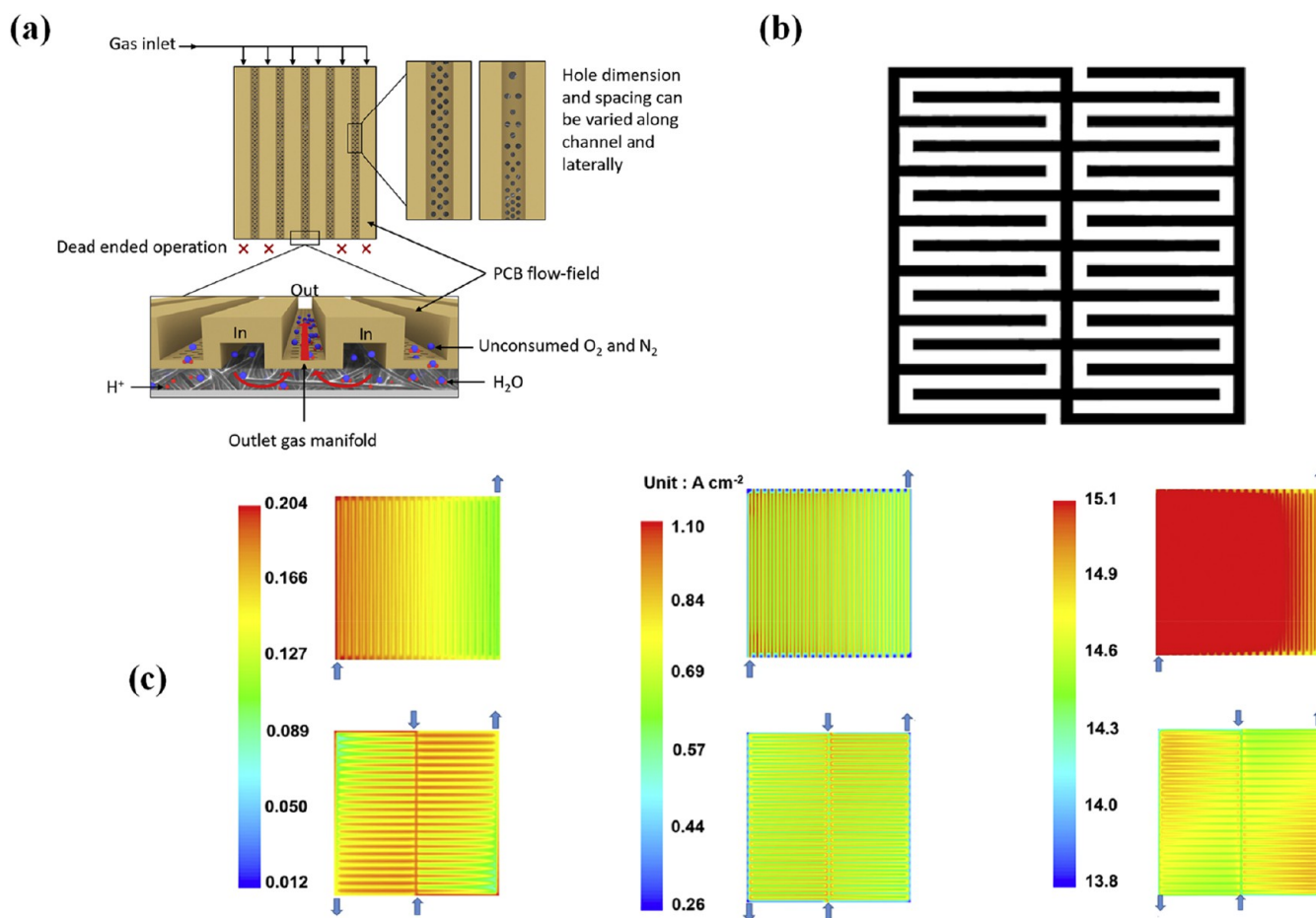
Figure 10. (a) Schematic of the novel flow field design incorporating a microhole array, proposed by Whiteley et al.;[128] (b) serpentine-interdigitated flow field configuration, and (c) comparison between the proposed design of Limjeerajarus and Santiprasertkul[129] and a conventional single-channel serpentine-type flow field in terms of oxygen mass fraction, current density, and water content, respectively.[129] Reprinted with permission from ref 128. Copyright 2019 Elsevier. Reprinted with permission from ref 129. Copyright 2020 Elsevier.

designed and simulated a nautilus-shaped field that outperformed conventional serpentine layouts. Kang et al.[131] proposed a ginkgo leaf-inspired design that enhanced water removal. Badduri et al.[132] drew inspiration from leaf veins and human lung vessels to create a layout that improved net power density. Lee et al.[133] demonstrated that a cylindrical flow field offered better performance than planar configurations across various current densities. Cylindrical and 3D spiral designs are also being investigated for nonplanar fuel cell modules, such as in rotorcraft, blended-wing body aircraft, or distributed propulsion systems, where stack shape must conform to aerodynamic structures.[134]

4.2. Flow Chanel Design Parameters. Flow channel parameters, such as aspect ratio (the channel's width to its height), land-to-channel ratio, and channel depth, affect pressure drop, water management, and gas delivery. Manso et al.,[135] Kiattamrong and Sripakagorn,[136] and Wang et al.[137] found that higher aspect ratios improve PEMFC performance by enhancing water removal while maintaining reactant supply. However, excessively high ratios can increase the pressure drop and manufacturing complexity. Kahraman and Orhan[138] studied the land-to-channel ratio (also known as the rib-to-channel ratio) and found that lower ratios enhance reactant diffusion but compromise water removal and thermal management due to reduced rib area. Higher ratios improve water and heat transport but can impede gas diffusion and increase

pressure drop, necessitating a design balance.[139] To further enhance flow performance, researchers have proposed various designs such as wave-shaped channels, divergent–convergent designs, and integrated multiplate configurations. Additional enhancements include internal blockages, baffles, and microstructured fins, all aiming to improve reactant distribution and water evacuation while managing flow resistance. These design strategies are listed in Table 3.

For aviation PEMFCs, high aspect ratio channels improve water removal at altitude but may exacerbate backpressure imbalances if cabin pressure fluctuates or ventilation is uneven.[140−142] Low land-to-channel ratios increase reactant access but can compromise mechanical sealing integrity, a concern in aviation where vibration and mechanical stress are high.[52,143] Wave-shaped, baffled, and gradient microstructure designs are increasingly favored for their ability to passively modulate flow without additional power, supporting the move toward low parasitic-load PEMFC stacks for airborne use.[144−146]

Unlike terrestrial PEMFCs, which operate in fixed orientations, aircraft-mounted stacks may undergo tilts, rolls, and rapid acceleration. Consequently, flow field asymmetry and multidirectional drainage paths are necessary to avoid flooding during flight phases.[144,160,161] Several demonstrator projects, such as HES Energy's UAV stack, have adopted angled serpentine and branched flow channels to manage
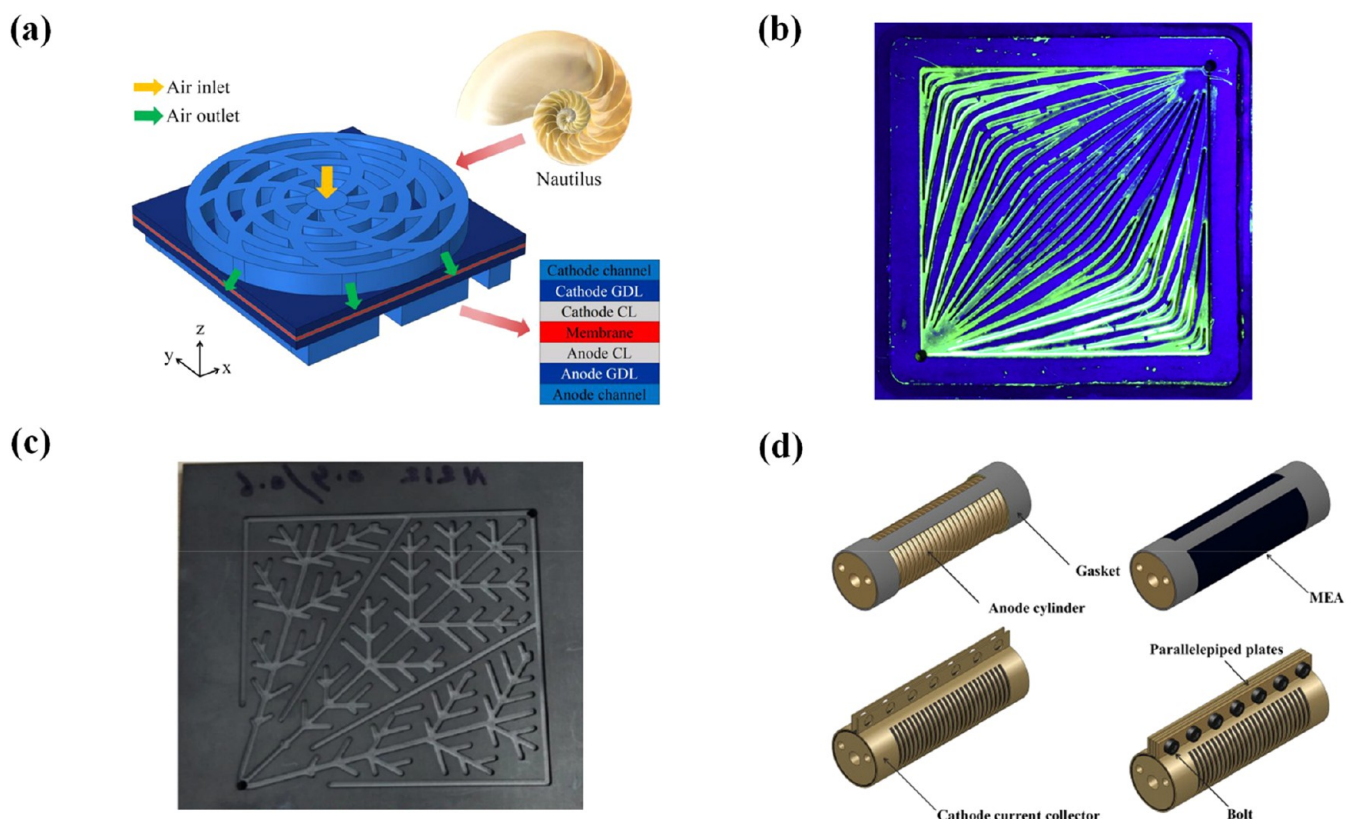
Figure 11. Schematic designs of novel flow field configurations proposed by (a) Li et al.;[130] (b) Kang et al.;[131] (c) Badduri et al.;[132] and (d) Lee et al.[133] Reprinted with permission from ref 130. Copyright 2023 Elsevier. Reprinted with permission from ref 131. Copyright 2019 Elsevier. Reprinted with permission from ref 132. Copyright 2020 Elsevier. Reprinted with permission from ref 133. Copyright 2010 Elsevier.

liquid water removal under dynamic orientations.[51,162−164] Based on the literature reviewed in this section, Table 4 summarizes the key design priorities for flow fields in aviation-grade PEMFC systems.

4.3. Manufacturability and Cost Analysis of Candidate BP Technologies.
Aviation PEMFC stacks must minimize mass per cell while maintaining low interfacial contact resistance (ICR), corrosion resistance, and scalability of manufacture.[63,68,69] Table 5 compares three leading BP options (thin titanium with coatings, aluminum alloys with coatings, and carbon-polymer composites) across mass, cost drivers, ICR stability, and process scalability. While thicker or more robust coatings improve corrosion resistance, they can raise ICR and reduce voltage efficiency over time, creating a design trade-off that must be quantified in qualification testing.[70,165,166]

4.3.1. Manufacturing Routes.

- Metal sheet stamping/hydroforming + PVD/CVD coating (DLC, TiN/ZrN, amorphous carbon): Highest throughput and best cost−scalability path for large volumes; requires postprocess surface finishing and coating quality control to manage ICR growth during aging (coating pinholes/porosity, adhesion).[167]

- Additive manufacturing (laser powder-bed or binder-jet metals; carbon-polymer AM tools): Enables integrated coolant plenums and thin, complex rib geometries that shorten stack height. Current limitations are surface roughness (affecting ICR), dimensional tolerance, and per-part cost; best suited to low-to-medium volumes or weight-critical bespoke architectures.[108,168,169]

- Compression molding of carbon-polymer composites (graphite platelets/CNT-filled): Excellent weight potential and in-plane conductivity, with tooling cycles compatible with medium volumes.[65,170] Challenges include through-plane conductivity and edge sealing; requires resin formulation control and postcure machining of flow features.[171−173]

4.3.2. ICR Evolution and Durability.
ICR is sensitive to coating thickness/chemistry and contact pressure. Metallic BPs rely on stable, low-defect coatings; coating thickening enhances corrosion resistance but tends to increase ICR over life.[174] Composite BPs avoid metal corrosion but need surface metallization or conductive skins in land areas to keep the ICR low and stable. Qualification should therefore report initial ICR ($m\Omega \cdot cm^2$) at defined clamping pressure and ICR drift after thermal/humidity/vibration cycling, alongside mass loss/corrosion rate.[175]

4.3.3. Production Readiness.
For transport-category aircraft, stamped/coated metal BPs are currently the most scalable path (mature tooling, roll-to-roll coating options).[81,176] Composites offer the largest mass reduction but require strong QA for porosity, fiber wet-out, and dimensional control. Additive metal BPs are promising for integrated, height-reduced stacks, pending cost, and roughness improvements.[81,177]

5. GAS DIFFUSION LAYER (GDL)

The gas diffusion layer (GDL) is a multifunctional component located between the flow field and the catalyst layer (CL) in a PEMFC. It facilitates the transport of reactant gases to the CL,

Table 3. Design Strategies for PEMFC Flow Channels[147−159]

Strategies	Illustration	Advantages	Disadvantages	Reference
Channel cross-section shapes configuration		Tailors pressure drop and flow characteristics; may enhance reactant distribution and water evacuation.	Complex fabrication; potential flow maldistribution at low flow rates.	Mohammedi et al. 147 Reprinted with permission from ref (147). Copyright 2020 Elsevier
Novel wave flow channel design		Promotes turbulence and reactant mixing; improves water removal.	Increased pressure drop; higher parasitic load.	Chen et al. 148 Reprinted with permission from ref (148). Copyright 2021 Elsevier
Divergent and convergent channel designs		Enhances gas acceleration and pressure gradient for water evacuation.	May cause flow instability or local drying.	Lei et al. 149 Reprinted with permission from ref (149). Copyright 2023 Elsevier
Condensing-tower-like curved flow channel design		Facilitates natural drainage paths; smoothens water removal.	Requires precise geometric tuning; fabrication complexity.	Jin et al. 150 Reprinted with permission from ref (150). Copyright 2023 Elsevier
Multi-plate structure and integrated structure channel design		Enables modular assembly and design flexibility; can improve mass transfer.	Risk of flow leakage between plates; increased sealing requirements.	Fan et al. 151 Reprinted with permission from ref (151). Copyright 2018 Elsevier

Table 3. continued

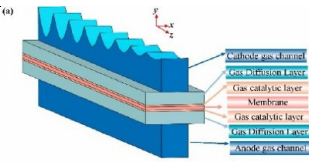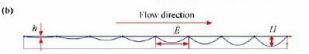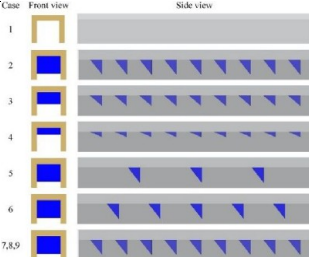| Strategies	Illustration	Advantages	Disadvantages	Reference
Flow channel indentation		Creates local turbulence and improves gas diffusion.	Potential flow obstruction or increased water retention in recessed areas.	Ghanbarian and Kermani 152 Reprinted with permission from ref (152). Copyright 2016 Elsevier
Blockages as flow-guide and the suppression		Directs reactant flow and promotes water removal from under ribs.	Increased flow resistance may cause non-uniform distribution.	Cai et al. 153 Reprinted with permission from ref (153). Copyright 2021 Elsevier
Blockages in the channel		Enhances reactant utilization and mitigates channel flooding.	Risk of pressure buildup and reactant starvation downstream.	Shen et al. 154 Reprinted with permission from ref (154). Copyright 2019 Elsevier
In-line and staggered blockages in the cathode flow channel		Improves mixing and oxygen distribution; controls water accumulation.	Higher pressure drop, challenging to optimize blockage size and spacing.	Heidary et al. 155 Reprinted with permission from ref (155). Copyright 2016 Elsevier
Different angle and height of trapezoid baffles in flow channel		Induces controlled turbulence; enhances heat and mass transfer.	Adds design and manufacturing complexity may affect durability.	Perng and Wu 156 Reprinted with permission from ref (156). Copyright 2015 Elsevier
Partially blocked flow channels		Balances between pressure drop and mass transfer; mitigates dry/flood zones.	Performance is extremely sensitive to blockage placement.	Dong et al. 157 Reprinted with permission from ref (157). Copyright 2020 Elsevier

Table 3. continued

Strategies	Illustration	Advantages	Disadvantages	Reference
Gradient sinusoidal-wave fins in the cathode flow channel		Facilitates gradual pressure variation and uniform reactant distribution.	May be hard to scale; potentially significant parasitic losses.	Chen et al. [158] Reprinted with permission from ref ([158]). Copyright 2024 Elsevier
Wedge-shaped fins in the cathode flow channel		Channels gas effectively toward the CL; improves water management and current density.	Risk of excessive flow disturbance if geometry is not optimized	Zhang et al. [159] Reprinted with permission from ref ([159]). Copyright 2021 Elsevier

Table 4. Summary of Key Aviation Design Priorities for Flow Fields

Design factor	Aviation requirement
Low pressure drop	Minimizes parasitic power and supports altitude-adjusted airflow systems
High reactant utilization	Essential in low-density air environments (e.g., cruising altitude)
Passive water removal	Reduces system mass by avoiding dedicated drainage subsystems
Orientation-independent drainage	Critical for nonhorizontal stack orientations and maneuvering flight
Mechanical robustness	Must withstand vibration, altitude cycling, and aerodynamic loads

the removal of product water, the distribution of heat, and electron conduction. Structurally, the GDL typically comprises a dual-layer configuration: a macroporous substrate[6] and a microporous layer (MPL). The macroporous substrate (MPS) is often made of carbon-based materials and provides bulk support and gas permeability, while the MPL—composed of fine carbon particles and hydrophobic agents—is coated onto the MPS to improve interfacial contact and water management.[6] The GDL must simultaneously satisfy several competing requirements: low electrical resistance, high gas permeability, efficient water removal, good mechanical strength, and compatibility with fabrication and operational conditions.[178] In open-cathode or fan-assisted systems often used in UAVs and short-range aircraft, the GDL must accommodate variable airflow and humidity without external humidification—placing additional emphasis on internal structure and wettability engineering.[179,180] Moreover, in cryogenic hydrogen systems, localized cold spots may cause risk condensation within GDL pores, requiring thermal conductivity tuning.[47] Given these functions, improvements to GDL materials and structures are crucial for enhancing PEMFC performance, especially under dynamic and high-current-density conditions, such as those found in aviation applications.

5.1. Materials and Hydrophobic Agent. *5.1.1. Material Composition.* Carbon fiber and carbon black remain the most widely used materials for MPS and MPL, respectively. To enhance performance, advanced carbon-based materials—such as carbon nanotubes (CNTs), nanofibers, and graphene—have

been incorporated into GDL structures.[181] In aviation, where stack compactness is crucial, emerging materials such as CNTs and electrospun nanofibers are attractive due to their lower thickness, higher porosity, and tunable pore structures. These attributes help maintain gas transport efficiency at low ambient pressure and improve power-to-weight ratios, a key metric for airborne propulsion systems. Kim et al.[182] experimentally demonstrated that CNT sheets used as MPLs significantly improved reactant diffusion and liquid water removal due to their highly porous structure. Optimal performance was observed at a thickness of 15 μm, beyond which mass transport limitations began to appear. Similarly, Wei et al.[183] fabricated an ultrathin GDL using a CNT-based MPS (Figure 12a,b), achieving higher specific volume and gravimetric power density due to reduced thickness and enhanced porosity. Graphene doping has also proven to be effective. Lee et al.[184] investigated the performance of graphene-doped carbon black MPLs and found that graphene content modulates the pore structure. At low humidity, a low graphene content preserved microporosity for water retention, while at high humidity, the increased graphene promoted mesoporosity and better water removal. For airborne PEMFCs, these improvements are particularly valuable under low ambient humidity, where the water balance becomes critical to membrane hydration. Notably, NASA and Airbus-funded studies have identified GDL thickness and porosity tuning as key levers for reducing system mass while maintaining stack integrity at altitude.[185]

5.1.2. Nanofiber-Based GDLs. Electrospun nanocarbon fibers represent a novel and promising GDL platform., They offer smaller pore sizes and tunable structures compared to conventional carbon fibers.[48,186] Balakrishnan et al.[187] fabricated a nanofiber-based GDL with a graded pore size (Figure 12c,d), which enhanced water management and mass transport. Particularly, their design eliminated the need for an MPL, suggesting that well-designed electrospun GDLs could simplify the MEA architecture.

5.1.3. Hydrophobic Agents. Polytetrafluoroethylene (PTFE) is the conventional hydrophobic agent used in both the MPS and MPL. It increases contact angle and promotes water removal, mitigating flooding.[188] However, several studies have shown that excessive PTFE content can reduce thermal conductivity,[189] decrease pore size and porosity, and increase mass transfer resistance.[190] To address these limitations,

Table 5. Manufacturability-Focused Comparison of Candidate Bipolar-Plate Technologies for Aviation PEMFCs[63,68−70,108,170−175]

Candidate	Mass per cell (relative)	Unit-cost drivers	ICR (initial → aged) and corrosion	Scalable production steps	Manufacturability note
Ti sheet (≤0.1−0.2 mm) + coating (DLC/TiN/ZrN)	Low−medium (thin sheet; higher density than Al but robust)	Ti sheet cost; coating line (PVD/CVD); finishing	Low ICR initially; good corrosion; ICR ↑ with thicker/aging coatings	Stamping/hydroforming → cleaning → coating → QA	Most TRL-ready for high volume; proven corrosion performance; watch coating-induced ICR drift
Al alloy sheet + barrier coating	Very low (best density)	Surface prep; robust barrier coating; passivation	Needs excellent coating to avoid pitting; ICR stability depends on coating integrity	Stamping → conversion coating/ceramic barrier → QA	Strong weight case; coating reliability is the key risk
Carbon-polymer composite (graphite/CNT-filled)	Very low (lightest)	Resin/filler cost; mold cycle time; machining	No metal corrosion; ICR depends on surface metallization/skins; moisture uptake management	Compounding → compression molding → machining → (optional) metallization → QA	Best mass potential; ensure through-plane conductivity and edge sealing

alternative hydrophobic agents have been explored. PVDF, FEP, and CF_4 plasma have shown promise. For example, Cho et al.[191] and Bottino et al.[192] reported that PVDF-based MPLs exhibited smoother surfaces, fewer cracks, and better gas permeability. Latorrata et al.[193] and Park and Park[194] demonstrated that FEP-treated GDLs achieved superhydrophobicity and reduced diffusion resistance, likely due to improved compressive strength and interfacial contact.

5.2. Structure Optimization. Structural parameters of GDL, such as porosity, pore size, thickness, and spatial distribution, have a decisive impact on the GDL performance. For instance, increasing porosity improves gas diffusion but may impede water removal if water accumulation clogs the pores. Conversely, smaller pores enhance capillary-driven water removal but raise diffusion resistance.[195] Therefore, achieving an optimal pore size distribution is key not only for terrestrial use but also for aviation PEMFCs.

5.2.1. GDL with Hydrophilic and Hydrophobic Regions. Balancing reactant transport, water removal, and wettability within the GDL is crucial for optimal fuel cell performance.[196] Introducing a hydrophobic agent creates distinct hydrophobic and hydrophilic regions. Water tends to migrate through the untreated (hydrophilic) areas, while reactants move more easily through hydrophobic regions with lower resistance. The hydrophilic zones also help retain moisture under low-humidity conditions. However, in conventional GDLs, the distribution of these regions is random, leading to inconsistent performance.

Niu et al.[197] numerically analyzed laser-perforated GDLs and found that perforation at the water breakthrough point significantly reduced liquid water saturation and improved oxygen availability at the CL interface. Optimum performance was achieved with a perforation size and depth of 100 μm. 2D contour images (Figure 13) revealed that perforations effectively created hydrophilic regions capable of collecting more liquid water. As a result, overall water content in the GDL decreased, and water saturation in the hydrophilic zones surrounding the perforations was reduced. This freed up more pores for oxygen transport, thereby enhancing mass transfer within the perforated GDL. Numerical simulations supported these findings, showing an increase in oxygen concentration at the GDL bottom to 101%.

Grooved GDLs have also been explored. Nishida et al.[198] incorporated vertical grooves in the cathode side aligned with gas flow to enhance water drainage, while Yin et al.[199] implemented microelliptical grooves to reduce water content at high current density. In both cases shown in Figure 14, the designs successfully mitigated flooding and improved the reactant delivery.

In addition to incorporating perforations and grooves, designing GDLs with distinct hydrophilic and hydrophobic regions presents another effective optimization strategy. As shown in Figure 15a, Wang et al.[200] fabricated MPLs with spatially separated hydrophilic and hydrophobic zones, which facilitated selective water drainage while preserving dry gas transport pathways. Final test results demonstrated that this design significantly reduced the oxygen transport resistance. Forner-Cuenca et al.[201] developed a similar single-layer GDL without MPL (Figure 15b), demonstrating that capillary forces drive water to hydrophilic areas, preserving dry regions for gas transport.

5.2.2. GDL with Graded Porosity. Gradient porosity can create directional capillary forces that aid in water transport.
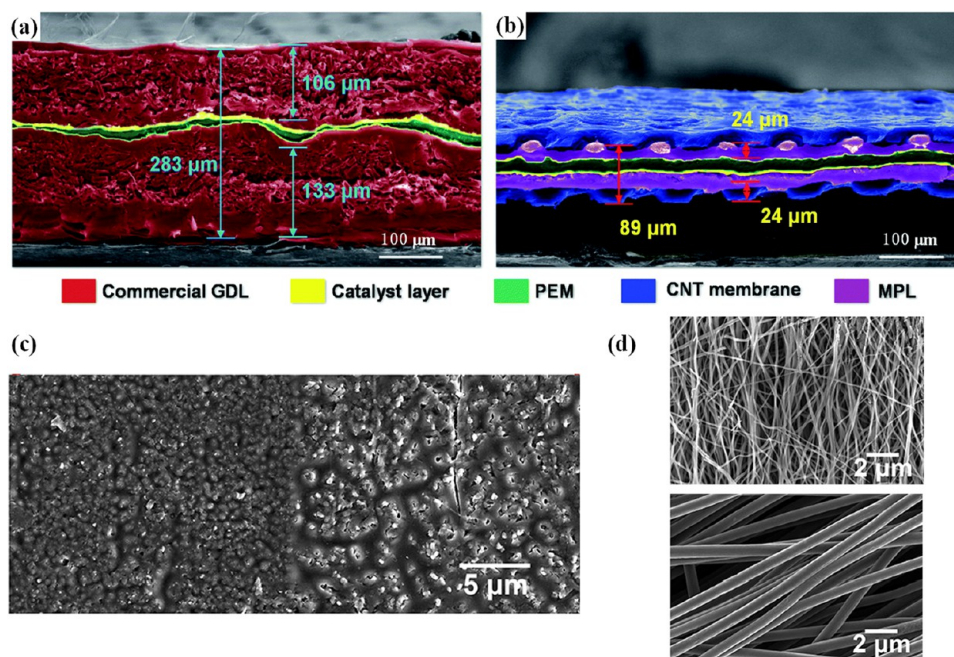
Figure 12. (a, b) Cross-sectional views comparing a conventional gas diffusion layer (GDL) with an ultrathin GDL incorporating a carbon nanotube (CNT) film-based microporous structure.[183] (c) Cross-section and (d) surface SEM images of the porosity graded e-GDL.[187] Reprinted with permission from ref 183. Copyright 2020 Royal Society of Chemistry. Reprinted from ref 187. Copyright 2020 American Chemical Society.
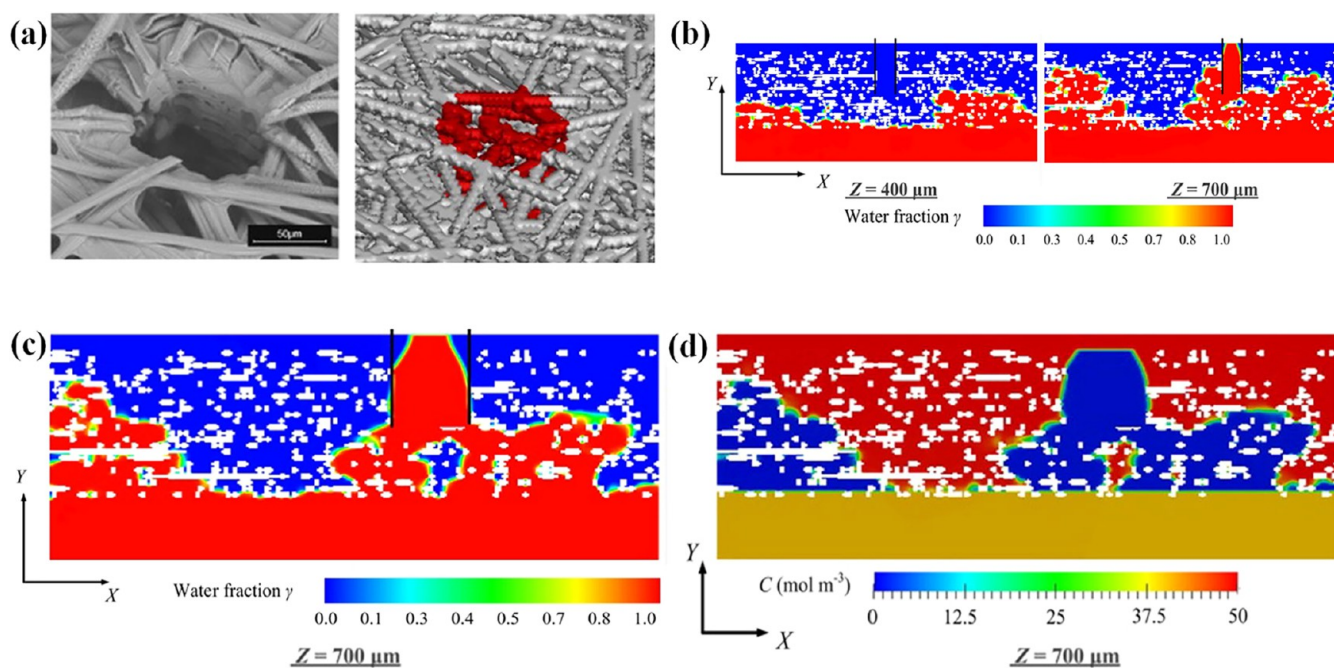

Figure 13. (a) SEM and reconstructed images of a laser-perforated GDL; (b) 2D contour plots of liquid water fraction at the center ($Z = 400\ \mu$m) and at the liquid water breakthrough point ($Z = 700\ \mu$m); (c, d) 2D contours of liquid water fraction and oxygen concentration with a perforation height and diameter of 100 μm.[197] Reprinted with permission from ref 197. Copyright 2019 Elsevier.

Lin et al.[202] constructed a double-layer MPL with coarse and fine pores (Figure 16a), enhancing power density by 25% at 60% RH. Verification experiments indicated that the performance enhancement was primarily attributed to the modified pore size distribution within the GDL. Wang and Wu[203] fabricated a microporous layer (MPL) featuring both uniform and gradient pore structures by controlling the pore-former content and applying a layered coating approach, as shown in Figure 16b. Performance tests in PEMFC operation demon-

strated that this MPL design outperformed conventional configurations, particularly under high current density and high relative humidity conditions. The gradient pore distribution significantly enhanced gas diffusion and liquid water removal. Consequently, the authors concluded that this design could improve the PEMFC performance under extreme operating conditions. Wang et al.[204] extended their study by incorporating porosity gradients in both through-plane and in-plane directions. Their simulations indicated that synergistic
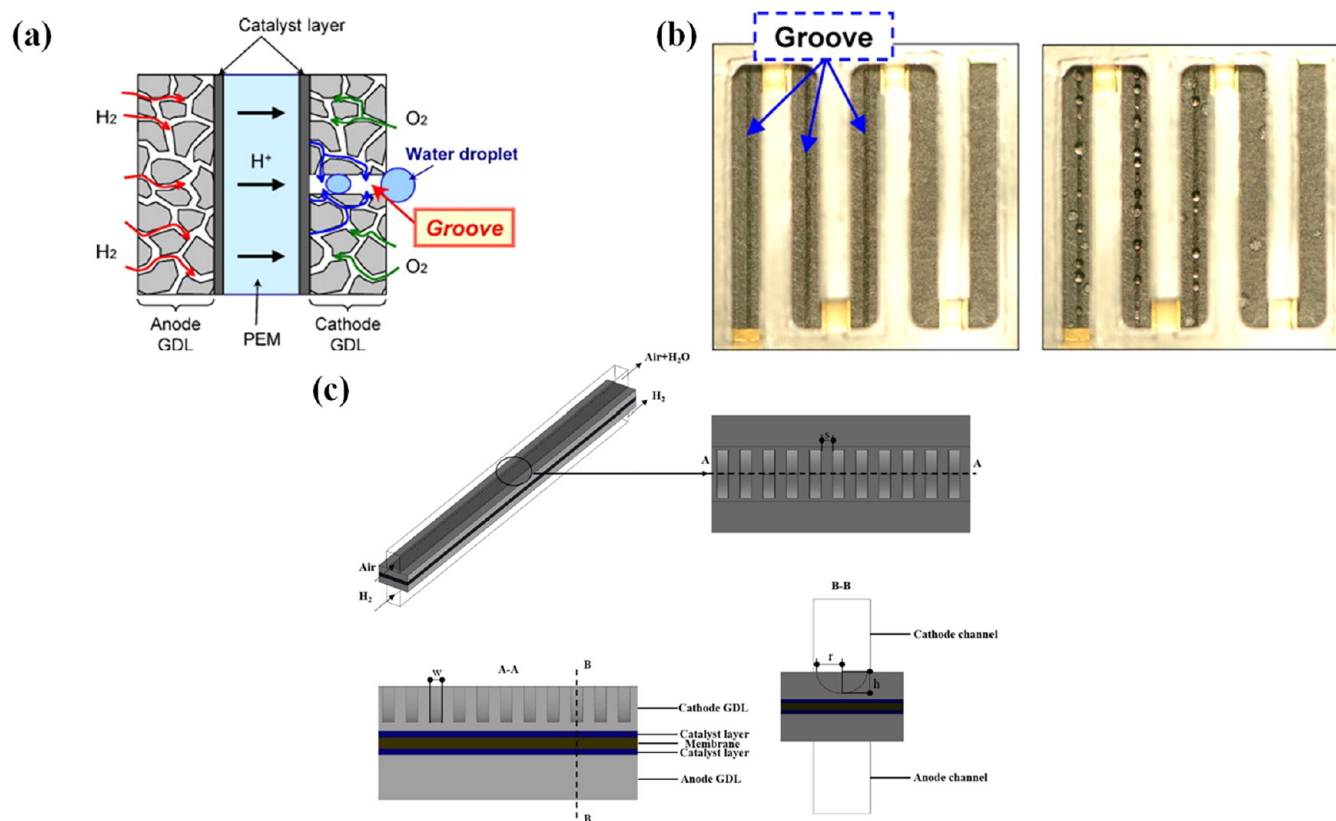
Figure 14. (a) Schematic of groove design;[198] (b) visualization of liquid water distribution in the cathode gas channel at $t = 0$ and 250 s;[198] (c) Illustration of microelliptical groove design.[199] Reprinted with permission from ref 198. Copyright 2010 Elsevier. Reprinted with permission from ref 199. Copyright 2021 Elsevier.
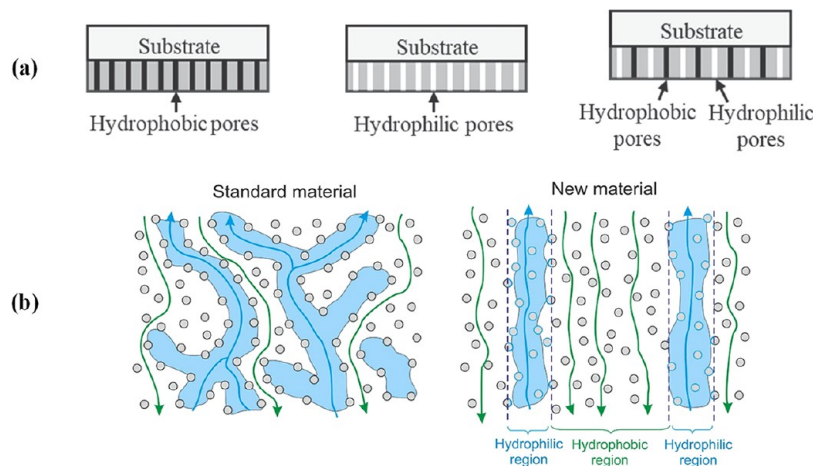

Figure 15. Design images of GDL with independent hydrophilic and hydrophobic areas from (a) Wang et al.[200] and (b) Forner-Cuenca et al.[201] Reprinted with permission from ref 200. Copyright 2024 IOP Publishing. Reprinted with permission from ref 201. Copyright 2015 John Wiley and Sons.

gradients produced the highest PEMFC performance, especially under transient load conditions.

5.2.3. Integrated GDL Designs. Thickness is another important factor influencing mass transport within the gas diffusion layer (GDL), as the GDL is significantly thicker than both the catalyst layer (CL) and the membrane. As a result, reactants must travel longer distances, encountering greater resistance. Additionally, the contact resistances between the GDL and both the BPs and CL represent a limitation, as these are typically much higher than the intrinsic resistance of the

GDL itself.[205] To address these challenges, an integrated GDL has been developed, which combines the functions of the gas flow field and the GDL. This integrated design offers several advantages, including reduced overall resistance, a more compact structure, and lower mass transport resistance due to shorter diffusion paths.

Park et al.[206] utilized graphite foam to fabricate an integrated GDL with a built-in gas flow field. Experimental results demonstrated that a unified membrane electrode assembly (MEA) incorporating this integrated GDL effectively reduced
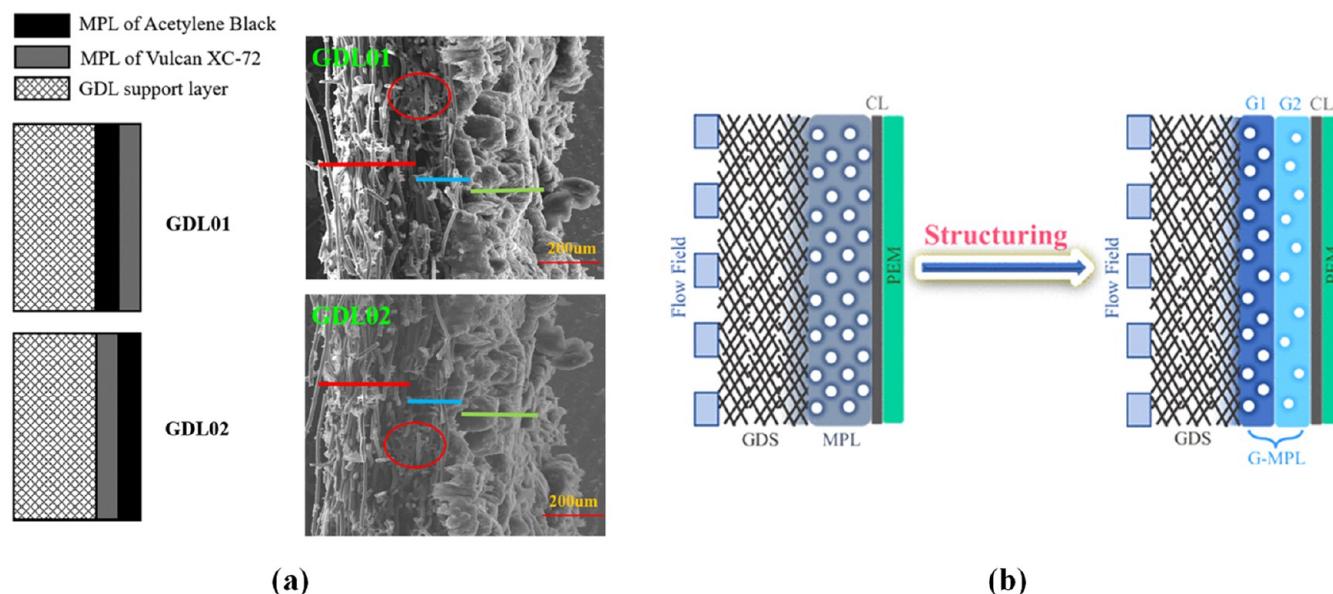
Figure 16. (a) SEM images of the proposed GDL design featuring dual microporous layers (MPLs);[202] (b) design strategy for a GDL incorporating a porosity gradient in the MPL structure.[203] Reprinted with permission from ref 202. Copyright 2020 John Wiley and Sons. Reprinted from ref 203. Copyright 2024 American Chemical Society.
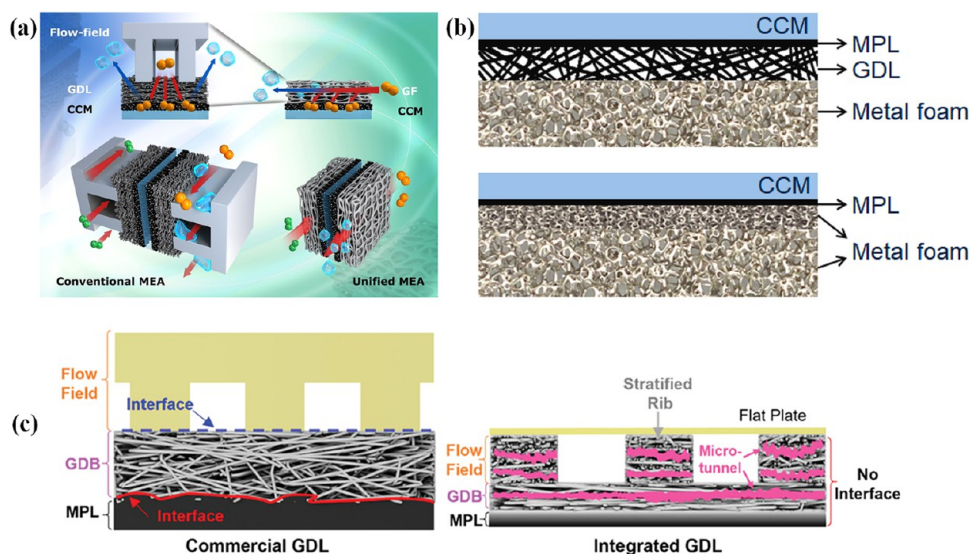

Figure 17. Schematic design of the integrated GDL by (a) Park et al.,[206] (b) Zhang et al.,[207] and (c) He et al.[208] Reprinted with permission from ref 206. Copyright 2019 Elsevier. Reprinted with permission from ref 207. Copyright 2022 Elsevier. Reprinted from ref 208. Copyright 2024 John Wiley and Sons.

both electrical and mass transport losses during the PEMFC operation. As a result, the system exhibited superior electrochemical performance compared to conventional designs. Furthermore, the reduced component volume contributed to an increase in the volumetric power density of the PEMFC. Zhang et al.[207] developed a similar system using nickel foam coated with carbon-based MPLs, achieving improved performance across humidity conditions. The use of metal foam provided higher electrical conductivity and reduced ohmic losses. Performance analysis revealed that the PEMFC incorporating this integrated GDL consistently outperformed conventional designs under both high and low relative humidity conditions. He et al.[208] further refined the design by introducing flow channels and microtunnels within the GDL, reducing pressure drop and enhancing water tolerance.

These integrated structures, shown in Figure 17, offer a promising pathway for lightweight, high-performance PEMFC stacks in aviation.

5.2.4. Summary of Structure Optimization. In summary, porosity gradients in the through-plane and in-plane directions enhance capillary-driven water removal without adding significant weight. Such designs are being explored in air–liquid-cooled stacks for aviation demonstrators. Hydrophilic–hydrophobic zoning within the GDL helps retain moisture in dry ambient conditions while channeling liquid water during high-load phases like takeoff and climb. This zoning mitigates membrane drying—one of the most critical failure risks in high-altitude PEMFCs. Grooved and perforated GDLs, especially those aligned with the airflow direction, have been shown to support directional drainage, critical in wing-

embedded fuel cell stacks or under varying pitch/yaw angles. Electrospun nanofiber-based GDLs have shown promise in reducing the thickness while maintaining high permeability. This directly supports stack volumetric energy density targets set by EU Clean Aviation programs for onboard hydrogen-electric propulsion.

In aviation, component integration is a key strategy to reduce the system weight, thermal resistance, and mechanical complexity. Integrated GDL designs, combining the functions of the gas flow field and diffusion layer, are being adopted to minimize contact resistance, reduce parasitic losses, and improve mechanical integrity. NASA's and DLR's recent PEMFC stack designs for aircraft applications have employed graphite or nickel foam GDLs with microchannel flow paths to unify gas delivery and diffusion functions.[14,32,90,185] These reduce the stack height and improve electrical contact reliability under vibrational stress. Furthermore, metal-foam-based integrated GDLs with hydrophobic MPL coatings offer superior water management,[48,209] making them ideal for midaltitude crewed flight where system redundancy and reliability are essential. Such designs also reduce the need for bulky external humidification systems, aligning with the goal of compact, self-regulating PEMFC subsystems in aviation. Based on the literature discussed in this section, Table 6 summarizes the key design priorities for gas diffusion layers (GDLs) in aviation PEMFC applications.

Table 6. Summary of the Key Aviation Design Priorities for GDLs

Design consideration	Aviation requirement
Water management	Orientation-independent drainage to prevent flooding during flight maneuvers
Gas diffusivity	High permeability under reduced atmospheric pressure
Mechanical integrity	Resistance to vibration, shock, and rapid thermal cycling
Thermal stability	Operability across wide temperature and pressure ranges
Lightweight structure	Minimize stack weight while preserving transport and support functions
Passive humidification	Retain moisture without external humidifiers, especially in high-altitude environments

5.3. Aerodynamic Coupling and Flight-Representative Validation. The aerodynamic environment of aircraft imposes nonuniform external pressure and temperature fields that directly influence gas transport and liquid water management within PEMFC stacks.[210] Under cruise conditions (i.e., Mach 0.3–0.8, Reynolds $\approx 10^6$–10^7), pressure gradients across the airframe and nacelle lead to differential cathode-inlet pressures of roughly 5–20 kPa depending on intake geometry and installation layout.[211,212] Computational-fluid-dynamics (CFD) analyses that incorporate such boundary conditions reveal oxygen concentration gradients of up to 15% across the flow field when simulated at 0.6 bar and 40–60% relative humidity, representative of 8–10 km altitude.[213–215] Orientation changes between the climb, cruise, and descent further modify two-phase flow paths. Multiphase CFD and side-view visualization studies coupling Navier–Stokes and species-transport equations under variable gravity vectors predict liquid water saturation zones of 0.25–0.40 near outlet ribs for 30° inclination.[216,217]

Integrating aerodynamic loads with stack-internal CFD has been demonstrated by Edwards et al.,[218] who compared channel geometries under fluctuating ambient pressure and found that serpentine channels maintain more uniform O_2 distribution than parallel designs, albeit with 10–15% higher pressure drop. Similar behavior is observed experimentally, where orientation-dependent drainage and oxygen starvation zones were validated through optical and neutron-imaging diagnostics.[219,220] Quantitative metrics extracted from these coupled analyses include the local oxygen partial pressure, liquid water saturation, and effective diffusion resistance within the gas diffusion layer. Under cruise-equivalent conditions, area-averaged O_2 mole fractions typically decrease from 0.21 to 0.18, while water saturation levels rise from 0.10 to 0.25 along the cathode channel.[213–216] These deviations reduce limiting current density by $\approx$5–12%, underscoring the importance of aerodynamically consistent flow field validation for aviation PEMFCs.

Future work should combine CFD–FEM cosimulation of flow field plates under vibrational and pressure loading with controlled-environment experiments using neutron or optical imaging to map oxygen distribution and water accumulation. Establishing such test matrices will bridge current laboratory designs with the aerodynamic realities of flight and provide essential validation for integrated aircraft power system models.[220–224]

6. CATALYST LAYER (CL)

The catalyst layer (CL) is the performance-defining component in a PEMFC. It facilitates the electrochemical reactions, the hydrogen oxidation reaction (HOR) at the anode and the oxygen reduction reaction (ORR) at the cathode, and largely determines the overall efficiency, power output, and durability of the cell. A typical CL comprises three primary constituents: (i) an electrocatalyst (commonly Pt-based),[53] an ionomer (e.g., Nafion) for proton transport, and (iii) a catalyst support (e.g., carbon) for electronic conduction and nanoparticle dispersion.[225]

The structure is designed to ensure effective transport of reactants, electrons, and protons and to manage water formed during the reaction. These three functions must occur simultaneously at the so-called three-phase boundary, where gas, ionomer, and catalyst coexist (Figure 18). While the HOR proceeds rapidly on the anode, the oxygen reduction reaction (ORR) on the cathode side is kinetically sluggish and therefore
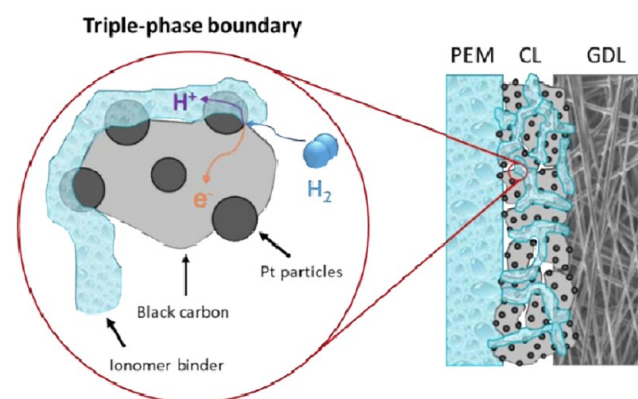

Figure 18. Schematic illustration of the reaction mechanism at the three-phase interface on the anode side.[227]
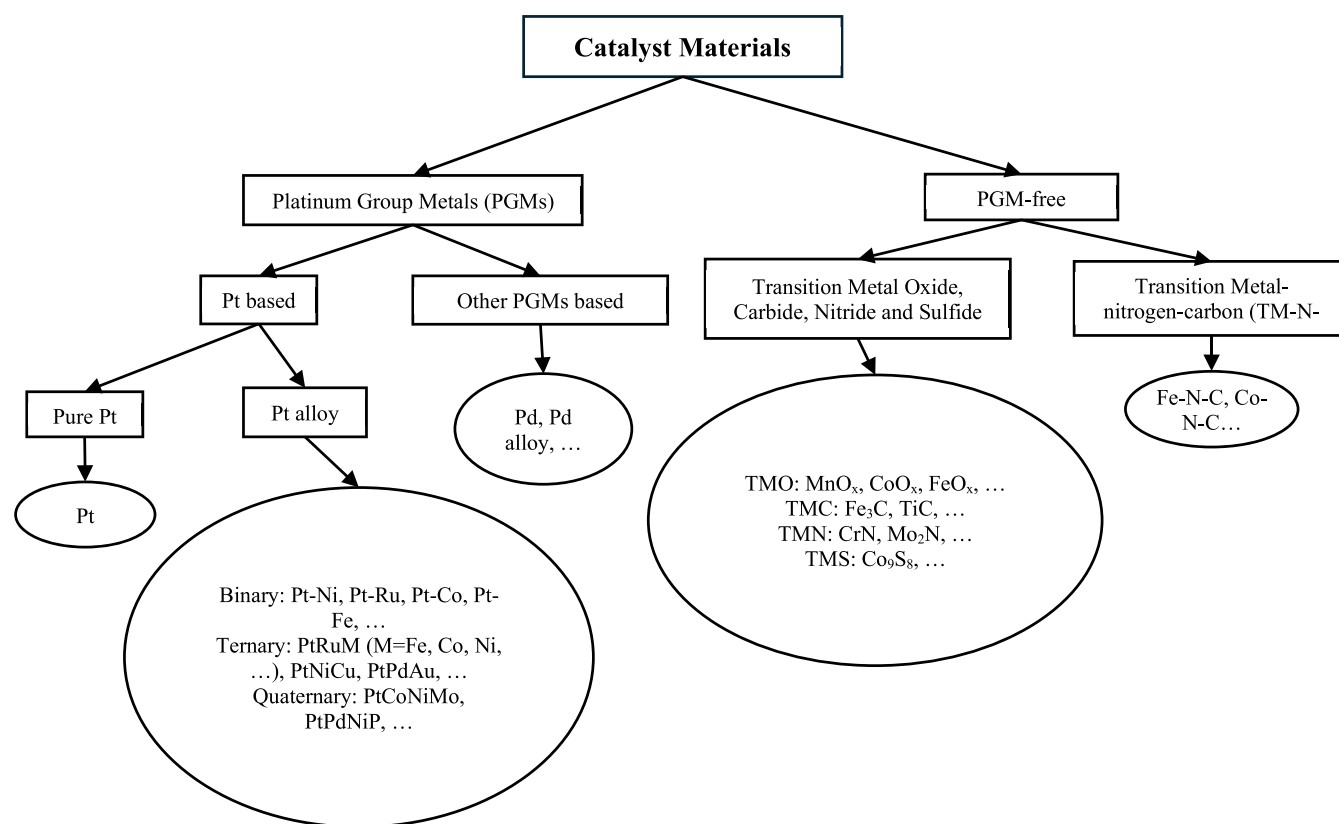
Figure 19. A range of materials studied and developed for the cathode catalyst layer (CL) in PEMFCs.

constitutes the rate-limiting step in PEMFC operation.[7] Consequently, optimization of cathode CLs, especially catalyst composition and structure, has received the most attention.

In aviation applications, the CL must satisfy ultralightweight, high-efficiency, and durability demands. Aircraft systems, especially those for mid- to long-range crewed flight, operate under variable load profiles, vibrational stress, and humidity/temperature fluctuations. This places significant pressure on the CL to maintain activity, prevent degradation, and minimize platinum group metal (PGM) usage.[18,226] Importantly, specific power (W/kg) and power density (W/L) must be optimized at the CL level to meet aviation propulsion targets.

6.1. Catalyst. *6.1.1. Catalyst Materials.* Platinum (Pt) remains the benchmark catalyst due to its high ORR activity and suitable adsorption energy for oxygen intermediates. The standard carbon-supported platinum (Pt/C) catalyst is widely used, but its high cost, limited availability, and susceptibility to degradation under acidic and high-potential conditions limit large-scale deployment for aerospace applications.[228] As a result, significant efforts have been directed toward developing alternative catalyst materials that maintain or enhance activity while reducing Pt content or eliminating precious metals entirely.[229−231]

PGM-free catalysts, especially those based on transition metal−nitrogen−carbon (TM−N-C) systems, have attracted growing interest. Among them, Fe−N−C is widely recognized as the most promising nonprecious catalyst. Wang et al.[232] and Martinaiou et al.[233] developed FeOx@graphitic carbon nanoparticles with a core−shell structure that exhibited ORR activity surpassing commercial Pt/C under acidic conditions and excellent durability after 10,000 potential cycles. Luo et al.[234] developed a transition metal chromium nitride (CrN)

catalyst and evaluated its oxygen reduction reaction (ORR) performance as a cathode material. While undoped CrN exhibited poor ORR activity in acidic media, Fe doping significantly improved its performance, making it only slightly less active than commercial Pt/C. These results suggest that Fe-doped CrN has potential as a competitive cathode catalyst.

Ren et al.[235] introduced a core−shell Fe_3C-based catalyst with comparable ORR activity to Pt/C and superior tolerance to CO poisoning. Although Co_9S_8 nanoparticles proposed by Illathvalappil and Kurungot[236] had slightly lower activity than Pt/C, they demonstrated much better long-term stability in acidic media. Fe−N−C catalysts have been shown to meet or approach the 2025 Department of Energy (DOE) targets in MEA testing.[237] However, their widespread deployment remains hindered by durability issues. Degradation primarily results from demetalation of FeNx active sites and corrosion of the carbon support.[233,237−240] To mitigate these challenges, researchers have explored atomic dispersion of active sites,[241−243] bimetallic site engineering,[244,245] and more robust carbon or noncarbon supports.[246] PGM-free catalysts offer promising ORR activity, particularly for unpressurized or open-cathode systems in UAVs. However, their durability under high-altitude and low-pressure conditions remains a barrier for crewed aviation.

Pt-alloy catalysts have also demonstrated great potential in reducing Pt usage while maintaining high activity. Alloying Pt with transition metals such as Ni, Fe, Co, or Cu alters its electronic structure and optimizes the adsorption energies of ORR intermediates.[247,248] Alloying improves the ORR kinetics, allowing for lower Pt loading without sacrificing activity. In flight-grade stacks, Pt-alloy catalysts contribute to weight

Table 7. Research Examples of Pt Alloy as a Cathode Catalyst. MA and SA Are the Mass Activity and Specific Activity, Respectively

Catalyst types	Electrochemical surface area (ECSA) (m^2/g_{Pt})	Mass activity (A/mg_{Pt}) @ 0.9 V	Specific activity (mA/cm^2) @ 0.9 V	Accelerated durability test (ADT)	refs
ordered fct- PtFe NPs	-	1.6	2.3	-	250
PtNi/C	44.39	0.2719	-	Maximum power density declined by 3.6% after 10,000 cycles	251
Pt$_3$Fe-ECNT	84 ± 4	0.45	0.535	93% initial limiting current density retention after 10,000 cycles	252
Pt−Ni−Ir/C	85	0.409	-	5 m^2/g_{Pt} and 58 A/mg_{Pt} losses in ECSA and MA after 5000 cycles	253
Pt$_{54}$Pd$_{46}$/B−C	79	0.549	0.463	22% and 25 mV losses in MA and cell voltage after 30,000 cycles	254
PtNi NW array	29	0.01444	0.0498	60% and 28% losses in ECSA and power density when tested in single cell after 3,000 cycles	255
L1$_0$−Pt$_2$CuGa/C	48.6	1.39	2.86	28 mV losses in cell voltage and 0.37 A/mg_{Pt} in MA after 30,000 cycles	256
PtCo40 @NG	65.2615	0.8195	1.2558	-	257
PtCo30Ni10 @NG	45.5206	1.3567	1.8933	18.15% losses in MA after 30,000 cycles	
PtCoNWs	73.2	1.06 ± 0.14	-	0.45 A/mg_{Pt} in MA after 30,000 cycles	258
PtCu$_{0.72}$Co$_{0.01}$	38.6	0.52	1.34	-	259
Pt$_4$Co$_1$ nanowires	41.2	0.148	0.279	5.6%, 22.3% and 19.4% degradation rate in ECSA, MA, and SA after 3000 cycles	260
Pt$_3$Fe/Fe$_3$C-NCB	51.75	0.97	1.89	30.93% and 14.28% decreases in MA and SA after 20,000 cycles	261
Pt/NbO/CNTs	81.62	0.057	1.14	7.4% and 7% decay in ECSA and MA after 30,000 cycles	53
Pt−Ni EDP-NCs-9	68.3	0.43	-	8.6% losses in MA after 10,000 cycles	262
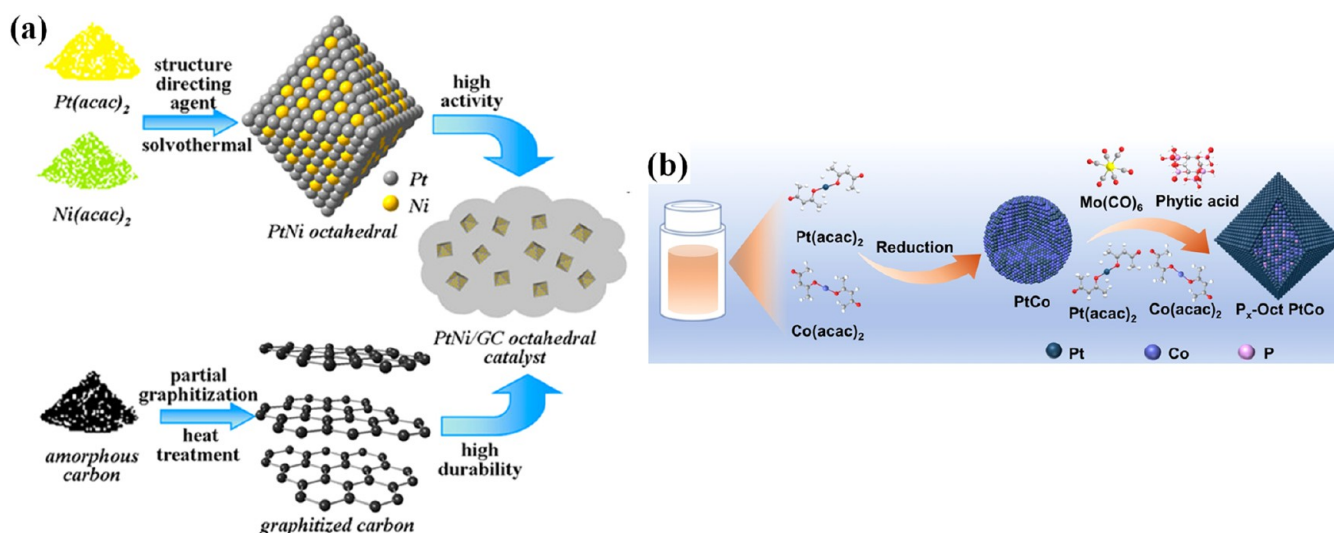
Figure 20. Schematic synthesis routine of (a) oh-PtNi/GC nanocrystal catalyst[267] and (b) codoping P and O oh-PtCo/C catalyst.[266] Reprinted from ref 267. Copyright 2020 American Chemical Society. Reprinted from ref 266. Copyright 2024 Elsevier.

savings, improved start-up/shutdown durability, and reduced performance decay under dynamic load cycles.[249]

Figure 19 shows a range of materials studied and developed for the cathode catalyst layer (CL) in PEMFCs. Numerous binaries and multimetallic Pt alloys have achieved significant enhancements in both mass activity (MA) and specific activity (SA), as listed in Table 7.

6.1.2. Catalyst Structures and Morphologies. Alongside material development, structural engineering of catalysts offers another powerful strategy to improve performance and reduce Pt loading. The shape, facet orientation, and nanoscale architecture of catalysts directly influence the availability of active sites and the kinetics of ORR.[263]

It is well established that different crystal facets exhibit varying ORR activity, following the order of (110) > (111) > (100) on the crystal facets in acidic media.[228,264,265] For Pt and its alloys, the (111) facet typically shows superior activity under acidic conditions. Therefore, octahedral (oh) Pt-based catalysts, which expose eight (111) facets, have received particular attention. Tian et al.[266] prepared P and O codoped oh-PtCo/C catalysts with mass activity (MA) and specific activity (SA) values 4.1 and 10.9 times greater than commercial Pt/C, respectively. Moreover, it exhibited good stability, with only a 25% loss in mass activity after 50,000 ADT cycles. Wang et al.[267] and Cai et al.[268] also reported oh-PtNi catalysts that demonstrated outstanding performance in
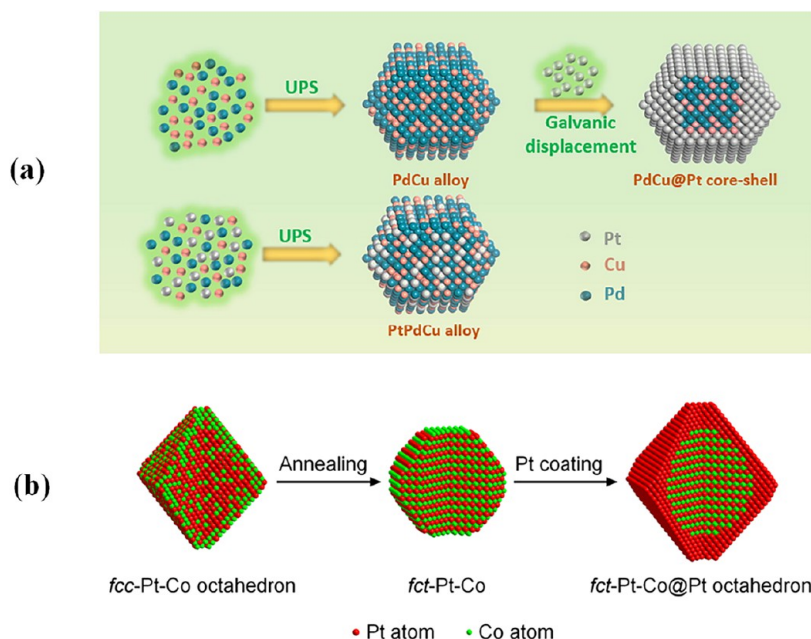
Figure 21. Illustrations of the preparation steps for the (a) core−shell PtPdCu/C nanoparticle catalyst[272] and (b) fct-PtCo@Pt octahedron catalyst with core−shell structure.[273] Reprinted with permission from ref 272. Copyright 2022 Elsevier. Reprinted from ref 273. Copyright 2021 American Chemical Society.
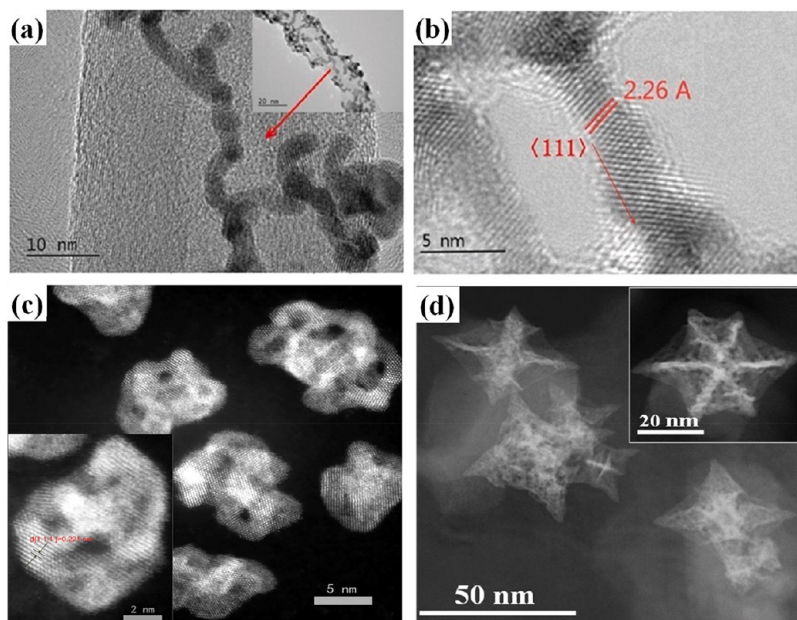
Figure 22. TEM images of (a) PtNW/NCNT catalyst[274] and (b) PtNi nanocage catalyst.[275] (c, d) HADDF-STEM images of PtCu nanoframe catalyst from different angles.[277] Reprinted with permission from ref 274. Copyright 2022 Elsevier. Reprinted with permission from ref 275. Copyright 2017 Elsevier. Reprinted with permission from ref 277. Copyright 2021 Elsevier.

MEA tests. Figure 20 shows the synthesis processes of both Tian et al.[266] and Wang et al.[267]

Pan et al.[269] and Danisman et al.[270] proposed and synthesized ternary nanoparticle catalysts, oh-PtNiRh/C and oh-PtNiMo/C, respectively. Their results demonstrated that introducing a third metal into the oh-PtNi catalyst could further enhance both the performance and durability. Building on this concept, Hornberger et al.[271] doped PtNi/C with two additional metals, developing the quaternary catalyst oh-PtNiRhMo/C. Test results indicated that this quaternary

catalyst offered improved structural stability compared to the binary oh-PtNi/C catalyst.

Core−shell architectures represent another effective design for reducing Pt consumption while retaining the catalytic activity. In this configuration, a Pt shell is deposited on a nonprecious metal or alloy core. Shi et al.[272] synthesized PtPdCu@Pt core−shell nanoparticles that exhibited an MA over three times higher than Pt/C and only 12.2% loss after 30,000 durability cycles, as shown in Figure 21a. Xie et al.[273] fabricated an fct-PtCo@Pt catalyst with an octahedral

Figure 23. Synthesis procedures of Pt monolayer@Pd core−shell catalyst.[280] Reprinted with permission from ref 280. Copyright 2020 Elsevier.

geometry (Figure 21b) that reached an MA of 2.82 A/mgPt and sustained performance over 30,000 cycles.

Nanowires, nanocages, and nanoframes have also been investigated for maximizing the Pt utilization. These structures offer high surface area, improved mass transport, and enhanced s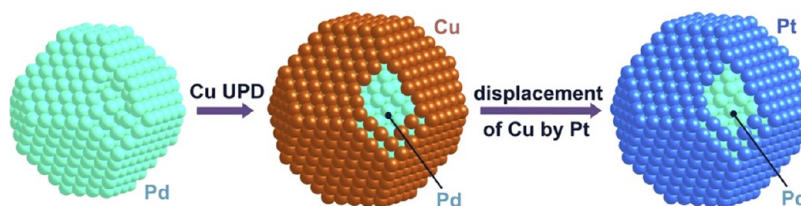tructural stability. Lu et al.[274] synthesized a nitrogen-doped carbon nanotube (NCNT) supported Pt nanowire (PtNW) catalyst. TEM analysis revealed that the Pt nanowires preferentially grew along with the (111) crystallographic facet. This observation was further confirmed by X-ray Diffraction (XRD) results, which showed a stronger (111) peak intensity for the PtNW/NCNT catalyst compared to the conventional Pt/C catalyst. The enhanced exposure of the (111) facet contributed to improved binding energy, thereby enhancing the catalyst's electrochemical activity. Peng et al.[275] fabricated a PtNi nanocage catalyst and evaluated its ORR performance. Owing to the nanocage structure, the catalyst achieved an electrochemical surface area (ECSA) of 71.16 m^2/gPt—more than twice that of Pt/C. As a result, despite a lower Pt loading (0.1 mgPt/cm^2), its PEMFC performance exceeded that of Pt/C. Similarly, Liu et al.[276] developed a high Pt content nanocage catalyst (60 wt %), which achieved performance comparable to commercial 60 wt % Pt/C, but with a lower Pt loading of 0.17 mgPt/cm^2, attributed to its larger ECSA. Gong et al.[277] proposed an atomically ordered PtCu nanoframe catalyst that exhibited both high activity and durability. It achieved mass activity (MA) of 0.82 A/mgPt, with only a 15% decline after 30,000 ADT cycles. These improvements were primarily attributed to the high ECSA provided by the nanoframe structure and the weakened oxygen intermediate binding energy resulting from alloying. The TEM images of these catalysts are displayed in Figure 22.

Surface morphology treatments can enhance both the distribution and the surface concentration of Pt on catalyst particles. Techniques such as controlled synthesis, surface atomic ordering, atomic displacement (internal and external), and dealloying are commonly employed to form surface structures like Pt-skin or Pt monolayers.[263] These approaches aim to achieve uniform Pt coverage and maximize surface reactions, critical for high-power applications such as aviation propulsion stack. Malheiro et al.[278] compared PtFe nanoparticle catalysts with and without a Pt-skin to assess their effect on performance. Their results showed that the presence of a Pt-skin doubled the ORR activity, although no significant improvement in PEMFC power density was observed. Sugawara et al.[279] investigated the influence of ordering treatments on Pt-skin formation and corrosion resistance in PtCo alloy catalysts. Ordered and disordered PtCo alloys were synthesized, and Pt-skin layers were generated via dealloying. The study found that ordering effectively suppressed Pt-skin dissolution, thereby enhancing the catalyst stability and durability. Sasaki et al.[280] fabricated a Pt monolayer@Pd core−shell catalyst via atomic displacement (Figure 23), which

significantly reduced Pt content while simultaneously improving ORR activity and stability.

To maximize catalyst utilization and reduce Pt demand, morphological engineering has been employed:

- Octahedral Pt-alloy nanoparticles, which expose high-activity (111) crystal facets, are ideal for compact stacks with high mass activity.[281]
- Core−shell structures (e.g., Pt@Pd, Pt@PtNi) reduce Pt content while preserving ORR performance.[282] These are suitable for aviation systems with strict specific power limits.
- Nanowires, nanocages, and nanoframes offer high surface area, lower internal resistance, and improved gas access[283,284]—essential under pressurized cabin or transient airflow conditions.
- Dealloyed or Pt-skin morphologies enhance stability under load cycling,[285] making them suitable for long-duration cruise where catalyst degradation via Pt dissolution is a major risk.

6.2. Ionomer Films in the Catalyst Layer. Within the catalyst layer (CL), ionomers perform two essential functions: they serve as proton-conducting media and act as binders that provide mechanical cohesion. To enable electrochemical reactions, the ionomer forms a thin film that coats the surface of catalyst particles, thereby facilitating the formation of a three-phase interface where the gas, ionomer, and catalyst converge. This interface is essential for enabling the oxygen reduction reaction (ORR), particularly at the cathode.

Taking ORR as an example, oxygen molecules first diffuse from the gas diffusion layer (GDL) through the gas channels into the CL. The gas navigates the interparticle voids until it reaches the surface of the ionomer film. From there, oxygen permeates through the ionomer film, dissolves in it, and ultimately reaches the ionomer/Pt interface, where it reacts with electrons and protons to form water. Given this sequence, the ionomer film influences CL performance primarily in two respects: (1) its ability to conduct protons[42] and (2) its resistance to oxygen transport.

The ionomer films used in PEMFCs are typically composed of perfluorosulfonic acid (PFSA), the same material as used in PEMs. However, due to the large difference in thickness (nanometers in ionomer films versus micrometers in PEMs), the transport properties of PFSA in these two contexts differ significantly. In bulk PEMs, proton conduction occurs via both the vehicle mechanism and the Grotthuss (hopping) mechanism, supported by adequate water content (see Section 7).[286]

In contrast, the thin ionomer films in the CL exhibit reduced water adsorption due to strong interactions between sulfonic acid groups and functional groups on the catalyst support surface. As summarized by Paul et al.[287] and Iden et al.,[288] this leads to reduced hydration and suppresses the fast Grotthuss mechanism, thereby forcing protons to travel via the slower

surface diffusion mechanism. Farzin et al.[289] further investigated the underlying reasons for the reduced proton conductivity in thin ionomer films. Their findings showed that the limited film thickness restricts ionomer chain mobility, resulting in smaller, poorly connected ion domains. Consequently, proton transport becomes dominated by surface diffusion, which is slower and less efficient, especially under low humidity. These insights suggest that enhancing ion domain formation and interconnectivity within the ionomer film is more critical than water uptake alone for improving proton conductivity.

To address these limitations, Chatterjee et al.[290] developed a polystyrene-based ionomer incorporating sulfonated macrocyclic calix[4]arene pendants (PS-calix). At the subnanometer scale, this ionomer exhibited proton conductivity 13 times higher than Nafion. The improved performance was attributed to its ability to effectively trap water within macrocyclic cavities, which promoted the formation of long-range coherent ion channels. In addition, enhanced interfacial phase separation between the ionomer and catalyst surface allowed more sulfonic acid groups to participate in proton conduction and increased the overall water adsorption. Notably, despite a lower sulfur content at the interface compared to Nafion, the PS-calix ionomer achieved higher conductivity, underscoring the significance of the ion domain architecture and interface interaction. These characteristics are particularly beneficial for aviation stacks operating under thin air and high cycle loads, where water retention is limited.

On the other hand, oxygen transport through the ionomer film presents a different set of challenges. For oxygen to reach the Pt surface, it must cross two interfaces—the gas/ionomer interface and the ionomer/Pt interface, as well as diffuse through the bulk of the film. While increasing film thickness can improve proton conductivity, it also raises diffusion resistance and impedes oxygen transport.[291] Importantly, several studies have revealed that interfacial resistance, especially at the ionomer/Pt interface, poses a more significant barrier to oxygen transport than bulk diffusion resistance.[292,293]

Strong adsorption of ionomer side chains onto Pt has been identified as the primary cause of this resistance.[294] As a result of this interaction, the ionomer side chains tend to adsorb onto the Pt surface, eventually forming a dense ultrathin film.[286,295−297] This dense ultrathin ionomer film poses significant resistance to oxygen transport. Moreover, due to the hydrophilic nature of the ionomer side chains, the film−Pt interface becomes increasingly hydrophilic, leading to greater water absorption and retention at the interface. The resulting high water content blocks oxygen transport pathways, further reducing the oxygen diffusion rates. The formation of a water film exacerbates interfacial resistance and hinders oxygen access to active sites.[295,298,299] As reported by Gao et al.,[294] sulfonic acid groups and ether linkages on the ionomer chains tend to interact with Pt surfaces, forming dense, ultrathin hydrophilic films that inhibit oxygen permeation. This structure not only limits oxygen access but also increases water uptake at the interface due to the hydrophilicity of the side chains. The accumulation of interfacial water further obstructs oxygen transport and raises interfacial resistance.[291] These findings highlight the need for interface engineering strategies to disrupt water film formation and restore oxygen accessibility, particularly important in low-pressure or air-cooled aviation stacks.

In aviation PEMFCs, ionomer performance must be optimized for low-humidity conditions at higher altitudes, dynamic temperature environments (subzero to 80+ °C), and resistance to flooding and drying cycles, especially in hybrid propulsion systems.[16,300−302] Thin ionomer films (<100 nm) are prone to low proton conductivity due to poor hydration at altitude. In addition, excessive side-chain adsorption to Pt surfaces leads to high interfacial resistance—a critical bottleneck in low-pressure cathodes used in aviation.[303,304] Advanced ionomers such as sulfonated macrocyclic polymers (e.g., PS-calix) or short-side-chain PFSA analogues (e.g., 3 M 870) demonstrate higher proton conductivity and enhanced oxygen permeability, making them promising for next-generation aerospace stacks.[305,306] Interface engineering to mitigate water film formation at the Pt−ionomer interface is particularly important in air-cooled or high-altitude PEMFCs, where water management is passive.[307−309]

6.3. Catalyst Supports. Catalyst support plays a vital role in stabilizing catalyst nanoparticles, enhancing electron transport, and maintaining structural integrity under the demanding conditions within a PEMFC. An ideal support must offer high surface area, excellent electrical conductivity, strong interaction with metal particles, and exceptional chemical and electrochemical stability—especially in acidic and oxidative environments characteristic of PEMFC operation.

6.3.1. Carbon and Carbon-Based Supports. Carbon-based materials remain the most commonly used supports due to their high electrical conductivity, low cost, large surface area, and structural tunability. While conventional carbon black (e.g., Vulcan XC-72) is widely adopted in commercial PEMFCs, its limited corrosion resistance and weak interaction with Pt often lead to particle agglomeration and detachment under high-potential cycling, especially in cathode environments. To address these limitations, various advanced carbon supports have been developed. These include carbon nanotubes (CNTs),[53,310−312] carbon nanofibers (CNFs),[313−316] graphene and graphite derivatives,[317−320] ordered mesoporous carbons (OMCs),[232,321−324] and carbon aerogels.[325−327] The unique tubular structure of CNTs and the high degree of graphitization provide superior conductivity and corrosion resistance. Similarly, CNFs offer high surface area, directional conductivity, and enhanced durability. Graphene-based materials provide excellent thermal and electrical properties, while the properties of the OMCs and aerogels are controllable and promote improved catalyst dispersion and mass transport. These nanostructured supports offer improved resistance to vibration-induced catalyst detachment and maintain electrical connectivity under flight-induced thermal stress.

One key challenge with carbon materials is insufficient anchoring of Pt nanoparticles.[328] Surface modification through heteroatom doping has been widely used to introduce binding sites and improve the catalytic performance. Nitrogen doping, in particular, can create defects and functional groups that promote uniform metal dispersion and may even introduce additional ORR-active sites.[329−333]

Roudbari et al.[334] investigated the effect of nitrogen-functionalized carbon nanotube (CNT) supports on the ORR performance of Pt-based catalysts in PEMFCs. The presence of nitrogen functional groups enhanced the anchoring of Pt nanoparticles, resulting in improved catalytic activity and stability. A PtCo nanocatalyst supported on N-doped ordered mesoporous carbon exhibited excellent performance with an electrochemical surface area (ECSA) of 98.19 m²/g. In single-

cell tests, the catalyst achieved a current density of 1.53 A/cm^2 at 0.6 V and a peak power density of 1.17 W/cm^2. Yang et al.[321] further showed that the synergistic effect of nitrogen doping and an ordered mesoporous structure resulted in high ECSA and peak power density.

Other dopants, such as oxygen, boron, sulfur, and phosphorus, have also been explored. Li et al.[335] introduced oxygen-containing functional groups, using ammonium persulfate (APS) as the modifier, on CMK-3 mesoporous carbon, significantly improving Pt dispersion and achieving nearly 5-fold enhancement in mass activity over commercial Pt/C. Yao et al.[336] demonstrated that boron doping enhanced Pt dispersion and facilitated oxygen adsorption and dissociation. Han and Chen[337] achieved stable performance using N/P codoped graphene supports, while Long et al.[338] presented a tridoped (N, P, S) porous carbon structure that outperformed single- and dual-doped materials, approaching the ORR activity of Pt/C in acidic environments.

6.3.2. Noncarbon Supports. To overcome the limitations of carbon corrosion, noncarbon supports based on transition metal compounds have been explored. These include carbides, nitrides, and oxides such as tungsten carbide,[339,340] molybdenum carbide (Mo$_2$C),[341] zirconium carbide (ZrC),[342] silicon dioxide (SiO$_2$),[343] and titanium nitride (TiN).[344] These materials offer excellent chemical stability and unique metal–support interactions that enhance the catalyst dispersion and activity.

Lori et al.[340] showed that Pt supported on WC exhibited enhanced activity and improved durability compared to Pt/C. Hamo et al.[341] used low-overpotential electrodeposition to achieve high Pt dispersion on Mo$_2$C, resulting in significantly increased mass activity at reduced Pt loading. ZrC demonstrated strong corrosion resistance and stability over 30,000 cycles, meeting DOE durability targets.[342] Similarly, SiO$_2$-anchored PtNi catalysts[343] and mesoporous TiN supports[344] provided high catalytic activity and improved utilization efficiency under various operating conditions.

MXenes, a recently developed class of 2D transition metal carbides, nitrides, and carbonitrides, have also emerged as promising catalyst supports. Their general formula Mn + 1XnTx (where M is a transition metal, X is carbon or nitrogen, and T represents surface terminations such as −OH, −O, or −F) allows for versatile surface engineering and high conductivity. Ti$_3$C$_2$Tx is the most widely studied MXene for PEMFCs.[345] Xu et al.[346] synthesized a hybrid catalyst by combining Ti$_3$C$_2$Tx MXene with CNTs, achieving a 3-fold improvement in mass activity over Pt/C and superior performance in MEA tests. Similar improvements were reported by Wang et al.,[347] Junaidi et al.,[348] and Chang et al.,[349] highlighting the robustness and scalability of MXene-based hybrids. Furthermore, theoretical studies by Yang et al.[350] predicted that V$_2$C MXenes exhibit strong metal–support interactions, enabling stable dispersion of catalytic metal monolayers. Zhang et al.[351] also proposed a scalable synthesis method for TiN-based MXene supports, showing competitive ORR activity under alkaline conditions. MXene-based catalysts offer compact, high-activity designs that are favorable for airborne fuel cells exposed to thermal gradients and vibration.

6.4. Catalyst Layer Structure Design. Beyond material composition, the internal structure of the catalyst layer significantly affects mass transport, electrochemical activity, and water management—especially under high current

densities. Parameters such as pore size, porosity, ionomer distribution, and spatial gradients in catalyst and ionomer content play key roles in determining the PEMFC performance and durability. Guan et al.[352] showed that increasing the average pore size of the CL (to 70−100 nm) reduced oxygen transport resistance, particularly under low Pt loading. Larger pores increased cumulative pore volume and facilitated reactant diffusion while also enhancing the effective electrochemical surface area. However, excessive enlargement of the pore size can reduce structural strength and water retention capacity, especially under dry conditions. This trade-off is particularly relevant for airborne systems operating at high altitudes, where humidity control is limited.

Garsany et al.[353] have suggested that wettability control may have a greater influence on performance than porosity alone. Introducing a wettability gradient—where hydrophilic regions promote water removal and hydrophobic regions support gas transport—can effectively mitigate flooding and dry-out. Lin et al.[354] and Wang et al.[355] demonstrated that such gradient-controlled CLs, created by doping PTFE nanoparticles at tailored concentrations, significantly enhanced power density and reduced mass transport losses at high current densities. Several studies have explored the effect of spatial gradients in Pt particle size, loading, and ionomer content across the CL thickness.[356−358] Zheng et al.[356] proposed placing small Pt particles and higher ionomer content near the membrane side to improve activity during early operation, while using larger particles toward the GDL side to resist dissolution and aggregation. Wang et al.[357] and Mu et al.[358] confirmed the positive effect of ionomer gradient distributions on oxygen accessibility and overall cell performance. Dong et al.[359] used a coupled performance degradation model to show that combining ionomer and Pt gradients in opposing directions (i.e., high ionomer content with small Pt particles) improved both beginning-of-life performance and long-term durability. In contrast, aligning the Pt particle size and loading gradients in the same direction enhanced durability toward end-of-life operation. However, Fan et al.[360] emphasized that optimizing a single parameter, such as ionomer content or Pt distribution, does not guarantee performance enhancement, due to the complex interplay between structural, electrochemical, and transport phenomena in the CL.

In summary, structural engineering of the catalyst layer, including pore morphology, wettability gradients, and functional gradient design, offers a powerful avenue for improving PEMFC performance, particularly in systems operating at high current density and under dynamic load conditions, as would be required for aviation propulsion. Table 8 summarizes the key aviation requirements for catalyst layers in the PEMFC systems.

6.5. Combined Electrochemical−Mechanical Durability. The durability of aviation fuel cell catalyst layers must be evaluated under coupled electrochemical, thermal, and mechanical stress, since aircraft operation imposes simultaneous load cycling, vibration, and temperature gradients.[361] Conventional automotive accelerated stress tests (ASTs) that isolate individual mechanisms (e.g., potential cycling between 0.6 and 1.0 V vs reversible hydrogen electrode (RHE) at 50 mV s^{-1} for 30,000 cycles) underestimate degradation rates observed under dynamic flight conditions.[362,363]

Recent studies combining ORR/Pt-loss ASTs with thermal and vibration cycling have reported electrochemically active surface area (ECSA) retention of only 60−80% after 500 h for

Table 8. Summary of Key Aviation Requirements for the Catalyst Layers

Design priority	Aviation-specific need
Pt utilization efficiency	Minimize stack mass and cost
Load-cycle durability	Maintain performance across takeoff, cruise, descent, and restart
Structural robustness	Survive vibration, thermal cycling, and rapid pressure changes
Oxygen transport optimization	Ensure reactant access under low-pressure or open-cathode conditions
Water management compatibility	Avoid flooding or drying under variable humidity and orientation
Thin, high-surface-area designs	Support stack compactness and integration in fuselage or wing structures

Pt/C catalysts operated between 20 and 80 °C with ± 2 °C min^{-1} temperature swings.[364] In parallel, particle growth from 3 to 6 nm and support corrosion currents exceeding 50 μA cm^{-2} have been observed during mixed thermal−electrochemical cycling.[365,366] For low-Pt ($\leq$0.1 mg Pt cm^{-2}) and PGM-free (Fe−N−C, Co−N−C) catalysts, activity losses of 30−50% after 200 h combined ASTs are typical, primarily due to carbon-support oxidation and active-site demetalation under humid, low-pressure operation.[367]

Incorporating mechanical excitation at 5−500 Hz and accelerations up to 5 g rms during electrochemical testing enables realistic simulation of vibration-induced particle detachment and interfacial delamination.[368] Quantitative metrics recommended for comparative reporting include ECSA retention (% initial), particle size growth (nm), support-corrosion current (μA cm^{-2}), and mass activity loss (% after 500 h).[369] Establishing such coupled-stress protocols will help identify catalyst and support formulations truly robust for aviation deployment and harmonize testing across research and industrial groups.[370]
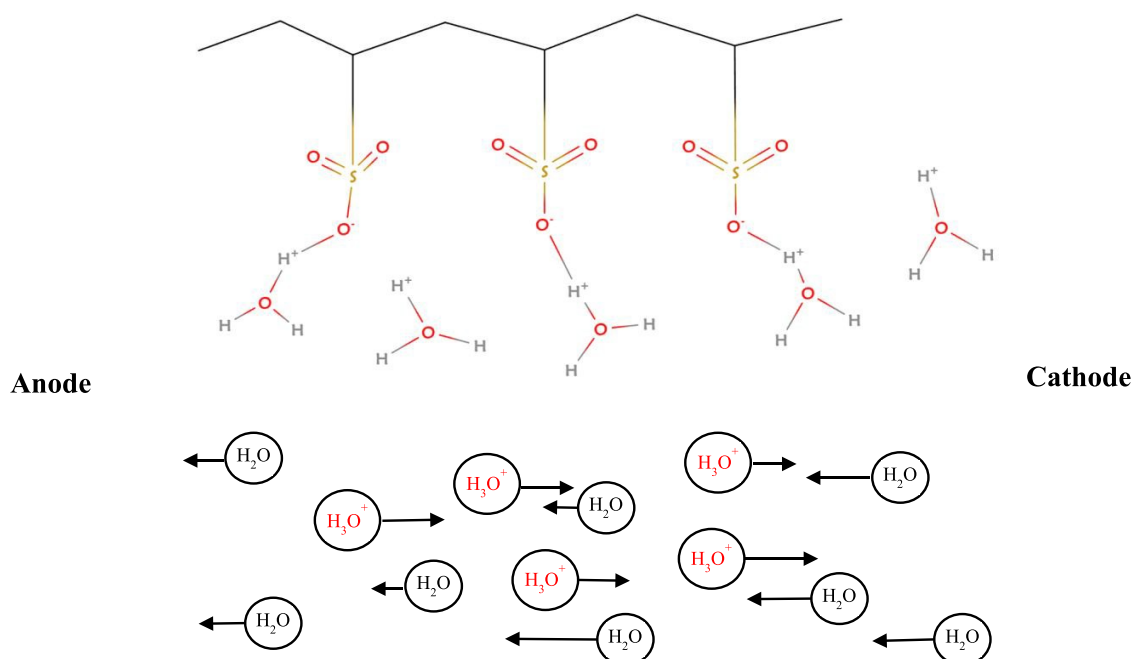
7. PROTON EXCHANGE MEMBRANE (PEM)

The proton exchange membrane (PEM) forms the electrochemical core of a PEMFC, enabling selective transport of protons (H$^+$) from the anode to the cathode while blocking electrons and reactant gases. Its performance significantly impacts the overall efficiency, durability, and power output of the cell. The PEM must simultaneously exhibit high proton conductivity, low gas permeability, thermal and chemical stability, and robust mechanical integrity over extended operating cycles.[371]

In aviation applications, PEMs must operate under conditions far more demanding than those in terrestrial or automotive fuel cells. Aircraft propulsion systems experience substantial environmental fluctuations, including sharp changes in temperature, pressure, and humidity. During high-altitude flight, ambient temperatures can fall below −40 °C and partial pressures of oxygen and water vapor can decline drastically.[309] Consequently, the membrane must retain conductivity under dry, low-pressure conditions, while maintaining mechanical strength and gas-separation capabilities.[372,373] In addition, the PEM must exhibit resilience to frequent start−stop cycles, vibrational loading, and accelerated degradation mechanisms, such as radical-induced oxidative stress, which are intensified during extended flight operations.[173,374]

Proton transport within PEMs primarily occurs through the Grotthuss mechanism (proton hopping between adjacent water molecules and sulfonic acid groups) and the vehicle mechanism (diffusion of hydrated protons such as H$_3$O$^+$).[286,371] As illustrated in Figure 24, both pathways are highly dependent on the membrane's hydration state. In airborne PEMFCs, where external humidification is often limited or absent, membrane designs must facilitate internal water retention or operate efficiently under a reduced water content.

7.1. PFSA-Based Membranes. Perfluorosulfonic acid (PFSA) membranes continue to serve as the benchmark in PEMFCs due to their exceptional chemical stability and high

Figure 24. Schematic illustration of proton transport mechanisms in a proton exchange membrane.
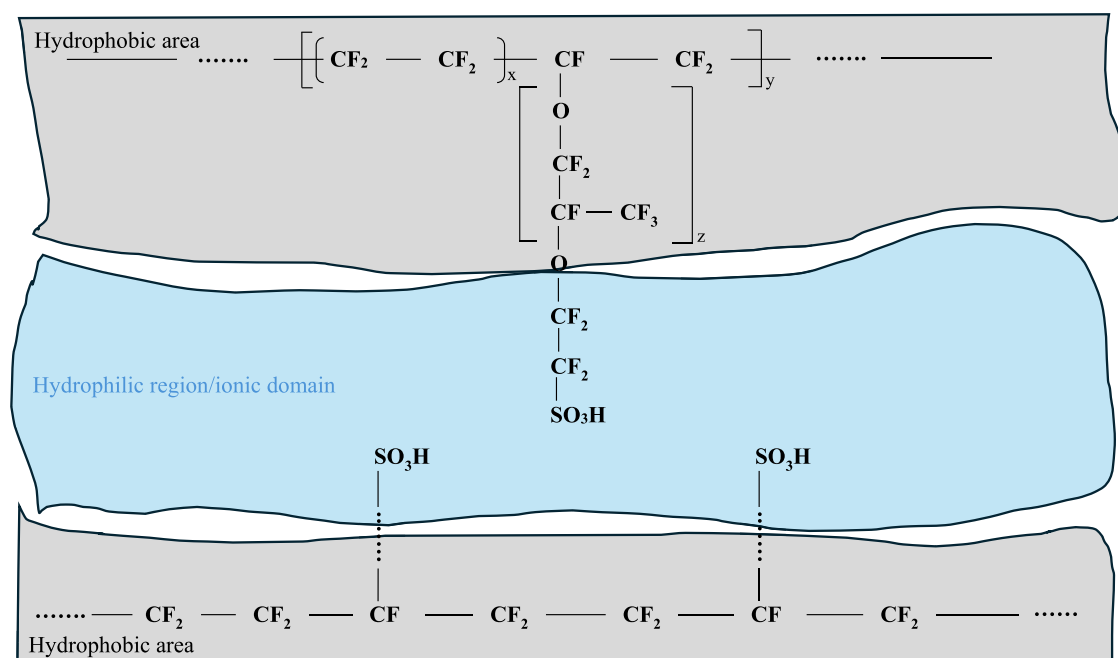
Figure 25. Chemical structure and ion transport channel of the PFSA membrane.

proton conductivity under humidified conditions. Their microstructure, based on a hydrophobic polytetrafluoroethylene (PTFE) backbone with hydrophilic sulfonic acid side chains ($-SO_3H$), supports the formation of ion-conducting channels when hydrated,[375] as shown in Figure 25. PFSA membranes offer excellent proton conductivity and electrochemical performance under low-temperature and high-humidity conditions.[375] However, they face several drawbacks such as the high production cost, reduced conductivity under low relative humidity (RH), limited thermal stability above 80 °C, susceptibility to mechanical swelling, and sensitivity to contaminants such as CO and NH_3.[375] Furthermore, in aviation environments, they encounter several limitations. Their proton conductivity drops sharply at low relative humidity, and they are prone to dimensional swelling and degradation at elevated temperatures.[376] These drawbacks complicate their integration into high-performance aviation stacks, which must remain compact, reliable, and self-regulating.

7.2. Alternative Membrane Types. To overcome the limitations of PFSA-based membranes, several alternative membrane types have been developed and are summarized in Table 9. Partially fluorinated sulfonic acid membranes, which employ polymer backbones such as polyvinylidene fluoride (PVDF) or ethylene-tetrafluoroethylene (ETFE) with sulfonated side chains,[377] provide better mechanical and oxidative resistance but exhibit lower proton conductivity than fully fluorinated PFSA materials. These membranes offer moderate performance in aircraft systems with partial pressure regulation or limited thermal variation.[378] They also provide better chemical resistance than hydrocarbon-based membranes but lower proton conductivity and hydrophobicity than fully fluorinated PFSAs. Ballard's BAM series exemplifies this class. These materials are promising for low-pressure aviation environments but require additional reinforcement to meet humidity cycling demands in pressurized cabins or high-altitude UAVs.

Nonfluorinated hydrocarbon membranes such as sulfonated polyether ether ketone (SPEEK) are attractive due to their low cost and environmental compatibility. With proper design, their performance can approach that of PFSA membranes.[379] Their tunable sulfonation levels allow for acceptable performance under controlled humidity; however, they typically suffer from reduced oxidative stability and mechanical degradation,[380] particularly under thermal cycling typical in aviation use.

Composite membranes, incorporating PFSA with reinforcing substrates such as expanded PTFE (ePTFE) or electrospun PVDF nanofibers,[381] offer an optimal balance for aerospace integration. These membranes combine high conductivity and chemical stability with low swelling and mechanical robustness even under fluctuating humidity and temperature. These attributes make composite membranes highly suitable for airborne platforms that experience frequent takeoff/landing cycles and power modulation. Products such as GORE-SELECT have demonstrated excellent performance under altitude simulation and are increasingly used in UAV and small aircraft fuel cell demonstrators.[382−386]

7.3. Membrane Modification Strategies. Membrane modification strategies are actively being pursued to enhance the PEM resilience and performance in aviation fuel cells. Various chemical and physical modifications have been explored.

7.3.1. Doping and Blending. Cali et al.[391] doped phosphorene−graphene oxide into PVDF membranes, achieving improved durability and electrochemical performance. Rajabalizadeh Mojarrad et al.[392] and Thmaini et al.[393] enhanced water retention and conductivity by doping sulfonated silica and $SiO_2@TiO_2$−palygorskite fibers into Nafion and PVDF-based membranes. More importantly, the nanocomposite membrane exhibited high proton conductivity at elevated temperatures (110 °C), addressing the performance limitations of conventional Nafion membranes under such conditions. This improvement is likely attributed to the membrane's enhanced water retention and thermal stability.

Table 9. Classification of Proton Exchange Membranes Used in PEMFCs

Types	Structure	Advantages	Disadvantages	Representative products
Perfluorosulfonic acid (PFSA) membrane[387]	Polytetrafluoroethylene (PTFE) as the main chain and the side chain contains sulfonic acid groups	High mechanical strength and good chemical stability. Best performance at low temperature and high humidity conditions (high proton conductivity and high current density).	High cost. Poor tolerance to impurity gas, easy to poison. Poor performance under high temperature and dry conditions, prone to degradation. Large swelling degree	Nafion, Aquivion, Flemion, Aciplex, Dow XUS-B204.
Partially fluorinated sulfonic acid polymer membrane[388]	Fluorocarbons are used as the main chain, such as polyvinylidene fluoride (PVDF), ethylene-tetrafluoroethylene copolymer (ETFE), or polytetrafluoroethylene (PTFE). Hydrocarbons or aromatic hydrocarbons are used as side chains, and sulfonic acid groups are introduced through sulfonation.	Good mechanical strength, thermal stability, and chemical resistance. Relative Low cost.	Hydrophobicity leads to poor water absorption ability. Bad mechanical stability. Low proton conductivity.	Ballard BAM
Nonfluorinated sulfonic acid polymer membrane[389]	Fluorine-free hydrocarbons such as polyarylether (PEEK), polyimide (PI), poly(ether imide) (PEI), and polystyrene (PS) are used as substrates, and sulfonic acid groups are introduced into the side chains by sulfonation.	Low cost, safe, and environmentally friendly. It can exhibit similar performance to PFSA membrane under appropriate design.	Poor proton conductivity and stability. The swelling degree at high sulfonation degree is greater than PFSA membrane. It is difficult to achieve high electrochemical performance and high mechanical properties at the same time.	DAIS
Composite membrane[390]	Porous PTFE (ePTFE) or PVDF electrospun nanofiber as substrate and is completely filled with PFSA solution to form PFSA/ePTFE or PFSA/PVDF composite membrane.	High mechanical strength, good thermal/chemical stability. Thin thickness. Excellent performance over a wide range of operating conditions. Low swelling degree.	The manufacturing process is relatively complex and immature. High requirements for filling accuracy and integrity of PFSA solvent.	GORE-SELECT

Table 10. Aviation PEMFC Performance Targets Compared with Current Best-Reported Values from Automotive and Stationary Fuel Cell Systems[a]

Parameter	Aviation target	Current best-reported	Gap/challenge	refs
Specific power (W kg^{-1})	>2000	1000−1500 (automotive stacks)	25−50% shortfall	90,338,430,51
Volumetric power (W L^{-1})	>2000	800−1200	40−60% lower	
Durability/life cycles	>30,000 h or >10,000 cycles	5000−8000 h (automotive)	60−80% improvement needed	169,410,342
Allowable performance loss	<10% over service life	15−20%	5−10% excess degradation	169,410
Membrane conductivity at 50% RH (S cm^{-1})	≥0.08	0.05−0.06 (PFSA/composite)	∼25−40% lower	387−391
Pt loading (mg Pt cm^{-2})	≤0.10	0.15−0.25 (automotive)	33−60% reduction required	247−249
Stack operating temperature (°C)	0−80 (ambient start to cruise)	20−80	Need robust cold-start	408,409
Operating pressure (bar)	0.5−1.0 (altitude range)	1.5−2.5 (pressurized)	Stable low-pO$_2$ operation required	399,426

[a]Quantitative gaps indicate research priorities for achieving lightweight, durable, and efficient hydrogen-electric propulsion in aircraft.

These modified membranes show particular promise for aircraft PEMFCs exposed to dry and hot operating conditions without external humidification systems. Bisht et al.[394] mixed SiO$_2$, sulfonated SiO$_2$, and MOF-5 in a ternary SPEEK-based composite. The result was improved mechanical strength and conductivity, although excessive swelling due to unstable silica crystals was noted. Therefore, the authors concluded that the synthesized ternary hybrid membrane holds promise as a potential membrane material for use in PEMFCs. This is particularly important in aircraft PEMFCs, where high-voltage operation and load cycling can increase ROS formation and accelerate membrane thinning.

7.3.2. Ionic Liquid Incorporation. Vázquez-Fernández et al.[395] introduced ionic liquids such as [Im][Hex] and [EHNH$_2$][H$_2$PO$_4$] into PVDF matrices. These materials boosted Grotthuss conduction and significantly improved hydrophilicity and ion mobility, especially at elevated temperatures, making them highly relevant for flight applications without active humidifiers.

7.3.3. Antioxidant Additives. To suppress chemical degradation caused by reactive oxygen species (ROS), Zheng et al.[396] embedded ferrocyanide-loaded silica particles into sulfonated polysulfone membranes, demonstrating improved radical scavenging and membrane stability. Xu et al.[397] further enhanced antioxidant properties by coating the membrane with a thin polyaniline/CeO$_x$ (PANI/CeO$_x$) layer. Kang et al.[398] developed a sandwich-structured Nafion membrane with ultrathin CeO$_x$ barriers on both sides, effectively balancing improved durability with minimal added resistance. However, it should be noted that excessive CeO$_x$ content can increase interfacial resistance, negatively impacting electrochemical performance. Therefore, the authors emphasize the importance of balancing PEMFC performance with long-term durability. These barrier strategies are critical in PEMFCs for high-altitude aviation, where ROS formation can accelerate under UV and thermal cycling conditions.

The structural alignment of ion channels and reduction of interfacial resistance remain ongoing design priorities.[399,400] Future membranes for crewed aircraft PEMFCs must demonstrate proton conductivities greater than 100 mS/cm under ambient RH < 50%, oxidative durability beyond 30,000 cycles, and minimal hydrogen crossover at operating pressures typical of aviation-grade hydrogen storage.[401,402] Emerging research suggests that membranes incorporating aligned nanofiber scaffolds and amphiphilic domain regulation could

achieve the desired balance of conductivity, stability, and weight for future aviation applications.[403−405]

The role of the PEM in determining stack thickness and energy density is also nontrivial. Aviation fuel cell systems must meet strict packaging constraints—especially in fuselage-integrated or wing-mounted stacks.[47,406] Composite membranes with sub-30 μm thicknesses can significantly reduce stack height and increase volumetric power density.[407,48] In addition, thinner membranes reduce ohmic losses and cooling loads, enabling simpler thermal management architectures.[408,409] However, thinner membranes are more susceptible to mechanical damage and hydrogen crossover, underscoring the need for integrated reinforcement and layered barrier technologies. Membranes below 30 μm also facilitate distributed propulsion designs where packaging constraints and airflow routing are major design bottlenecks.

In summary, while PFSA-based membranes remain dominant, future aviation PEMFCs will increasingly rely on composite and modified membranes that combine high conductivity with structural integrity under aviation-specific environmental stresses. The ongoing development of membranes with tailored nanostructures, embedded antioxidants, and humidity-insensitive transport mechanisms is critical to enabling durable, high-efficiency hydrogen-electric propulsion in aircraft.[169,410]

Quantitative characterization of thin membranes (20−40 μm) under low-humidity and variable-pressure conditions is essential for aviation PEMFCs, where active humidification is limited.[411,412] Reported proton conductivities of 0.05−0.06 S cm^{-1} at 50% RH and 80 °C for standard PFSA membranes (e.g., Nafion 211, Aquivion E79−05S) decrease to ≈0.03 S cm^{-1} at 30% RH, indicating a 30−40% loss in proton transport compared with fully hydrated operation.[413−415] Hydrogen crossover through 20−25 μm films typically ranges from 1.0×10^{-6} to 2.5×10^{-6} mol cm^{-2} s^{-1}, approaching the upper safety limit for stack operation.[416−418] Mechanical puncture and tear resistance values for unreinforced membranes (15−25 MPa tensile strength, elongation ≤ 150%) are generally insufficient for vibration-rich aircraft environments.[419−421]

Reinforcement strategies under investigation include electro-spun nanofiber scaffolds (PVDF, PTFE, or PPS supports), inorganic fillers such as SiO$_2$, ZrP, TiO$_2$, or layered clays to retain water, and hybrid composite architectures (e.g., PFSA + sulfonated poly(ether ketone)) that enhance both strength and water retention.[375,422] These reinforced membranes can sustain >0.07 S cm^{-1} conductivity at 40−50% RH while

Table 11. PEMFC Component-Level Degradation Modes and Mitigation Strategies under Aviation Operating Environments

Component	Aviation-specific failure modes/Stressors	Underlying mechanisms	Mitigation/Design strategies
Bipolar Plates (BPs)	Corrosion under humid, low-pressure cathode	Electrochemical oxidation of metal surfaces	Ultrafine coated metallic BPs (Ti, SS, Al + DLC/TiB$_2$/ZrN)
	Coating delamination due to vibration and thermal cycling	Differential thermal expansion between base and coating	Carbon-polymer composites with graphite/CNT fillers
	Mass penalty from thick coatings	Mechanical fatigue	In situ monitoring of interfacial contact resistance (ICR)
Gas Flow Fields	Water accumulation and local flooding at variable orientations	Gravitational asymmetry, condensation, and low-density airflow	Hybrid serpentine−interdigitated or bioinspired geometries, microgroove drainage, hydrophobic patterning
	Nonuniform air distribution during climb/descent• Pressure drop rise at altitude		Adaptive flow control via aircraft ECS coupling
Gas Diffusion Layers (GDLs)	Water/ice retention during low-T or low-pO$_2$	Freeze−thaw cycling, hydrophobicity loss, carbon oxidation	Graded hydrophobic/hydrophilic microstructure
			Nickel/graphite foams with integrated channels
	Fiber fracture or compression under vibration		Surface coatings (PTFE-treated carbon paper)
	Increased electrical resistance over time		Mechanical reinforcement with woven carbon fabrics
Catalyst Layers (CLs)	Pt dissolution/agglomeration during high-altitude transients	Potential cycling; hydroxyl radical formation; mass transport limitation	Low-Pt or PGM-free catalysts on corrosion-resistant supports (graphitized carbon, TiO$_2$, doped oxides)
	Ionomer degradation (radical attack)		Radical scavengers (CeO$_2$, MnO$_x$)
	ORR kinetic loss at low humidity		Optimized ionomer content and distribution
Membrane (PEM)	Dehydration/cracking under low RH	PFSA chain scission; pressure fluctuations; cycling	Composite membranes with reinforcement (e.g., ePTFE, hydrocarbon blends)
	Oxidative thinning from radicals, hydrogen crossover, and mechanical fatigue		Embedded antioxidant additives self-humidifying designs with hygroscopic fillers (SiO$_2$, ZrP)
Seals and Gaskets	Compression set, leakage under pressure change• Chemical attack by peroxide radicals	Elastomer aging, ozone/oxidant exposure	Fluoroelastomers with peroxide stabilizers
			Precision compression control and redundancy in sealing zones
Stack/System Level	Thermal imbalance between cells	Nonuniform current density and heat generation	Lightweight manifolds with active cooling loops
	Uneven humidification at altitude		Smart balance-of-plant (BOP) control
	Electrical contact loss under vibration		Vibration-isolated mounting and structural damping

reducing crossover by ≈50% relative to neat PFSA.[423] Durability testing shows that mechanical endurance declines approximately exponentially with membrane thinning: a doubling of cycle count (to >20,000 AST cycles) is often achieved when reinforcement layers are introduced.[424] The trade-off between thickness, conductivity, and mechanical stability can be illustrated by conductivity−RH and endurance−cycle count trends reported in refs 399,425−429, which clearly show that sub-30 μm membranes require structural reinforcement to meet aviation reliability targets.

Building on the preceding discussion of membrane and stack component characteristics, Table 10 summarizes the key aviation performance targets and compares them with current state-of-the-art PEMFC metrics reported in the literature. The data illustrate the quantitative shortfalls that must be overcome for viable aviation deployment.

7.4. Cross-Component Degradation Modes and Mitigation Strategies. While Sections 3−7 have examined individual PEMFC stack components, their in-service reliability under aviation environments depends on coupled degradation mechanisms acting across interfaces. Table 11 consolidates major aviation-specific failure modes, underlying physical or chemical mechanisms, and representative mitigation strategies reported in recent studies. The mapping highlights the interdependence of electrochemical, thermal, and mechanical stressors and provides a foundation for durability testing protocols and certification planning.

8. CHALLENGES AND PERSPECTIVES

The integration of PEMFCs into aviation systems represents a pivotal opportunity for decarbonizing short- and medium-range flights. However, aircraft propulsion imposes system-level demands that differ significantly from automotive or stationary fuel cell applications. These system-level differences arise from the unique operational and environmental constraints of aviation. Unlike automotive or stationary systems, aircraft power units must achieve exceptionally high specific power (>2 kW/kg) and volumetric power density (>2 kW/L) under stringent weight and space limits. They must also operate reliably across wide altitude, temperature, and humidity variations where ambient pressure and oxygen partial pressure change substantially, influencing reactant supply and water management. Furthermore, vibration, orientation changes, and limited onboard cooling capacity impose additional challenges on gas and thermal management. In contrast, automotive PEMFCs benefit from near-constant ambient pressure and moderate vibration, while stationary systems prioritize lifetime and efficiency overweight. These distinctions justify a dedicated review of PEMFC technology tailored for aviation applications.

Achieving competitive performance requires that PEMFCs deliver high power-to-weight and power-to-volume ratios, maintain operational stability across altitude profiles, and ensure system durability under mechanical, thermal, and environmental stress. Table 12 outlines key design considerations that require careful attention for aviation applications. The subsections below critically examine these aviation-specific

Table 12. Key Design Aspects for PEMFCs in Aviation

Design challenge	Critical requirements for aviation
Power-to-Weight Ratio	Lightweight, compact stack components; ultrathin bipolar plates
Catalyst Performance	High activity at low Pt loading; long-term durability under cyclic and high-altitude operation
Membrane Reliability	Stable proton conductivity without external humidification; thermal and oxidative resilience
Gas and Water Management	Efficient reactant delivery and water removal via tailored GDL and flow field designs
System Integration	Co-optimization with aircraft structure, airflow, and hybrid energy systems

challenges in the context of PEMFC design and component-level constraints.

8.1. Power Density and Weight Constraints. Aircraft systems impose exceptionally strict mass and volume requirements. Aircraft propulsion systems typically require PEMFC stacks to achieve specific power levels exceeding 2 kW/kg and volumetric power densities of over 2 kW/L, depending on the platform and mission envelope.[90,339,430,431] In comparison, current state-of-the-art PEMFC systems designed for automotive applications deliver around 1−1.5 kW/kg and less than 1 kW/L.[14,399,426] The gap between the available and required performance highlights a central bottleneck in aviation PEMFC development. The bipolar plate[432] remains the most mass-intensive component, often accounting for up to 80% of stack weight.[58,59,339] Efforts to reduce weight focus on ultrathin metallic plates with corrosion-resistant coatings, and the use of carbon-polymer composite BPs with embedded conductive fillers.[63,432−435] Reducing overall stack height is also critical for increasing volumetric power density, especially in fuselage-embedded or wing-integrated PEMFC configurations.[399,436,437] This objective is being addressed through thin membrane technologies, integrated GDL−flow field interfaces, and multifunctional component designs.[438−440] Notably, stacks designed for modular integration in distributed propulsion architectures are constrained by both aerodynamic packaging and thermal management zones,[441] necessitating aggressive power density optimization.

8.2. Catalyst Cost, Activity, and Durability. Catalyst performance plays a central role in determining the PEMFC system efficiency, lifetime, and cost. Aviation applications introduce specific challenges related to catalyst durability under high-load cycling, long-duration missions, and altitude-induced partial pressure variations. While significant progress has been made in developing Pt-alloy catalysts and PGM-free materials, much of the reported activity and stability are demonstrated at the MEA or single-cell level.[284,411,442,443] Translating these results to multikilowatt flight-ready stacks remains an active area of research. Platinum dissolution and nanoparticle agglomeration remain major degradation mechanisms, especially during start−stop cycles, rapid current ramping, and high-potential idling,[444] all of which are common in aviation use-cases such as taxi, takeoff, and descent. Catalyst degradation during start−stop and descent−ascent cycles remains a bottleneck for long-haul aviation platforms, necessitating more resilient support−ionomer interfaces. Durability targets established by several aviation projects exceed 30,000 operational cycles with less than 10% voltage decay.[32,430,445,446] Meeting these targets requires combined advances in Pt utilization efficiency, catalyst−ionomer interface engineering, and support stability, particularly under simulated flight conditions where RH and ambient pressure vary significantly. Furthermore, costs remain a limiting factor. Despite reduced Pt loading strategies (<0.1 mgPt/cm^2), scaling fuel cells for aviation requires economically viable recovery or recycling pathways.[447−449] Research into reclaimable catalyst substrates, in situ degradation monitoring, and end-of-life refurbishing is being explored to meet both economic and environmental sustainability standards for future hydrogen-powered aircraft.[43,47,450−452]

8.3. Membrane Stability and Water Management. PEM must remain chemically and mechanically stable throughout extended flight operations. In contrast to ground-based systems, aviation PEMFCs are often operated with little or no external humidification, especially in UAVs or aircraft using open-cathode designs to reduce system complexity and mass.[375] Traditional PFSA membranes such as Nafion suffer from reduced proton conductivity under low humidity and are prone to oxidative degradation in the presence of ROS.[375,453] In high-altitude or cold-soak scenarios, inadequate hydration can lead to irreversible membrane thinning, gas crossover, and catastrophic voltage drops.[454] This necessitates a move toward reinforced composite membranes that retain conductivity under subsaturated conditions and incorporate radical scavengers, dimensional stabilizers, or humidity-insensitive ionomers. Emerging membrane platforms, including PFSA/ePTFE composites, ionic liquid-enhanced PVDF membranes, and nanofiber-reinforced structures, are showing promise under altitude-simulated PEMFC testing.[455] For instance, GORE-SELECT membranes tested in the Hy4 demonstrator showed stable operation at 60 °C under 20% RH,[456] validating their suitability for high-efficiency aviation stacks. Aircraft also face temperature swings from cold starts (−40 °C) to operational peaks (>80 °C), especially in hybrid electric architectures. Membranes must thus accommodate a broad thermal range, ideally without reliance on active thermal conditioning subsystems. To achieve this, advanced membranes are increasingly being developed with cross-linked domains and amphiphilic block morphologies, which stabilize internal water channels across diverse environmental conditions.[457,458]

8.4. Oxygen and Water Transport in the Cathode. At high current densities and under altitude-simulated conditions, oxygen transport resistance at the cathode becomes a primary performance limiter. Flooding of the gas flow field and GDL, particularly in condensing environments or during throttle transients, can lead to localized oxygen starvation and voltage degradation.[459,460] Many aviation PEMFC prototypes have adopted open-cathode configurations, using the aircraft's forward motion or integrated cooling fans to facilitate airflow.[437,461] While this simplifies system design, it also creates a highly dynamic reactant environment, subject to changing airflow rates, humidity, and external pressure. Under these conditions, cathode performance becomes tightly linked to GDL wettability, flow field orientation, and CL−ionomer microstructure.[355,462] Future systems for crewed aviation, which operate under sealed cabin pressure and require longer duration missions, may need actively pressurized cathode systems or humidifier bypass modules to support consistent oxygen and water transport. In either case, the cathode subsystem must be carefully co-optimized with aircraft aerodynamics, cabin ventilation, and fuel cell packaging to ensure reliable and efficient reactant delivery. Future research directions include: (i) integrated GDL−flow field designs that improve oxygen distribution and minimize parasitic loads; (ii) gradient wettability and pore size control in the GDL to direct water removal passively; and customized flow field orientation aligned with aircraft airflow (e.g., propeller-induced streams) to enhance convective delivery of reactants. While gas channel design may be less critical in UAV-scale PEMFCs, it will likely become essential for multikilowatt stacks used in crewed aircraft, where stack geometry, aircraft layout, and airflow direction must be co-optimized. Cathode designs for aviation must anticipate changes in altitude, angle of attack, and cabin pressure—all of which influence oxygen availability and water removal strategies.

Table 13. Key Technical Challenges for Aviation-Grade PEMFCs

Component	Primary challenge	Aviation-specific impact
Bipolar Plates (BPs)	High mass fraction; corrosion; contact resistance	Limits power-to-weight; affects durability and voltage efficiency
Catalyst Layer (CL)	Pt cost; degradation; mass transport under dynamic load	Reduces system lifetime; increases cost and operational uncertainty
Membrane (PEM)	Humidity dependence; swelling; gas crossover; oxidative damage	Affects conductivity and durability at altitude and under variable RH
GDL and Flow Fields	Flooding; oxygen starvation; uneven gas distribution	Compromises performance in orientation-variable flight regimes
Ionomer Films	Oxygen diffusion resistance; interface wetting	Reduces cathode voltage under low-pressure or high-humidity operation
Supports and Structures	Corrosion, mechanical failure, or cracking under vibration	Threatens reliability during flight, especially in hybrid architectures
System Integration	Trade-offs between cooling, weight, redundancy, and layout	Requires co-optimization with airframe, powertrain, and mission architecture

Table 14. Matrix of Flight-Representative PEMFC Validation Parameters and Corresponding Ranges for the Pressure, Humidity, Temperature, Electrical Loading, and Vibration

Test domain	Parameter range	Purpose/relevance	refs
Pressure cycling	0.5−1.0 bar (altitude 0−10 km)	Simulates cabin/ambient pressure variation	140,302,477,478
Relative humidity cycling	20−90% RH	Evaluates water management robustness	303,373
Temperature cycling	−30 to +80 °C	Captures cold-start and cruise operation	479,480
Electrical load profile	0.1−1.5 A cm^{-2} (takeoff/cruise/idle)	Reproduces mission-phase power demand	52,483−485
Potential cycling (AST)	0.6−1.0 V, 50 mV s^{-1}, ≥5000 cycles	Assesses catalyst/CL degradation	249,443,487
Vibration testing	5−500 Hz, ≤5 g rms (3-axis)	Evaluates mechanical integrity under flight loads	472,474,488,489
Combined testing	Pressure + vibration + thermal	Captures multistress coupling	173,213,490,491
Pass/fail criteria	<10% voltage loss/500 h; ≥90% membrane conductivity retained	Defines durability threshold	492−495

8.5. Trade-Offs in Component Design. PEMFC systems for aviation require careful balancing of competing parameters across all components. For example, increasing membrane thickness may reduce gas crossover but adds to ohmic resistance and stack mass.[463−465] Increasing GDL porosity improves oxygen diffusion but can undermine mechanical integrity under pressure cycling and vibration.[466] Similarly, thicker coatings on metallic BPs improve corrosion resistance but raise interfacial contact resistance, reducing system voltage efficiency.[467,468] These trade-offs are further complicated by aviation-specific considerations, such as emergency safety protocols, redundancy requirements, and volume packaging constraints. Optimization strategies must therefore adopt multiobjective design frameworks, incorporating flight mission profiles, environmental conditions, system-level performance metrics, and regulatory standards. In the context of aircraft operations, trade-offs also occur at the system level. For instance, adopting passive water management may simplify system weight and volume, but risks reduced reliability under variable pitch and yaw.[469,470] Conversely, incorporating humidifiers and active cooling may improve stack robustness but increase parasitic loads and system mass.[50,471] Aircraft-specific PEMFC design must be modular, fault-tolerant, and responsive to platform-specific constraints. Based on the critical issues discussed and analysis presented throughout this review, Table 13 summarizes the key technical challenges associated with aviation-grade PEMFCs.

8.6. Flight-Representative Test Matrix for Aviation PEMFC Validation. Reliable evaluation of aviation fuel cell stacks requires testing protocols that reproduce the coupled electrochemical, thermal, and mechanical stresses encountered in flight.[15,437,472,473] Generic automotive durability tests cannot capture the combined effects of low-pressure operation, rapid load changes, and vibration experienced by airborne systems.[474−476] A dedicated flight-representative test matrix is therefore proposed in Table 14, consolidating procedures recommended in recent aerospace-fuel cell studies,[140,213,214,218,220,221] environmental/altitude and cold-start simulation work,[302] and component-durability analyses relevant to humidity/temperature stress.[303,373]

Pressure and humidity cycling should reflect altitude transitions between sea level and ≈10 km, corresponding to 0.5−1.0 bar absolute pressure and 20−90% RH.[140,302,373,477,478] Temperature should vary between −30 °C and +80 °C, representing ground cold-start and in-flight steady operation.[479−482] Electrical loading must follow a realistic mission profile: takeoff (>1.5 A cm^{-2} for ≤2 min), cruise (0.6−0.8 A cm^{-2} for 1−2 h), and descent/idle (0.1−0.3 A cm^{-2} intermittent), consistent with aircraft-specific operating-window studies and altitude demonstrations.[52,483−485] Combined electrochemical accelerated stress tests (ASTs) should include potential cycling between 0.6 and 1.0 V at 50 mV s^{-1} for ≥5000 cycles and load cycling at 1−2 Hz to emulate transient power demands.[249,443,486,487] Mechanical endurance testing should be conducted in a pressure chamber equipped with triaxial vibration capability, applying frequencies of 5−500 Hz and accelerations up to 5 g rms, representative of airframe/nacelle spectra and consistent with vibration-sensitivity of stack elements, and with coupled condensation/transport behavior under dynamic conditions.[472,474,488,489] Such coupling of vibration, temperature, and pressure variations enables concurrent evaluation of gas-tightness, contact resistance stability, and water management.[173,213,490,491]

Quantitative pass-fail criteria are essential for comparability:

(i) voltage loss <10% at rated power after 500 h combined cycling;

(ii) no leakage or delamination; and

(iii) retention of ≥90% initial membrane proton conductivity.

These limits align with preliminary aerospace-stack specifications.[492−495] Implementing harmonized test conditions will

allow both research institutions and industry to benchmark new designs and accelerate technology readiness for hydrogen-electric aircraft propulsion.

8.7. System-Level Safety and Certification Considerations.

Aviation PEMFC systems must meet stringent airworthiness and safety requirements comparable to those defined by EASA CS-25, FAA Part 33/35, and RTCA DO-160 environmental standards.[496,497] Achieving certification readiness requires systematic identification of potential failure modes and mapping them to detection, isolation, and mitigation strategies,[498−500] ensuring that component-level R&D aligns with regulatory expectations. Primary failure modes include:[173,432,496,499,501,502]

(i) Membrane rupture or pinhole formation, leading to cross-gas leakage or internal shorting;

(ii) Bipolar-plate shorting or coating delamination, causing localized heating and electrical faults;

(iii) Hydrogen leakage from manifolds, valves, or seals;

(iv) Coolant or condensate intrusion into electrical paths; and

(v) Loss of stack electrical isolation under vibration or condensation.

Mitigation strategies incorporate multilayer safety architectures: redundant hydrogen sensors in each compartment (response time <1 s, detection threshold <0.4 vol %), isolation valves actuated automatically upon leak detection, double-sealed fittings, and ventilation ducts ensuring buoyant hydrogen dispersal away from ignition sources.[503−505] BP electrical faults are mitigated by stack-level insulation monitoring, coating QA verification, and fault-tolerant busbar designs. Membrane rupture protection involves differential-pressure sensors across anode/cathode manifolds, with automated purge and stack isolation upon exceeding 10 kPa imbalance.[506−508] Regulatory testing expectations include hydrogen-leak localization and rate quantification (ISO 14687:2025,[509] SAE J2579[510]), electrical isolation resistance under humidity and vibration (RTCA DO-160), fire-propagation and flammability tests for composite BPs and GDLs (CS-25.863) 500, and shock/vibration endurance at 5−500 Hz to demonstrate mechanical integrity (DO-160).[511] Certification evidence will also require failure-mode-and-effects analysis (FMEA), fault-tree analysis, and demonstrated safe venting of hydrogen under worst-case fault conditions.[512]

Integrating these safety and certification requirements at the research stage is critical to avoiding late-stage redesigns. Coordinating laboratory testing and simulation results with the EASA/FAA framework ensures that innovations in membrane, catalyst, and BP design contribute directly to the evidence base needed for aviation qualification and eventual type certification of hydrogen-electric aircraft powertrains.

8.8. Future Research Directions.

Future research should focus on developing aviation-specific PEMFC components that achieve durability targets exceeding 30,000 cycles, with performance degradation under 10% across full flight envelopes. For membranes, emphasis should be placed on materials with high proton conductivity under low humidity and embedded radical scavenging capabilities to resist oxidative thinning. In catalyst layers, the transition toward low-Pt or non-PGM systems must be accompanied by support materials that retain electrical and mechanical integrity under vibrational and thermal stress. Lightweight and highly conductive bipolar plate designs, using novel composites or ultrathin coated metals, remain essential for improving system-specific power.

Furthermore, multifunctional integration—where flow fields, GDLs, and thermal management elements are codesigned—should be explored to reduce component redundancy and increase packing density. Ultimately, flight-representative testing protocols, including altitude chambers, vibration exposure, and accelerated load cycling, are urgently needed to provide reliable lifetime and safety assessments. Collaboration among material scientists, aerospace engineers, and fuel cell developers will be key to realizing the full potential of PEMFCs for clean, efficient, and certifiable hydrogen-powered aviation.

9. CONCLUSIONS

PEMFCs represent one of the most promising zero-emission propulsion technologies for future aviation, especially in the context of short-haul, regional, and unmanned aerial platforms. However, their adaptation from ground-based systems to airborne applications introduces a host of design and performance challenges that require significant reengineering across all components. This review has demonstrated that the key barriers to aviation deployment lie in achieving high power-to-weight and power-to-volume ratios, ensuring long-term operational durability under fluctuating altitude, humidity, and thermal conditions, and optimizing system integration without excessive parasitic mass. Component-level analysis shows that while automotive PEMFC technology provides a foundation, aircraft fuel cells demand tailored solutions: ultralightweight bipolar plates with corrosion-resistant coatings, catalyst layers with maximized Pt utilization and support stability, membranes that maintain conductivity without external humidification, and gas diffusion structures that regulate oxygen and water transport under pressure and orientation changes. Current research is progressively addressing these challenges through the development of multifunctional components, graded material architectures, and integrated flow field GDL systems. Demonstrator platforms such as HY4, Dornier 228, and Airbus ZEROe are validating the feasibility of aviation-adapted PEMFCs, but further material and structural innovations are needed to close the gap between laboratory-scale performance and aerospace system readiness.

■ ASSOCIATED CONTENT

Data Availability Statement

No data is associated with this paper.

■ AUTHOR INFORMATION

Corresponding Author

Mohammad Alnajideen − *College of Physical Sciences and Engineering, Cardiff University, Cardiff CF24 3AA, U.K.;* orcid.org/0000-0001-9408-6893; Email: AlnajideenMI@cardiff.ac.uk

Authors

Yifan Xue − *College of Physical Sciences and Engineering, Cardiff University, Cardiff CF24 3AA, U.K.*

Rukshan Navaratne − *College of Physical Sciences and Engineering, Cardiff University, Cardiff CF24 3AA, U.K.*

Complete contact information is available at:
https://pubs.acs.org/10.1021/acs.energyfuels.5c03463

Author Contributions

Yifan Xue: Writing—original draft, methodology, investigation, formal analysis, data curation, conceptualization. **Mohammad Alnajideen**: Writing—original draft, writing—review and editing, methodology, investigation, formal analysis, visualization, validation, conceptualization, supervision. **Rukshan Navaratne**: Conceptualization, investigation, visualization, validation, supervision, resources, project administration, funding acquisition.

Notes

The authors declare no competing financial interest.

Biographies

Yifan Xue is currently a PhD candidate in Aerospace Engineering at the College of Physical Sciences and Engineering, Cardiff University. He holds a master's degree in Sustainable Energy and Environment from Cardiff University, UK, and a bachelor's degree in chemical engineering from Xiamen University, China. His research focuses on the development of proton exchange membrane (PEM) fuel cells for aviation applications.

Mohammad Alnajideen is the Manager of the Centre of Excellence on Ammonia Technologies at Cardiff University and an EPSRC−UKRI Research Associate, leading innovations in alternative fuels for combustion engine systems. He holds a PhD in Energy Engineering Systems from Cardiff University and is a Chartered Engineer with the IMechE and IET, as well as a member of ASME, IEEE, and InsLM. With over 15 years of experience in renewable energy R&D&I, his expertise spans both academia and industry. He has served as an Assistant Professor and as a Gas Turbine and Balance of Plant Engineer. His work focuses on renewable fuels for net-zero energy solutions and the advancement of sustainable energy systems.

Rukshan Navaratne is a Reader in Power & Propulsion, the Director of Aerospace Centre, and the Director of MSc course in Sustainable Energy & Environment at Cardiff University. With a PhD in Aerospace Engineering from Cranfield University, he brings extensive industry experience as an engineer, project manager, and senior executive. His experimental research focuses on novel propulsion systems, electric machines, and sustainable aviation technologies, advancing concepts from initial design to commercial readiness. Dr Navaratne is a Chartered Engineer and member of IMechE, ASME, and AIAA.

■ ACKNOWLEDGMENTS

■ ABBREVIATIONS

APU:Auxiliary Power Unit
ASR:Area-Specific Resistance
AST:Accelerated Stress Test
BOL:Beginning of Life
BP:Bipolar Plate
CL:Catalyst Layer
CNF:Carbon Nanofiber
CNT:Carbon Nanotube
DOE:Department of Energy (US)
ECSA:Electrochemically Active Surface Area
EOL:End of Life
ePTFE:Expanded PTFE
Fe−N−C:Iron−Nitrogen−Carbon (catalyst class)
FEM:Finite Element Methods
FEP:Fluorinated Ethylene Propylene
GDL:Gas Diffusion Layer
HOR:Hydrogen Oxidation Reaction
ICR:Interfacial Contact Resistance
IEA:International Energy Agency
MA:Mass Activity
MEA:Membrane Electrode Assembly
MOF:Metal−Organic Framework
MPL:Microporous Layer
MPS:Macroporous Substrate
MXene:2D transition metal carbides/nitrides
OCV:Open Circuit Voltage
OMC:Ordered Mesoporous Carbon
ORR:Oxygen Reduction Reaction
PANI:Polyaniline
PEM:Proton Exchange Membrane
PEMFC:Proton Exchange Membrane Fuel Cell
PFSA:Perfluorosulfonic Acid
PGM:Platinum Group Metal
PGM-free:Platinum Group Metal-free
PS-calix:Polystyrene-calix [4] arene-based ionomer
Pt:Platinum
Pt@Core or Pt@Shell:Core−Shell Pt-based catalyst structure
PTFE:Polytetrafluoroethylene
PVDF:Polyvinylidene Fluoride
RH:Relative Humidity
ROS:Reactive Oxygen Species
SA:Specific Activity
SEM:Scanning Electron Microscopy
SiO_2:Silicon Dioxide
SOFC:Solid Oxide Fuel Cell
SPEEK:Sulfonated Poly Ether Ether Ketone
TiN:Titanium Nitride
UAV:Unmanned Aerial Vehicle
XRD:X-ray Diffraction

■ NOMENCLATURE

CO_2:Carbon dioxide
e^-:Electron
$GtCO_2$:Gigatonnes of carbon dioxide
$GtCO_2$-e:Gigatonnes of carbon dioxide equivalent
H^+:Proton
H_2:Hydrogen
H_2O:Water
mA/cm^2:Milliampere per square centimeter
$MtCO_2$:Million tons of carbon dioxide
mW/cm^2:Milliwatt per square centimeter (power density)
$m\Omega\cdot cm^2$:Milliohm square centimeter 70
Mach:Mach number—dimensionless speed ratio
NO_x:Nitrogen oxides
O_2:Oxygen
pO_2:Oxygen Partial Pressure
Re:Reynold number
S/cm:Siemens per centimeter (conductivity)
wt %:Weight percent
μm:Micrometer

■ REFERENCES

(1) Bergero, C.; Gosnell, G.; Gielen, D.; Kang, S.; Bazilian, M.; Davis, S. J. Pathways to net-zero emissions from aviation. *Nat. Sustainability* **2023**, *6* (4), 404−414.

(2) International Energy Agency Aviation https://www.iea.org/energy-system/transport/aviation (02/07/2025).

(3) Gössling, S.; Humpe, A.; Fichert, F.; Creutzig, F. COVID-19 and pathways to low-carbon air transport until 2050. *Environ. Res. Lett.* **2021**, *16* (No. 034063).

(4) Schubert, I.; Sohre, A.; Ströbel, M. The role of lifestyle, quality of life preferences and geographical context in personal air travel. *J. Sustainable Tourism* **2020**, *28* (10), 1519−1550.

(5) Higham, J.; Font, X. Decarbonising academia: Confronting our climate hypocrisy. *J. Sustainable Tourism* **2020**, *28* (1), 1−9.

(6) Avila, D.; Sherry, L.; Thompson, T. Reducing global warming by airline contrail avoidance: A case study of annual benefits for the contiguous United States. *Transp. Res. Interdiscip. Perspect.* **2019**, *2*, No. 100033.

(7) Sui, S.; Wang, X.; Zhou, X.; Su, Y.; Riffat, S.; Liu, C.-j. A comprehensive review of Pt electrocatalysts for the oxygen reduction reaction: Nanostructure, activity, mechanism and carbon support in PEM fuel cells. *J. Mater. Chem. A* **2017**, *5* (5), 1808−1825.

(8) Evro, S.; Oni, B. A.; Tomomewo, O. S. Carbon neutrality and hydrogen energy systems. *Int. J. Hydrogen Energy* **2024**, *78*, 1449−1467.

(9) Gao, J.; Wang, X.; Song, P.; Tian, G.; Ma, C. Review of the backfire occurrences and control strategies for port hydrogen injection internal combustion engines. *Fuel* **2022**, *307*, No. 121553.

(10) Voglar, J.; Teržan, J.; Kroflič, A.; Huš, M.; Likozar, B. Mechanistic modelling of catalytic NOX reduction reactions after hydrogen or ammonia combustion on multiple scales. *Renewable Sustainable Energy Rev.* **2023**, *186*, No. 113666.

(11) Ali, A. B.; Nemah, A. K.; Al Bahadli, Y. A.; Ehsan, k. Principles and performance and types, advantages and disadvantages of fuel cells: A review. *Case Stud. Chem. Environ. Eng.* **2024**, *10*, No. 100920.

(12) Keles, O. K.; Hakyemez, I.; Bagriyanik, M.; Kalenderli, O. A Study on Power System Retrofit for Cessna-172S Aircraft by Using Hydrogen Fuel Cell and Battery Hybrid. *IEEE Access* **2025**, *13*, 6089−6101, DOI: 10.1109/ACCESS.2025.3526633.

(13) Toledo-Carrillo, E. A.; García-Rodríguez, M.; Sánchez-Moren, L. M.; Dutta, J. Decoupled supercapacitive electrolyzer for membrane-free water splitting. *Sci. Adv.* **2024**, *10* (10), No. eadi3180.

(14) Qasem, N. A. A.; Abdulrahman, G. A. A recent comprehensive review of fuel cells: history, types, and applications. *Int. J. Energy Res.* **2024**, *2024* (1), No. 7271748.

(15) Kazula, S.; de Graaf, S.; Enghardt, L. Review of fuel cell technologies and evaluation of their potential and challenges for electrified propulsion systems in commercial aviation. *J. Glob. Power Propulsion Soc.* **2023**, *7*, 43−57.

(16) Seddiq, M.; Alnajideen, M.; Navaratne, R. Thermal Transient Performance of PEM Fuel Cells in Aerospace Applications: A Numerical Study. *Energy Fuels* **2025**, *39*, 7876−7889, DOI: 10.1021/acs.energyfuels.4c04834.

(17) Baroutaji, A.; Wilberforce, T.; Ramadan, M.; Olabi, A. G. Comprehensive investigation on hydrogen and fuel cell technology in the aviation and aerospace sectors. *Renewable Sustainable Energy Rev.* **2019**, *106*, 31−40.

(18) Nicolay, S.; Karpuk, S.; Liu, Y.; Elham, A. Conceptual design and optimization of a general aviation aircraft with fuel cells and hydrogen. *Int. J. Hydrogen Energy* **2021**, *46* (64), 32676−32694.

(19) Ayar, M.; Karakoc, T. H. Decision mechanism between fuel cell types: A case study for small aircraft. *Int. J. Hydrogen Energy* **2023**, *48* (60), 23156−23167.

(20) Peyrani, G.; Marocco, P.; Gandiglio, M.; Biga, R.; Santarelli, M. Solid oxide fuel cells for aviation: A comparative evaluation against alternative propulsion technologies. *eTransportation* **2025**, *24*, No. 100408.

(21) Colpan, C. O.; Kovač, A. *Fuel Cell and Hydrogen Technologies in Aviation*; Springer, 2022.

(22) Huang, K.; Goodenough, J. B. 1 - Introduction to solid oxide fuel cells (SOFCs). In *Solid Oxide Fuel Cell Technology*; Huang, K.; Goodenough, J. B., Eds.; Woodhead Publishing, 2009; pp 1−9.

(23) Singh, L.; Nafees, A.; Dubey, K. *Hydrogen Fuel Cell Hybrid Technology in Aviation: An Overview*; Shukla, A. K.; Sharma, B. P.; Arabkoohsar, A.; Kumar, P., Eds.; Recent Advances in Mechanical Engineering, Singapore, 2023; Springer Nature: Singapore, 2023; pp 803−821.

(24) Fernandes, M. D.; de P Andrade, S. T.; Bistritzki, V. N.; Fonseca, R. M.; Zacarias, L. G.; Gonçalves, H. N. C.; de Castro, A. F.; Domingues, R. Z.; Matencio, T. SOFC-APU systems for aircraft: A review. *Int. J. Hydrogen Energy* **2018**, *43* (33), 16311−16333.

(25) Malik, V.; Srivastava, S.; Bhatnagar, M. K.; Vishnoi, M. Comparative study and analysis between Solid Oxide Fuel Cells (SOFC) and Proton Exchange Membrane (PEM) fuel cell − A review. *Mater. Today: Proc.* **2021**, *47*, 2270−2275.

(26) Intelligent Energy, Boeing to develop fuel cell plane. *Fuel Cells Bulletin* **2003**, *2003*, (7), 2−3.

(27) Airbus Airbus commits to ambitious environmental targets and calls for sector to become Eco-Efficient. https://www.airbus.com/en/newsroom/press-releases/2007-06-airbus-commits-to-ambitious-environmental-targets-and-calls-for (02/07/2025).

(28) Aerospace, G. GKN AEROSPACE LEADS DEVELOPMENT OF GROUND-BREAKING HYDROGEN PROPULSION SYSTEM FOR AIRCRAFT. https://www.gknaerospace.com/en/newsroom/news-releases/2021/gkn-aerospace-leads-development-of-ground-breaking-hydrogen-propulsion-system-for-aircraft2/.

(29) Alcock, C. H2FLY IS READY FOR THE NEXT LEG OF ITS FLIGHT PATH TO HYDROGEN-POWERED COMMERCIAL AVIATION. https://www.futureflight.aero/news-article/2022-02-18/h2fly-ready-next-leg-its-flight-path-hydrogen-powered-commercial-aviation.

(30) Universal Hydrogen Announces $20.5M in Series A Funding to Build and Test Full-Scale Hardware for Hydrogen Commercial Aircraft. https://hydrogen.aero/press-releases/universal-hydrogen-announces-20-5m-in-series-a-funding-to-build-and-test-full-scale-hardware-for-hydrogen-commercial-aircraft/.

(31) Rolls-Royce Power Electronics for Advanced Air Mobility: one step closer to take off. https://www.rolls-royce.com/media/our-stories/discover/2024/power-electronics-for-advanced-air-mobility-one-step-closer-to-take-off.aspx.

(32) Datta, A. *PEM Fuel Cell MODEL for Conceptual Design of Hydrogen eVTOL Aircraft*; NASA Technical Reports Server, 2021.

(33) Stroman, R.; Kellogg, J. C.; Swider-Lyons, K., Testing of a PEM fuel cell system for small UAV propulsion. *Power* **2000**, *60*, (80).

(34) Dudek, M.; Tomczyk, P.; Wygonik, P.; Korkosz, M.; Bogusz, P.; Lis, B. Hybrid Fuel Cell − Battery System as a Main Power Unit for Small Unmanned Aerial Vehicles (UAV). *Int. J. Electrochem. Sci.* **2013**, *8* (6), 8442−8463.

(35) Rhoads, G.; Bradley, T.; Wagner, N.; Taylor, B.; Keen, D. Design and Flight Test Results for a 24 h Fuel Cell Unmanned Aerial Vehicle. In *8th Annual International Energy Conversion Engineering Conference*; American Institute of Aeronautics and Astronautics, 2010.

(36) Ward, T. A.; Jenal, N. Design and Initial Flight Tests of a Hydrogen Fuel Cell Powered Unmanned Air Vehicle (UAV). *ECS Trans.* **2010**, *26* (1), 433.

(37) Erdör Türk, B.; Sarul, M. H.; Çengelci, E.; İyigün Karadağ, Ç.; Boyacı San, F. G.; Kılıç, M.; Okumuş, E.; Yazıcı, S. Integrated Process Control-Power Management System Design and Flight Performance Tests for Fuel Cell Powered Mini-Unmanned Aerial Vehicle. *Energy Technol.* **2021**, *9* (3), No. 2000879.

(38) Lapeña-Rey, N.; Blanco, J. A.; Ferreyra, E.; Lemus, J. L.; Pereira, S.; Serrot, E. A fuel cell powered unmanned aerial vehicle for low altitude surveillance missions. *Int. J. Hydrogen Energy* **2017**, *42* (10), 6926−6940.

(39) ZeroAvia First Breakthrough Flight. https://zeroavia.com/flight-testing/.

(40) Hydrogen, U. First flight of world's largest hydrogen fuel cell airliner. https://hydrogen.aero/timeline/.

(41) Romeo, G.; Borello, F.; Correa, G.; Cestino, E. ENFICA-FC: Design of transport aircraft powered by fuel cell & flight test of zero emission 2-seater aircraft powered by fuel cells fueled by hydrogen. *Int. J. Hydrogen Energy* **2013**, *38* (1), 469–479.

(42) H2FLY H2FLY Sets Hydrogen-Electric Flight World Record. https://www.h2fly.de/2022/04/19/h2fly-accelerates-progress-towards-zero-emission-commercial-flight-8/.

(43) El-Adawy, M.; Hamdy, M.; Khedr, A. M.; Ismael, M. A.; Elserfy, K.; Moral, A.; Nemitallah, M. A. Hydrogen-Powered Aviation: Status and Perspectives. *Energy Fuels* **2025**, *39* (24), 11469–11503, DOI: 10.1021/acs.energyfuels.5c01319.

(44) Staszczyk, K.; Tylingo, R. Bio-Based Proton Exchange Membranes from Chitosan: A Review of Progress and Challenges. *Energy Fuels* **2025**, *39* (28), 13242–13259.

(45) Wani, A. A.; Shaari, N.; Kamarudin, S. K.; Raduwan, N. F.; Yusoff, Y. N.; Khan, A. M.; Yousuf, S.; MNM, A. Critical review on composite-based polymer electrolyte membranes toward fuel cell applications: Progress and perspectives. *Energy Fuels* **2024**, *38* (19), 18169–18193.

(46) Wang, J.; He, H.; Wu, Y.; Yang, C.; Zhang, H.; Zhang, Q.; Li, J.; Cheng, H.; Cai, W. Review on electric resistance in proton exchange membrane fuel cells: advances and outlook. *Energy Fuels* **2024**, *38* (4), 2759–2776.

(47) Adler, E. J.; Martins, J. R. R. A. Hydrogen-powered aircraft: Fundamental concepts, key technologies, and environmental impacts. *Prog. Aerospace Sci.* **2023**, *141*, No. 100922.

(48) Lee, F. C.; Ismail, M. S.; Ingham, D. B.; Hughes, K. J.; Ma, L.; Lyth, S. M.; Pourkashanian, M. Alternative architectures and materials for PEMFC gas diffusion layers: A review and outlook. *Renewable Sustainable Energy Rev.* **2022**, *166*, No. 112640.

(49) Pourrahmani, H.; Siavashi, M.; Yavarinasab, A.; Matian, M.; Chitgar, N.; Wang, L.; Van Herle, J. A review on the long-term performance of proton exchange membrane fuel cells: From degradation modeling to the effects of bipolar plates, sealings, and contaminants. *Energies* **2022**, *15* (14), 5081.

(50) Xu, J.; Zhang, C.; Wan, Z.; Chen, X.; Chan, S. H.; Tu, Z. Progress and perspectives of integrated thermal management systems in PEM fuel cell vehicles: A review. *Renewable Sustainable Energy Rev.* **2022**, *155*, No. 111908.

(51) Pan, Z. F.; An, L.; Wen, C. Y. Recent advances in fuel cells based propulsion systems for unmanned aerial vehicles. *Appl. Energy* **2019**, *240*, 473–485.

(52) Dyantyi, N.; Parsons, A.; Sita, C.; Pasupathi, S. PEMFC for aeronautic applications: A review on the durability aspects. *Open Eng.* **2017**, *7* (1), 287–302.

(53) Alipour MoghadamEsfahani, R.; Vankova, S. K.; Easton, E. B.; Ebralidze, I. I.; Specchia, S. A hybrid Pt/NbO/CNTs catalyst with high activity and durability for oxygen reduction reaction in PEMFC. *Renewable Energy* **2020**, *154*, 913–924.

(54) Li, X.; Sabir, I. Review of bipolar plates in PEM fuel cells: Flow-field designs. *Int. J. Hydrogen Energy* **2005**, *30* (4), 359–371.

(55) Middelman, E.; Kout, W.; Vogelaar, B.; Lenssen, J.; de Waal, E. Bipolar plates for PEM fuel cells. *J. Power Sources* **2003**, *118* (1), 44–46.

(56) Sutharssan, T.; Montalvao, D.; Chen, Y. K.; Wang, W.-C.; Pisac, C.; Elemara, H. A review on prognostics and health monitoring of proton exchange membrane fuel cell. *Renewable Sustainable Energy Rev.* **2017**, *75*, 440–450.

(57) Pelz, P. F.; Leise, P.; Meck, M. Sustainable aircraft design — A review on optimization methods for electric propulsion with derived optimal number of propulsors. *Progr. Aerospace Sci.* **2021**, *123*, No. 100714.

(58) Hu, Q.; Zhang, D.; Fu, H.; Huang, K. Investigation of stamping process of metallic bipolar plates in PEM fuel cell—Numerical simulation and experiments. *Int. J. Hydrogen Energy* **2014**, *39* (25), 13770–13776.

(59) Tsuchiya, H.; Kobayashi, O. Mass production cost of PEM fuel cell by learning curve. *Int. J. Hydrogen Energy* **2004**, *29* (10), 985–990.

(60) Siengchin, S. A review on lightweight materials for defence applications: Present and future developments. *Defence Technol.* **2023**, *24*, 1–17.

(61) Suwaileh, W.; Bicer, Y.; Al Hail, S.; Farooq, S.; Mohamad Yunus, R.; Rosman, N. N.; Karajagi, I. Exploring hydrogen fuel as a sustainable solution for zero-emission aviation: Production, storage, and engine adaptation challenges. *Int. J. Hydrogen Energy* **2025**, *121*, 304–325.

(62) Anderson, T.; Balaban, C. *Hydrogen Research for Spaceport and Space-Based Applications: Fuel Cell Projects*; 2008.

(63) Irshad, H. M.; Shahgaldi, S. Comprehensive review of bipolar plates for proton exchange membrane fuel cells with a focus on materials, processing methods and characteristics. *Int. J. Hydrogen Energy* **2025**, *111*, 462–487.

(64) Leng, Y.; Ming, P.; Yang, D.; Zhang, C. Stainless steel bipolar plates for proton exchange membrane fuel cells: Materials, flow channel design and forming processes. *J. Power Sources* **2020**, *451*, No. 227783.

(65) Planes, E.; Flandin, L.; Alberola, N. Polymer Composites Bipolar Plates for PEMFCs. *Energy Procedia* **2012**, *20*, 311–323.

(66) Mehta, V.; Cooper, J. S. Review and analysis of PEM fuel cell design and manufacturing. *J. Power Sources* **2003**, *114* (1), 32–53.

(67) Hermann, A.; Chaudhuri, T.; Spagnol, P. Bipolar plates for PEM fuel cells: A review. *Int. J. Hydrogen Energy* **2005**, *30* (12), 1297–1302.

(68) Xu, Z.; Qiu, D.; Yi, P.; Peng, L.; Lai, X. Towards mass applications: A review on the challenges and developments in metallic bipolar plates for PEMFC. *Prog. Nat. Sci.: Mater. Int.* **2020**, *30* (6), 815–824.

(69) Tang, A.; Crisci, L.; Bonville, L.; Jankovic, J. An overview of bipolar plates in proton exchange membrane fuel cells. *J. Renewable Sustainable Energy* **2021**, *13* (2), No. 022701.

(70) Asri, N. F.; Husaini, T.; Sulong, A. B.; Majlan, E. H.; Daud, W. R. W. Coating of stainless steel and titanium bipolar plates for anticorrosion in PEMFC: A review. *Int. J. Hydrogen Energy* **2017**, *42* (14), 9135–9148.

(71) Lin, C.-H.; Tsai, S.-Y. An investigation of coated aluminium bipolar plates for PEMFC. *Appl. Energy* **2012**, *100*, 87–92.

(72) Madadi, F.; Rezaeian, A.; Edris, H.; Zhiani, M. Improving performance in PEMFC by applying different coatings to metallic bipolar plates. *Mater. Chem. Phys.* **2019**, *238*, No. 121911.

(73) Bian, H.; Li, C.; Peng, H.; Jiang, L.; Ma, Y.; Gu, J.; Yang, B.; Bin, D.; Tang, S.; Lu, H.; Meng, X. Recent advances in conducting polymer coatings for metal bipolar plates in PEMFC. *Prog. Org. Coat.* **2024**, *192*, No. 108502.

(74) He, R. Y.; Jiang, J.; Wang, R. F.; Yue, Y.; Chen, Y.; Pan, T. J. Anti-corrosion and conductivity of titanium diboride coating on metallic bipolar plates. *Corros. Sci.* **2020**, *170*, No. 108646.

(75) Dur, E.; Cora, Ö. N.; Koç, M. Experimental investigations on the corrosion resistance characteristics of coated metallic bipolar plates for PEMFC. *Int. J. Hydrogen Energy* **2011**, *36* (12), 7162–7173.

(76) Alaefour, I.; Shahgaldi, S.; Zhao, J.; Li, X. Synthesis and Ex-Situ characterizations of diamond-like carbon coatings for metallic bipolar plates in PEM fuel cells. *Int. J. Hydrogen Energy* **2021**, *46* (19), 11059–11070.

(77) Lee, S. H.; Pukha, V. E.; Vinogradov, V. E.; Kakati, N.; Jee, S. H.; Cho, S. B.; Yoon, Y. S. Nanocomposite-carbon coated at low-temperature: A new coating material for metallic bipolar plates of polymer electrolyte membrane fuel cells. *Int. J. Hydrogen Energy* **2013**, *38* (33), 14284–14294.

(78) Yu, L.; Shang, L.; Zhang, G.; Li, X.; Meng, Q. High-performance amorphous carbon films on titanium foils: Toward industrial preparation of coated metallic bipolar plates for proton exchange membrane fuel cells. *Int. J. Hydrogen Energy* **2023**, *48* (87), 34055–34066.

(79) Beck, M.; Riedmüller, K. R.; Liewald, M.; Bertz, A.; Aslan, M. J.; Carl, D. *Investigation on the Influence of Geometric Parameters on the Dimensional Accuracy of High-Precision Embossed Metallic Bipolar Plates*; Liewald, M.; Verl, A.; Bauernhansl, T.; Möhring, H.-C., Eds.;

Production at the Leading Edge of Technology, Cham, 2023; Springer International Publishing: Cham, 2023; pp 427−438.

(80) Wang, H.; Turner, J. A. Reviewing Metallic PEMFC Bipolar Plates. *Fuel Cells* **2010**, *10* (4), 510−519.

(81) Tawfik, H.; Hung, Y.; Mahajan, D. Metal bipolar plates for PEM fuel cell—A review. *J. Power Sources* **2007**, *163* (2), 755−767.

(82) Fu, Y.; Hou, M.; liang, D.; Yan, X.; Fu, Y.; Shao, Z.; Hou, Z.; Ming, P.; Yi, B. The electrical resistance of flexible graphite as flowfield plate in proton exchange membrane fuel cells. *Carbon* **2008**, *46* (1), 19−23.

(83) Wang, H.; Sweikart, M. A.; Turner, J. A. Stainless steel as bipolar plate material for polymer electrolyte membrane fuel cells. *J. Power Sources* **2003**, *115* (2), 243−251.

(84) Jeong, K. I.; Oh, J.; Song, S. A.; Lee, D.; Lee, D. G.; Kim, S. S. A review of composite bipolar plates in proton exchange membrane fuel cells: Electrical properties and gas permeability. *Composite Struct.* **2021**, *262*, No. 113617.

(85) Mathew, C.; Naina Mohamed, S.; Devanathan, L. S. A comprehensive review of current research on various materials used for developing composite bipolar plates in polymer electrolyte membrane fuel cells. *Polym. Compos.* **2022**, *43* (7), 4100−4114.

(86) Chari, C. S.; Hofer, R. R.; McEnerney, B. W.; Arestie, S. M.; Lobbia, R. B.; Marrese-Reading, C. M.; Faber, K. T. Evaluation of Graphite/h-BN Bimaterials for Electric Propulsion. *J. Electric Propulsion* **2025**, *4* (1), No. 31.

(87) Nigar, B.; Dönmez, S.; Çöker, D.; Özerinç, S. Understanding mechanical failure of graphite rocket nozzle throats under thermal stresses. *Aerospace Sci. Technol.* **2021**, *119*, No. 107152.

(88) Hamzat, A. K.; Murad, M. S.; Adediran, I. A.; Asmatulu, E.; Asmatulu, R. Fiber-reinforced composites for aerospace, energy, and marine applications: an insight into failure mechanisms under chemical, thermal, oxidative, and mechanical load conditions. *Adv. Compos. Hybrid Mater.* **2025**, *8* (1), No. 152.

(89) Liu, L. *Model-Based Technology Roadmapping of Sustainable Aviation Technologies*; Massachusetts Institute of Technology, 2023.

(90) Bhatti, W.; Wu, W.; Doyle, F.; Llambrich, J.; Webber, H.; Town, N. *Fuel Cells Roadmap. Report: FZO-PPN-COM-0033*; Aerospace Technology Institute: Cranfield, UK; 2022.

(91) Ross, S.; Pettinato, B.; Scavo-Fulk, S.; Hantz, B.; Supak, K. Future trends. In *Energy Transport Infrastructure for a Decarbonized Economy*; Elsevier, 2025; pp 413−428.

(92) Vroom, M. Preliminary Sizing of Balance-of-Plant Systems for Liquid Hydrogen Fuel Cell-Electric Propulsion in Regional Retrofitted Aircraft. 2025.

(93) Hoogendoorn, J. Fuel Cella and Battery Hybrid System Optimization. Student Theses, TU Delft Aerospace Engineering, 2018.

(94) Wu, J.; Ji, Y. Analysis and Prospects of Key Technologies for Hydrogen-Electric Regional Aircraft. In *China Aeronautical Science and Technology Conference*; Springer, 2023; pp 587−595.

(95) Gollnow, M. Passenger aircraft towards zero emission with hydrogen and fuel cells. In *Deutscher Luft-und Raumfahrtkongress*; Hamburg University of Applied Sciences; Aircraft Design and Systems Group (AERO)*, Hamburg, Germany, 2022.

(96) Corcau, J.-I.; Dinca, L.; Cican, G.; Ionescu, A.; Negru, M.; Bogateanu, R.; Cucu, A.-A. Studies Concerning Electrical Repowering of a Training Airplane Using Hydrogen Fuel Cells. *Aerospace* **2024**, *11* (3), 218.

(97) Hölzen, J. Hydrogen-powered aviation—techno-economics of flying with green liquid hydrogen. 2024.

(98) Airbus The ZEROe demonstrator has arrived - A giant leap towards hydrogen-powered aircraft by 2035. https://www.airbus.com/en/newsroom/stories/2022-02-the-zeroe-demonstrator-has-arrived (02/07/2025).

(99) Ramachandrarao, M.; Khan, S. H.; Abdullah, K. Carbon nanotubes and nanofibers − reinforcement to carbon fiber composites - synthesis, characterizations and applications: A review. *Composites, Part C* **2025**, *16*, No. 100551.

(100) Datta, A. PEM fuel cell model for conceptual design of hydrogen eVTOL aircraft. 2021.

(101) Hu, B.; He, G.; Chang, F.; Yang, H.; Cao, X.; Yin, X. Low filler and highly conductive composite bipolar plates with synergistic segregated structure for enhanced proton exchange membrane fuel cell performance. *Energy* **2022**, *251*, No. 123982.

(102) Rigail-Cedeño, A. F.; Espinoza-Andaluz, M.; Vera, J.; Orellana-Valarezo, M.; Villacis-Balbuca, M. Influence of different carbon materials on electrical properties of epoxy-based composite for bipolar plate applications. *Mater. Today: Proc.* **2020**, *33*, 2003−2007.

(103) Darıcık, F.; Topcu, A.; Aydın, K.; Çelik, S. Carbon nanotube (CNT) modified carbon fiber/epoxy composite plates for the PEM fuel cell bipolar plate application. *Int. J. Hydrogen Energy* **2023**, *48* (3), 1090−1106.

(104) Hu, B.; Chang, F.-L.; Xiang, L.-Y.; He, G.-J.; Cao, X.-W.; Yin, X.-C. High performance polyvinylidene fluoride/graphite/multi-walled carbon nanotubes composite bipolar plate for PEMFC with segregated conductive networks. *Int. J. Hydrogen Energy* **2021**, *46* (50), 25666−25676.

(105) Yao, D.; Zheng, J.; Jin, L.; Meng, X.; Zhan, Z.; Fan, R.; Feng, C.; Ming, P. Effect of surface oxidation on the interfacial and mechanical properties in graphite/epoxy composites composite bipolar plates. *Chin. Chem. Lett.* **2024**, *35*, No. 109382.

(106) Tang, A.; Crisci, L.; Bonville, L.; Jankovic, J. An overview of bipolar plates in proton exchange membrane fuel cells. *J. Renewable Sustainable Energy* **2021**, *13* (2), No. 022701, DOI: 10.1063/5.0031447.

(107) Mishra, S.; Verma, V.; Kishore, V.; Kumar, R. A review of polymeric bipolar plates for proton exchange membrane fuel cells: Materials, fabrication, applications, cost analysis, and current status. *Energy Environ.* **2024**, *35* (8), 4408−4444.

(108) Khalifa, R. E.; Shalaby, A. A.; Špitalský, Z. Toward revolutionizing PEMFC manufacturing for clean energy conversion: a review on the innovative contribution of 3D printing techniques. *Int. J. Adv. Manuf. Technol.* **2024**, *135* (9), 4119−4146.

(109) Müller, M.-V.; Giorgio, M.; Hausmann, P.; Kinlechner, L.; Heinzel, A.; Schwämmlein, J. Investigation of the effect of carbon post- vs pre-coated metallic bipolar plates for PEMFCs − start-up and shut-down. *Int. J. Hydrogen Energy* **2022**, *47* (13), 8532−8548.

(110) Liang, C.-H.; Huang, C.-F.; Tsai, H.-Y. The influence of substrate bias voltages on structure, mechanical properties and anti-corrosion performance of Cr doped diamond-like carbon films deposited by steered cathodic arc evaporation. *Thin Solid Films* **2015**, *597*, 88−96.

(111) Rajak, D. K.; Kumar, A.; Behera, A.; Menezes, P. L. Diamond-like carbon (DLC) coatings: classification, properties, and applications. *Appl. Sci.* **2021**, *11* (10), 4445.

(112) Rahimi-Esbo, M.; Ranjbar, A. A.; Ramiar, A.; Alizadeh, E.; Aghaee, M. Improving PEM fuel cell performance and effective water removal by using a novel gas flow field. *Int. J. Hydrogen Energy* **2016**, *41* (4), 3023−3037.

(113) Xu, S.; Liao, P.; Yang, D.; Li, Z.; Li, B.; Ming, P.; Zhou, X. Liquid water transport in gas flow channels of PEMFCs: A review on numerical simulations and visualization experiments. *Int. J. Hydrogen Energy* **2023**, *48* (27), 10118−10143.

(114) Rajalakshmi, N.; Pandiyan, S.; Dhathathreyan, K. S. Design and development of modular fuel cell stacks for various applications. *Int. J. Hydrogen Energy* **2008**, *33* (1), 449−454.

(115) Viola, N.; Cavini, L.; Liscouët-Hanke, S. Fuel Cell Simulation Model for Aircraft Integration Analysis in Early Design Phases. 2024.

(116) Liu, H.; Li, P.; Juarez-Robles, D.; Wang, K.; Hernandez-Guerrero, A. Experimental Study and Comparison of Various Designs of Gas Flow Fields to PEM Fuel Cells and Cell Stack Performance. *Front. Energy Res.* **2014**, *2*, 2 DOI: 10.3389/fenrg.2014.00002.

(117) Guo, N.; Leu, M. C.; Koylu, U. O. Network based optimization model for pin-type flow field of polymer electrolyte membrane fuel cell. *Int. J. Hydrogen Energy* **2013**, *38* (16), 6750−6761.

(118) Atyabi, S. A.; Afshari, E. Three-dimensional multiphase model of proton exchange membrane fuel cell with honeycomb flow field at the cathode side. *J. Cleaner Prod.* **2019**, *214*, 738−748.

(119) Ghasabehi, M.; Ashrafi, M.; Shams, M. Performance analysis of an innovative parallel flow field design of proton exchange membrane fuel cells using multiphysics simulation. *Fuel* **2021**, *285*, No. 119194.

(120) Atyabi, S. A.; Afshari, E. A numerical multiphase CFD simulation for PEMFC with parallel sinusoidal flow fields. *J. Therm. Anal. Calorim.* **2019**, *135* (3), 1823−1833.

(121) Liu, X.; Guo, H.; Ma, C. Water flooding and two-phase flow in cathode channels of proton exchange membrane fuel cells. *J. Power Sources* **2006**, *156* (2), 267−280.

(122) Cao, Y.; El-Shorbagy, M. A.; Dahari, M.; Cao, D. N.; Din, E. M. T. E.; Huynh, P. H.; Wae-hayee, M. Examining the relationship between gas channel dimensions of a polymer electrolyte membrane fuel cell with two-phase flow dynamics in a flooding situation using the volume of fluid method. *Energy Rep.* **2022**, *8*, 9420−9430.

(123) Kaiser, R.; Ahn, C.-Y.; Lee, S.-Y.; Kim, Y.-H.; Park, J.-C. Numerical analysis of water management and reactant distribution in PEM fuel cells with a convergent 5-channel serpentine flow field for emission-free ships. *Int. J. Naval Architect. Ocean Eng.* **2025**, *17*, No. 100649.

(124) Velisala, V.; Pullagura, G.; Yarramsetty, N.; Vadapalli, S.; Boni, M. K.; Gorantla, K. K. Three-Dimensional CFD Modeling of Serpentine Flow Field Configurations for PEM Fuel Cell Performance. *Arab. J. Sci. Eng.* **2021**, *46* (12), 11687−11700.

(125) Rostami, L.; Haghshenasfard, M.; Sadeghi, M.; Zhiani, M. A 3D CFD model of novel flow channel designs based on the serpentine and the parallel design for performance enhancement of PEMFC. *Energy* **2022**, *258*, No. 124726.

(126) Liu, H. C.; Yang, W. M.; Cheng, L. S.; Tan, J. Numerical Analysis of Different Multi-serpentine Flow Fields for Proton Exchange Membrane Fuel Cells. *Fuel Cells* **2018**, *18* (2), 173−180.

(127) Abdulla, S.; Patnaikuni, V. S. Performance evaluation of Enhanced Cross flow Split Serpentine Flow Field design for higher active area PEM fuel cells. *Int. J. Hydrogen Energy* **2020**, *45* (48), 25970−25984.

(128) Whiteley, M.; Cho, J. I. S.; Rasha, L.; Neville, T.; Millichamp, J.; Luca, R.; Shearing, P. R.; Brett, D. J. L. A novel polymer electrolyte fuel cell flow-field: The through-plane array. *J. Power Sources* **2019**, *442*, No. 227218.

(129) Limjeerajarus, N.; Santiprasertkul, T. Novel hybrid serpentine-interdigitated flow field with multi-inlets and outlets of gas flow channels for PEFC applications. *Int. J. Hydrogen Energy* **2020**, *45* (25), 13601−13611.

(130) Li, N.; Wang, W.; Xu, R.; Zhang, J.; Xu, H. Design of a novel nautilus bionic flow field for proton exchange membrane fuel cell by analyzing performance. *Int. J. Heat Mass Transfer* **2023**, *200*, No. 123517.

(131) Kang, H. C.; Jum, K. M.; Sohn, Y. J. Performance of unit PEM fuel cells with a leaf-vein-simulating flow field-patterned bipolar plate. *Int. J. Hydrogen Energy* **2019**, *44* (43), 24036−24042.

(132) Badduri, S. R.; Srinivasulu, G. N.; Rao, S. S. Influence of bio-inspired flow channel designs on the performance of a PEM fuel cell. *Chin. J. Chem. Eng.* **2020**, *28* (3), 824−831.

(133) Lee, K. I.; Lee, S. W.; Park, M. S.; Chu, C. N. The development of air-breathing proton exchange membrane fuel cell (PEMFC) with a cylindrical configuration. *Int. J. Hydrogen Energy* **2010**, *35* (21), 11844−11854.

(134) Wang, B.; Zhu, J.; Zhong, S.; Liang, W.; Guan, C. Space deployable mechanics: A review of structures and smart driving. *Mater. Des.* **2024**, *237*, No. 112557.

(135) Manso, A. P.; Marzo, F. F.; Mujika, M. G.; Barranco, J.; Lorenzo, A. Numerical analysis of the influence of the channel cross-section aspect ratio on the performance of a PEM fuel cell with serpentine flow field design. *Int. J. Hydrogen Energy* **2011**, *36* (11), 6795−6808.

(136) Kiattamrong, S.; Sripakagorn, A. Effects of the Geometry of the Air Flowfield on the Performance of an Open-Cathode PEMFC − Transient Load Operation. *Energy Procedia* **2015**, *79*, 612−619.

(137) Wang, X.-D.; Duan, Y.-Y.; Yan, W.-M.; Lee, D.-J.; Su, A.; Chi, P.-H. Channel aspect ratio effect for serpentine proton exchange membrane fuel cell: Role of sub-rib convection. *J. Power Sources* **2009**, *193* (2), 684−690.

(138) Kahraman, H.; Orhan, M. F. Flow field bipolar plates in a proton exchange membrane fuel cell: Analysis & modeling. *Energy Convers. Manage.* **2017**, *133*, 363−384.

(139) Zhang, G.; Duan, F.; Qu, Z.; Bai, H.; Zhang, J. Airfoil flow field for proton exchange membrane fuel cells enhancing mass transfer with low pressure drop. *Int. J. Heat Mass Transfer* **2024**, *225*, No. 125420.

(140) Willich, C.; Frank, D.; Graf, T.; Wazlawik, S.; Brandao, S.; Bauer, C. High-Altitude Operation of a Commercial 100 kW PEM Fuel Cell System. *Energies* **2024**, *17* (24), No. 19961073.

(141) Wei, L.; Zhu, X.; Wang, X.; Hu, Z.; Wang, M. Research on the coordinated control of oxygen excess ratio and air pressure for PEMFC's air supply system. *Int. J. Hydrogen Energy* **2024**, *69*, 122−133.

(142) Parlak, M.; Özsunar, A.; Koşar, A. High aspect ratio microchannel heat sink optimization under thermally developing flow conditions based on minimum power consumption. *Appl. Ther. Eng.* **2022**, *201*, No. 117700.

(143) Zhou, Y.; Chen, B. Investigation of optimization and evaluation criteria for flow field in proton exchange membrane fuel cell: A critical review. *Renewable Sustainable Energy Rev.* **2023**, *185*, No. 113584.

(144) Bunyan, S. T.; Dhahad, H. A.; Khudhur, D. S.; Yusaf, T. The effect of flow field design parameters on the performance of PEMFC: A review. *Sustainability* **2023**, *15* (13), 10389.

(145) Wan, Z.; Pan, D.; Zhu, X.; Chen, Y.; Huang, T.; Wang, X. Numerical study on the performance of a novel three-dimensional stepped wavy flow field in PEMFC. *Energy Convers. Manage.: X* **2023**, *20*, No. 100469.

(146) Zhu, K.-Q.; Ding, Q.; Zhang, B.-X.; Xu, J.-H.; Yang, Y.-R.; Lee, D.-J.; Wan, Z.-M.; Wang, X.-D. An integrated experimental and numerical investigation of performance and heat-mass transport dynamics in air-cooled PEMFCs with a bamboo-shaped flow field design. *Appl. Energy* **2025**, *377*, No. 124484.

(147) Mohammedi, A.; Sahli, Y.; Ben Moussa, H. 3D investigation of the channel cross-section configuration effect on the power delivered by PEMFCs with straight channels. *Fuel* **2020**, *263*, No. 116713.

(148) Chen, X.; Yu, Z.; Yang, C.; Chen, Y.; Jin, C.; Ding, Y.; Li, W.; Wan, Z. Performance investigation on a novel 3D wave flow channel design for PEMFC. *Int. J. Hydrogen Energy* **2021**, *46* (19), 11127−11139.

(149) Lei, J.; Zhao, S.; Liu, Y.; Deng, X.; Song, G.; Peng, H. Effect of cathode channel structure on the performance of open-cathode proton exchange membrane fuel cell in dry environments. *Energy Rep.* **2023**, *9*, 3022−3034.

(150) Jin, H.; Zou, S.; Wen, Q.; Li, Y.; Ning, F.; Xu, P.; Pan, S.; Zhou, X. Performance improvement of air-breathing proton exchange membrane fuel cell (PEMFC) with a condensing-tower-like curved flow field. *Chin. Chem. Lett.* **2023**, *34* (4), No. 107441.

(151) Fan, L.; Niu, Z.; Zhang, G.; Jiao, K. Optimization design of the cathode flow channel for proton exchange membrane fuel cells. *Energy Convers. Manage.* **2018**, *171*, 1813−1821.

(152) Ghanbarian, A.; Kermani, M. J. Enhancement of PEM fuel cell performance by flow channel indentation. *Energy Convers. Manage.* **2016**, *110*, 356−366.

(153) Cai, Y.; Wu, D.; Sun, J.; Chen, B. The effect of cathode channel blockages on the enhanced mass transfer and performance of PEMFC. *Energy* **2021**, *222*, No. 119951.

(154) Shen, J.; Tu, Z.; Chan, S. H. Enhancement of mass transfer in a proton exchange membrane fuel cell with blockage in the flow channel. *Appl. Ther. Eng.* **2019**, *149*, 1408−1418.

(155) Heidary, H.; Kermani, M. J.; Advani, S. G.; Prasad, A. K. Experimental investigation of in-line and staggered blockages in parallel flowfield channels of PEM fuel cells. *Int. J. Hydrogen Energy* **2016**, *41* (16), 6885−6893.

(156) Perng, S.-W.; Wu, H.-W. A three-dimensional numerical investigation of trapezoid baffles effect on non-isothermal reactant transport and cell net power in a PEMFC. *Appl. Energy* **2015**, *143*, 81−95.

(157) Dong, P.; Xie, G.; Ni, M. The mass transfer characteristics and energy improvement with various partially blocked flow channels in a PEM fuel cell. *Energy* **2020**, *206*, No. 117977.

(158) Chen, Z.; Zuo, W.; Zhou, K.; Li, Q.; Yi, Z.; Huang, Y. Numerical investigation on the performance enhancement of PEMFC with gradient sinusoidal-wave fins in cathode channel. *Energy* **2024**, *288*, No. 129894.

(159) Zhang, S.-y.; Qu, Z.-g.; Xu, H.-t.; Talkhoncheh, F.-K.; Liu, S.; Gao, Q. A numerical study on the performance of PEMFC with wedge-shaped fins in the cathode channel. *Int. J. Hydrogen Energy* **2021**, *46* (54), 27700−27708.

(160) Ijaodola, O.; El-Hassan, Z.; Ogungbemi, E.; Khatib, F.; Wilberforce, T.; Thompson, J.; Olabi, A. Energy efficiency improvements by investigating the water flooding management on proton exchange membrane fuel cell (PEMFC). *Energy* **2019**, *179*, 246−267.

(161) Li, Z.; Wang, S.; Li, W.; Zhu, T.; Fan, Z.; Xie, X. Droplet dynamics in a proton exchange membrane fuel cell flow field design with 3D geometry. *Int. J. Hydrogen Energy* **2021**, *46* (31), 16693−16707.

(162) Dudek, M.; Lis, B.; Raźniak, A.; Krauz, M.; Kawalec, M. Selected aspects of designing modular PEMFC stacks as power sources for unmanned aerial vehicles. *Appl. Sci.* **2021**, *11* (2), 675.

(163) De Wagter, C.; Remes, B.; Smeur, E.; van Tienen, F.; Ruijsink, R.; van Hecke, K.; van der Horst, E. The NederDrone: A hybrid lift, hybrid energy hydrogen UAV. *Int. J. Hydrogen Energy* **2021**, *46* (29), 16003−16018.

(164) Mus, J.; Madhav, D.; Vanierschot, M.; Vandeginste, V.; Buysschaert, F. A review of the impact of ambient conditions and degradation in hybrid fuel cell powered unmanned aerial vehicles. *J. Power Sources* **2024**, *624*, No. 235571.

(165) Turan, C.; Cora, Ö. N.; Koç, M. Contact resistance characteristics of coated metallic bipolar plates for PEM fuel cells − investigations on the effect of manufacturing. *Int. J. Hydrogen Energy* **2012**, *37* (23), 18187−18204.

(166) Hinds, G. Performance and durability of PEM fuel cells: a review. 2004.

(167) Oladoye, A. M. Design and characterisation of metallic bipolar plates for proton exchange membrane fuel cells; Dublin City University2016.

(168) He, C.; Wen, Q.; Ning, F.; Shen, M.; He, L.; Li, Y.; Tian, B.; Pan, S.; Dan, X.; Li, W.; et al. A new integrated GDL with wavy channel and tunneled rib for high power density PEMFC at low back pressure and wide humidity. *Adv. Sci.* **2023**, *10* (28), No. 2302928.

(169) Wang, C. R.; Stansberry, J. M.; Mukundan, R.; Chang, H.-M. J.; Kulkarni, D.; Park, A. M.; Plymill, A. B.; Firas, N. M.; Liu, C. P.; Lang, J. T.; et al. Proton Exchange Membrane (PEM) Water Electrolysis: Cell-Level Considerations for Gigawatt-Scale Deployment. *Chem. Rev.* **2025**, *125* (3), 1257−1302, DOI: 10.1021/acs.chemrev.3c00904.

(170) Dhakate, S. R.; Mathur, R. B.; Kakati, B. K.; Dhami, T. L. Properties of graphite-composite bipolar plate prepared by compression molding technique for PEM fuel cell. *Int. J. Hydrogen Energy* **2007**, *32* (17), 4537−4543.

(171) Kumar, R.; Subramanian, K. A. Performance enhancement of hydrogen PEM fuel cell using graphene coated graphite electrodes. *Process Saf. Environ. Protect.* **2024**, *190*, 48−59.

(172) Yuan, X.-Z.; Nayoze-Coynel, C.; Shaigan, N.; Fisher, D.; Zhao, N.; Zamel, N.; Gazdzicki, P.; Ulsh, M.; Friedrich, K. A.; Girard, F.; Groos, U. A review of functions, attributes, properties and measurements for the quality control of proton exchange membrane fuel cell components. *J. Power Sources* **2021**, *491*, No. 229540.

(173) Liu, Z.; Cai, S.; Tu, Z.; Chan, S. H. Recent development in degradation mechanisms of proton exchange membrane fuel cells for vehicle applications: problems, progress, and perspectives. *Energy Storage Saving* **2024**, *3* (2), 106−152.

(174) Orsi, A.; Kongstein, O. E.; Hamilton, P. J.; Oedegaard, A.; Svenum, I. H.; Cooke, K. An investigation of the typical corrosion parameters used to test polymer electrolyte fuel cell bipolar plate coatings, with titanium nitride coated stainless steel as a case study. *J. Power Sources* **2015**, *285*, 530−537.

(175) Xu, R.; Zhu, Y.; Zhu, R.; Li, M. Corrosion Resistance and Surface Conductivity of 446 Stainless Steel with Electrochemical Cr-Enrichment and Nitridation for Proton Exchange Membrane Fuel Cell (PEMFC) Bipolar Plates. *Metals* **2025**, *15* (5), 566.

(176) Porstmann, S.; Wannemacher, T.; Drossel, W. G. A comprehensive comparison of state-of-the-art manufacturing methods for fuel cell bipolar plates including anticipated future industry trends. *J. Manuf. Process.* **2020**, *60*, 366−383.

(177) Yoo, H.; Kwon, O.; Kim, J.; Cha, H.; Kim, H.; Choi, H.; Jeong, S.; Lee, Y. J.; Kim, B.; Jang, G. E.; Koh, J.-S.; Cho, G. Y.; Park, T. 3D-printed flexible flow-field plates for bendable polymer electrolyte membrane fuel cells. *J. Power Sources* **2022**, *532*, No. 231273.

(178) Li, X.; Yao, Y.; Tian, Y.; Jia, J.; Ma, W.; Yan, X.; Liang, J. Recent advances in key components of proton exchange membrane water electrolysers. *Mater. Chem. Front.* **2024**, *8* (13), 2493−2510.

(179) Ferreira, R. B.; Santos, D. F. M.; Pinto, A. M. F. R.; Falcão, D. S. Development and testing of a PEM fuel cell stack envisioning unmanned aerial vehicles applications. *Int. J. Hydrogen Energy* **2024**, *51*, 1345−1353.

(180) Shen, Z.; Liu, S.; Zhu, W.; Ren, D.; Xu, Q.; Feng, Y. A Review on Key Technologies and Developments of Hydrogen Fuel Cell Multi-Rotor Drones. *Energies* **2024**, *17* (16), 4193.

(181) Kwon, O.; Park, J.; Park, G.; Yang, S.; Park, T. Current progress of carbon nanotubes applied to proton exchange membrane fuel cells: a comprehensive review. *Int. J. Precis. Eng. Manuf.-Green Technol.* **2024**, *11* (2), 659−684.

(182) Kim, J.; Kim, H.; Song, H.; Kim, D.; Kim, G. H.; Im, D.; Jeong, Y.; Park, T. Carbon nanotube sheet as a microporous layer for proton exchange membrane fuel cells. *Energy* **2021**, *227*, No. 120459.

(183) Wei, J.; Ning, F.; Bai, C.; Zhang, T.; Lu, G.; Wang, H.; Li, Y.; Shen, Y.; Fu, X.; Li, Q.; Jin, H.; Zhou, X. An ultra-thin, flexible, low-cost and scalable gas diffusion layer composed of carbon nanotubes for high-performance fuel cells. *J. Mater. Chem. A* **2020**, *8* (12), 5986−5994.

(184) Lee, F. C.; Ismail, M. S.; Zhang, K.; Ingham, D. B.; Aldakheel, F.; Hughes, K. J.; Ma, L.; El-Kharouf, A.; Pourkashanian, M. Optimisation and characterisation of graphene-based microporous layers for polymer electrolyte membrane fuel cells. *Int. J. Hydrogen Energy* **2024**, *51*, 1311−1325.

(185) Okereke, I. *Novel gas diffusion layers for proton exchange membrane fuel cells*; University of Sheffield, 2022.

(186) Athanasaki, G.; Jayakumar, A.; Kannan, A. M. Gas diffusion layers for PEM fuel cells: Materials, properties and manufacturing − A review. *Int. J. Hydrogen Energy* **2023**, *48* (6), 2294−2313.

(187) Balakrishnan, M.; Shrestha, P.; Ge, N.; Lee, C.; Fahy, K. F.; Zeis, R.; Schulz, V. P.; Hatton, B. D.; Bazylak, A. Designing Tailored Gas Diffusion Layers with Pore Size Gradients via Electrospinning for Polymer Electrolyte Membrane Fuel Cells. *ACS Appl. Energy Mater.* **2020**, *3* (3), 2695−2707.

(188) Chen, T.; Liu, S.; Zhang, J.; Tang, M. Study on the characteristics of GDL with different PTFE content and its effect on the performance of PEMFC. *Int. J. Heat Mass Transfer* **2019**, *128*, 1168−1174.

(189) Sadeghifar, H.; Djilali, N.; Bahrami, M. Effect of Polytetrafluoroethylene (PTFE) and micro porous layer (MPL) on thermal conductivity of fuel cell gas diffusion layers: Modeling and experiments. *J. Power Sources* **2014**, *248*, 632−641.

(190) Park, G.-G.; Sohn, Y.-J.; Yang, T.-H.; Yoon, Y.-G.; Lee, W.-Y.; Kim, C.-S. Effect of PTFE contents in the gas diffusion media on the performance of PEMFC. *J. Power Sources* **2004**, *131* (1), 182−187.

(191) Cho, J.; Kim, D.; Yi, J. S.; Park, S. Microarchitecture of polyvinylidene fluoride-bound self-standing microporous layer and its implication to water management in fuel cells. *J. Power Sources* **2021**, *506*, No. 230129.

(192) Bottino, A.; Capannelli, G.; Comite, A.; Costa, C.; Ong, A. L. Microporous layers based on poly(vinylidene fluoride) and sulfonated poly(vinylidene fluoride). *Int. J. Hydrogen Energy* **2015**, *40* (42), 14690−14698.

(193) Latorrata, S.; Balzarotti, R.; Gallo Stampino, P.; Cristiani, C.; Dotelli, G.; Guilizzoni, M. Design of properties and performances of innovative gas diffusion media for polymer electrolyte membrane fuel cells. *Prog. Org. Coat.* **2015**, *78*, 517−525.

(194) Park, S. B.; Park, Y.-i. Fabrication of gas diffusion layer (GDL) containing microporous layer using flourinated ethylene prophylene (FEP) for proton exchange membrane fuel cell (PEMFC). *Int. J. Precis. Eng. Manuf.* **2012**, *13* (7), 1145−1151.

(195) Guan, R.; Shrestha, P.; Lee, J. K.; Bazylak, A. Determining local transport properties of gas diffusion layer land-channel regions via pore network modelling. *J. Power Sources* **2023**, *562*, No. 232770.

(196) Zhang, P.; Li, Y.; Lv, X.; Zhou, Z.; Wu, W.-T.; Wei, L.; Hu, C.; Lyu, J.; Li, Y.; Song, Y. Study of liquid water dynamics in Zoned PEMFC GDLs with different wettability. *Fuel* **2025**, *394*, No. 135171.

(197) Niu, Z.; Wu, J.; Bao, Z.; Wang, Y.; Yin, Y.; Jiao, K. Two-phase flow and oxygen transport in the perforated gas diffusion layer of proton exchange membrane fuel cell. *Int. J. Heat Mass Transfer* **2019**, *139*, 58−68.

(198) Nishida, K.; Murakami, T.; Tsushima, S.; Hirai, S. Measurement of liquid water content in cathode gas diffusion electrode of polymer electrolyte fuel cell. *J. Power Sources* **2010**, *195* (11), 3365−3373.

(199) Yin, B.; Xu, S.; Yang, S.; Dong, F. Influence of Microelliptical Groove Gas Diffusion Layer (GDL) on Transport Behavior of Proton Exchange Membrane Fuel Cell (PEMFC). *Int. J. Heat Mass Transfer* **2021**, *180*, No. 121793.

(200) Wang, P.; Nakajima, H.; Kitahara, T. Hydrophilic and Hydrophobic Composite Microporous Layer Coated Gas Diffusion Layers for Performance Enhancement of Polymer Electrolyte Fuel Cells. *J. Electrochem. Soc.* **2024**, *171* (1), No. 014501.

(201) Forner-Cuenca, A.; Biesdorf, J.; Gubler, L.; Kristiansen, P. M.; Schmidt, T. J.; Boillat, P. Engineered Water Highways in Fuel Cells: Radiation Grafting of Gas Diffusion Layers. *Adv. Mater.* **2015**, *27* (41), 6317−6322.

(202) Lin, G.; Liu, S.; Yu, B.; Wang, H.; Yu, K.; Hu, Y. Preparation of graded microporous layers for enhanced water management in fuel cells. *J. Appl. Polym. Sci.* **2020**, *137* (47), No. 49564.

(203) Wang, X.; Wu, G.-P. Graded Structure Design of the Microporous Layer for Improving the Mass Transfer Performance of Proton-Exchange Membrane Fuel Cells. *ACS Sustainable Chem. Eng.* **2024**, *12* (17), 6596−6605.

(204) Wang, Y.; Wang, X.; Qin, Y.; Zhang, L.; Wang, Y. Three-dimensional numerical study of a cathode gas diffusion layer with a through/in plane synergetic gradient porosity distribution for PEM fuel cells. *Int. J. Heat Mass Transfer* **2022**, *188*, No. 122661.

(205) Netwall, C. J.; Gould, B. D.; Rodgers, J. A.; Nasello, N. J.; Swider-Lyons, K. E. Decreasing contact resistance in proton-exchange membrane fuel cells with metal bipolar plates. *J. Power Sources* **2013**, *227*, 137−144.

(206) Park, J. E.; Lim, J.; Lim, M. S.; Kim, S.; Kim, O.-H.; Lee, D. W.; Lee, J. H.; Cho, Y.-H.; Sung, Y.-E. Gas diffusion layer/flow-field unified membrane-electrode assembly in fuel cell using graphene foam. *Electrochim. Acta* **2019**, *323*, No. 134808.

(207) Zhang, Y.; Tao, Y.; Ren, H.; Wu, M.; Li, G.; Wan, Z.; Shao, J. A metallic gas diffusion layer and porous media flow field for proton exchange membrane fuel cells. *J. Power Sources* **2022**, *543*, No. 231847.

(208) He, C.; Wen, Q.; Ning, F.; Shen, M.; He, L.; Tian, B.; Li, W.; Xu, L.; Liu, Y.; Dan, X.; Chai, Z.; Zou, S.; Zhou, X. A Highly Integrated Component with Tri-Part Significantly Enhances Fuel Cell Power Density by Reducing Mass Transfer Resistance and Excellent Humidity Tolerance. *Adv. Funct. Mater.* **2024**, *34*, No. 2401261.

(209) Jo, A.; Ahn, S.; Oh, K.; Kim, W.; Ju, H. Effects of metal foam properties on flow and water distribution in polymer electrolyte fuel cells (PEFCs). *Int. J. Hydrogen Energy* **2018**, *43* (30), 14034−14046.

(210) Jahanbakhsh, M. Advances in Fuel Cell Stack Level Correlations and Formulations: A Review of Recent Research. Available at SSRN 5249582 2025 DOI: 10.2139/ssrn.5249582.

(211) Hintermayr, D.; Kazula, S. Design and Analysis of the Air Inlet System for Fuel Cell-powered Electric Propulsion Systems in Regional Aviation. 2023.

(212) Chakravarthula, V. A.; Roberts, R. A. Transient analysis of an innovative cycle integrating a sofc and a turbogenerator for electric propulsion. In *Turbo expo: power for land, sea, and air*; American Society of Mechanical Engineers, 2017V003T06A029.

(213) Benkovic, D.; Fink, C.; Iranzo, A. Qualitative and quantitative determination of liquid water distribution in a PEM fuel cell. *Int. J. Hydrogen Energy* **2024**, *52*, 1360−1370.

(214) Schmitz, M.; Matthiesen, F.; Dirkes, S.; Pischinger, S. Predicting Liquid Water Condensation in PEM Fuel Cells by Coupling CFD with 1D Models. *Energies* **2024**, *17* (5), 1259.

(215) Gao, W.; Li, Q.; Sun, K.; Chen, R.; Che, Z.; Wang, T. Mass transfer and water management in proton exchange membrane fuel cells with a composite foam-rib flow field. *Int. J. Heat Mass Transfer* **2023**, *216*, No. 124595.

(216) Guo, H.; Zhao, Q.; Ye, F. An experimental study on gas and liquid two-phase flow in orientated-type flow channels of proton exchange membrane fuel cells by using a side-view method. *Renewable Energy* **2022**, *188*, 603−618.

(217) Kim, J. H.; Kim, W. T. Numerical investigation of gas-liquid two-phase flow inside PEMFC gas channels with rectangular and trapezoidal cross sections. *Energies* **2018**, *11* (6), 1403.

(218) Edwards, H.; Pereira, M. P.; Gharaie, S.; Omrani, R.; Shabani, B. Computational fluid dynamics modelling of proton exchange membrane fuel cells: Accuracy and time efficiency. *Int. J. Hydrogen Energy* **2024**, *50*, 682−710.

(219) Park, J.; Li, X.; Tran, D.; Abdel-Baset, T.; Hussey, D. S.; Jacobson, D. L.; Arif, M. Neutron imaging investigation of liquid water distribution in and the performance of a PEM fuel cell. *Int. J. Hydrogen Energy* **2008**, *33* (13), 3373−3384.

(220) Sławiński, D.; Bykuć, S.; Gliński, M.; Chaja, P. Numerical studies on Vibro-creep of PEM fuel cell elements used in mobile applications. *Int. J. Hydrogen Energy* **2023**, *48* (78), 30570−30584.

(221) Schröder, M.; Becker, F.; Kallo, J.; Gentner, C. Optimal operating conditions of PEM fuel cells in commercial aircraft. *Int. J. Hydrogen Energy* **2021**, *46* (66), 33218−33240.

(222) Schmelcher, M.; Häßy, J. Hydrogen fuel cells for aviation? A potential analysis comparing different thrust categories. In *International Society of Air Breathing Engines, Proceedings*, 2022.

(223) Boehm, R. C.; Yang, Z.; Bell, D. C.; Faulhaber, C.; Mayhew, E.; Bauder, U.; Eckel, G.; Heyne, J. S. Perspective on Fuel Property Blending Rules for Design and Qualification of Aviation Fuels: A Review. *Energy Fuels* **2024**, *38* (18), 17128−17145.

(224) Schmidtchen, U.; Behrend, E.; Pohl, H.-W.; Rostek, N. Hydrogen aircraft and airport safety. *Renewable Sustainable Energy Rev.* **1997**, *1* (4), 239−269.

(225) Lu, Y.; Li, S.-A.; Qi, R. Review of ionomers in catalyst layers of proton exchange membrane (PEM) modules: key parameters, characterization and manipulation methods. *Int. J. Green Energy* **2024**, *21* (12), 2872−2897.

(226) Deng, X.; Huang, C.; Pei, X.; Hu, B.; Zhou, W. Recent progresses and remaining issues on the ultrathin catalyst layer design strategy for high-performance proton exchange membrane fuel cell with further reduced Pt loadings: a review. *Int. J. Hydrogen Energy* **2022**, *47* (3), 1529−1542.

(227) Robert, M. Impact of degradation and aging on properties of PFSA membranes for fuel cells/Impact des dégradations et du vieillissement sur les propriétés des membranes PFSA pour piles à combustible. 2021.

(228) Hou, J.; Yang, M.; Ke, C.; Wei, G.; Priest, C.; Qiao, Z.; Wu, G.; Zhang, J. Platinum-group-metal catalysts for proton exchange membrane fuel cells: From catalyst design to electrode structure optimization. *EnergyChem* 2020, *2* (1), No. 100023.

(229) Wei, Z. D.; Ran, H. B.; Liu, X. A.; Liu, Y.; Sun, C. X.; Chan, S. H.; Shen, P. K. Numerical analysis of Pt utilization in PEMFC catalyst layer using random cluster model. *Electrochim. Acta* 2006, *51* (15), 3091−3096.

(230) Zhang, J.; Cao, P.; Xu, L.; Wang, Y. Modeling nanostructured catalyst layer in PEMFC and catalyst utilization. *Front. Chem. Sci. Eng.* 2011, *5* (3), 297−302.

(231) Gasteiger, H. A.; Kocha, S. S.; Sompalli, B.; Wagner, F. T. Activity benchmarks and requirements for Pt, Pt-alloy, and non-Pt oxygen reduction catalysts for PEMFCs. *Appl. Catal., B* 2005, *56* (1), 9−35.

(232) Wang, K.; Chen, H.; Zhang, X.; Tong, Y.; Song, S.; Tsiakaras, P.; Wang, Y. Iron oxide@graphitic carbon core-shell nanoparticles embedded in ordered mesoporous N-doped carbon matrix as an efficient cathode catalyst for PEMFC. *Appl. Catal., B* 2020, *264*, No. 118468.

(233) Martinaiou, I.; Monteverde Videla, A. H. A.; Weidler, N.; Kübler, M.; Wallace, W. D. Z.; Paul, S.; Wagner, S.; Shahraei, A.; Stark, R. W.; Specchia, S.; Kramm, U. I. Activity and degradation study of an Fe-N-C catalyst for ORR in Direct Methanol Fuel Cell (DMFC). *Appl. Catal., B* 2020, *262*, No. 118217.

(234) Luo, J.; Qiao, X.; Jin, J.; Tian, X.; Fan, H.; Yu, D.; Wang, W.; Liao, S.; Yu, N.; Deng, Y. A strategy to unlock the potential of CrN as a highly active oxygen reduction reaction catalyst. *J. Mater. Chem. A* 2020, *8* (17), 8575−8585.

(235) Ren, G.; Lu, X.; Li, Y.; Zhu, Y.; Dai, L.; Jiang, L. Porous Core−Shell Fe3C Embedded N-doped Carbon Nanofibers as an Effective Electrocatalysts for Oxygen Reduction Reaction. *ACS Appl. Mater. Interfaces* 2016, *8* (6), 4118−4125.

(236) Illathvalappil, R.; Kurungot, S. Co9S8 Nanoparticle-Supported Nitrogen-doped Carbon as a Robust Catalyst for Oxygen Reduction Reaction in Both Acidic and Alkaline Conditions. *ChemElectroChem* 2020, *7* (14), 3123−3134.

(237) Zhang, X.; Truong-Phuoc, L.; Asset, T.; Pronkin, S.; Pham-Huu, C. Are Fe−N−C Electrocatalysts an Alternative to Pt-Based Electrocatalysts for the Next Generation of Proton Exchange Membrane Fuel Cells? *ACS Catal.* 2022, *12* (22), 13853−13875.

(238) Ma, Q.; Jin, H.; Zhu, J.; Li, Z.; Xu, H.; Liu, B.; Zhang, Z.; Ma, J.; Mu, S. Stabilizing Fe−N−C Catalysts as Model for Oxygen Reduction Reaction. *Adv. Sci.* 2021, *8* (23), No. 2102209.

(239) Weiss, J.; Zhang, H.; Zelenay, P. Recent progress in the durability of Fe-N-C oxygen reduction electrocatalysts for polymer electrolyte fuel cells. *J. Electroanal. Chem.* 2020, *875*, No. 114696.

(240) Müller-Hülstede, J.; Schmies, H.; Schonvogel, D.; Meyer, Q.; Nie, Y.; Zhao, C.; Wagner, P.; Wark, M. What determines the stability of Fe-N-C catalysts in HT-PEMFCs? *Int. J. Hydrogen Energy* 2024, *50*, 921−930.

(241) Deng, Y.; Luo, J.; Chi, B.; Tang, H.; Li, J.; Qiao, X.; Shen, Y.; Yang, Y.; Jia, C.; Rao, P.; Liao, S.; Tian, X. Advanced Atomically Dispersed Metal−Nitrogen−Carbon Catalysts Toward Cathodic Oxygen Reduction in PEM Fuel Cells. *Adv. Energy Mater.* 2021, *11* (37), No. 2101222.

(242) Fu, X.; Gao, R.; Jiang, G.; Li, M.; Li, S.; Luo, D.; Hu, Y.; Yuan, Q.; Huang, W.; Zhu, N.; Yang, L.; Mao, Z.; Xiong, J.; Yu, A.; Chen, Z.; Bai, Z. Evolution of atomic-scale dispersion of FeNx in hierarchically porous 3D air electrode to boost the interfacial electrocatalysis of oxygen reduction in PEMFC. *Nano Energy* 2021, *83*, No. 105734.

(243) Zhan, Y.; Zeng, H.; Zhao, T.; Situ, A.; Yang, L.; Zhang, Z.; Li, P.; Wang, Z.; Wen, J.; Xie, F.; Chen, J.; Tang, X.; Meng, H. Densely accessible single atom Fe sites dispersed on porous carbon as highly stable and active ORR catalyst for PEMFC. *Int. J. Hydrogen Energy* 2024, *56*, 1049−1056.

(244) Cheng, Y.; He, S.; Veder, J.-P.; De Marco, R.; Yang, S.-z.; Ping Jiang, S. Atomically Dispersed Bimetallic FeNi Catalysts as Highly Efficient Bifunctional Catalysts for Reversible Oxygen Evolution and Oxygen Reduction Reactions. *ChemElectroChem* 2019, *6* (13), 3478−3487.

(245) Liu, F.; Shi, L.; Lin, X.; Zhang, B.; Long, Y.; Ye, F.; Yan, R.; Cheng, R.; Hu, C.; Liu, D.; Qiu, J.; Dai, L. Fe/Co dual metal catalysts modulated by S-ligands for efficient acidic oxygen reduction in PEMFC. *Sci. Adv.* 2023 *9*, (23), eadg0366..

(246) Moschkowitsch, W.; Cavaliere, S.; Jaouen, F. Fe-N-C Catalysts Synthesized on Conductive Non-Carbon Support Materials for Improved PEMFC Durability. *ECS Meeting Abstracts* 2023, *MA2023−02* (40), 1937.

(247) Duan, Z.; Wang, G. A first principles study of oxygen reduction reaction on a Pt(111) surface modified by a subsurface transition metal M (M = Ni, Co, or Fe). *Phys. Chem. Chem. Phys.* 2011, *13* (45), 20178−20187.

(248) Wu, D.; Shen, X.; Pan, Y.; Yao, L.; Peng, Z. Platinum Alloy Catalysts for Oxygen Reduction Reaction: Advances, Challenges and Perspectives. *ChemNanoMat* 2020, *6* (1), 32−41.

(249) Chen, C. H.; Coats, M.; Chabot, F.; Morimoto, Y.; Atanassov, P.; Tamura, N.; Braaten, J.; Stühmeier, B. M.; Johnston, C.; Pylypenko, S.; Cheng, L.; Zenyuk, I. V. Durability of Pt-Alloy Catalyst for Heavy-Duty Polymer Electrolyte Fuel Cell Applications under Realistic Conditions. *ChemElectroChem* 2025, *12* (8), No. e202400643.

(250) Chung, D. Y.; Jun, S. W.; Yoon, G.; Kwon, S. G.; Shin, D. Y.; Seo, P.; Yoo, J. M.; Shin, H.; Chung, Y.-H.; Kim, H.; Mun, B. S.; Lee, K.-S.; Lee, N.-S.; Yoo, S. J.; Lim, D.-H.; Kang, K.; Sung, Y.-E.; Hyeon, T. Highly Durable and Active PtFe Nanocatalyst for Electrochemical Oxygen Reduction Reaction. *J. Am. Chem. Soc.* 2015, *137* (49), 15478−15485.

(251) Wang, H.; Lin, R.; Cai, X.; Liu, S.; Zhong, D.; Hao, Z. Transition metal dissolution control in Pt-alloy catalyst layers for low Pt-loaded PEMFCs for improving mass transfer. *Int. J. Heat Mass Transfer* 2021, *178*, No. 121615.

(252) Ganguly, D.; Ramanujam, K.; Sundara, R. Low-Temperature Synthesized Pt3Fe Alloy Nanoparticles on Etched Carbon Nanotubes Catalyst Support Using Oxygen-Deficient Fe2O3 as a Catalytic Center for PEMFC Applications. *ACS Sustainable Chem. Eng.* 2023, *11* (8), 3334−3345.

(253) Lin, R.; Che, L.; Shen, D.; Cai, X. High durability of Pt-Ni-Ir/ C ternary catalyst of PEMFC by stepwise reduction synthesis. *Electrochim. Acta* 2020, *330*, No. 135251.

(254) Gao, S.; Zhao, H.; Gao, P.; Bi, J.; Liu, D.; Zhu, D.; Wang, B.; Yang, S. Hydrogenated Boride-Assisted Gram-Scale Production of Platinum−Palladium Alloy Nanoparticles on Carbon Black for PEMFC Cathodes: A Study from a Practical Standpoint. *ACS Appl. Mater. Interfaces* 2022, *14* (30), 34750−34760.

(255) Mardle, P.; Thirunavukkarasu, G.; Guan, S.; Chiu, Y.-L.; Du, S. Comparative Study of PtNi Nanowire Array Electrodes toward Oxygen Reduction Reaction by Half-Cell Measurement and PEMFC Test. *ACS Appl. Mater. Interfaces* 2020, *12* (38), 42832−42841.

(256) Liu, X.; Zhao, Z.; Liang, J.; Li, S.; Lu, G.; Priest, C.; Wang, T.; Han, J.; Wu, G.; Wang, X.; Huang, Y.; Li, Q. Inducing Covalent Atomic Interaction in Intermetallic Pt Alloy Nanocatalysts for High-Performance Fuel Cells. *Angew. Chem., Int. Ed.* 2023, *62* (23), No. e202302134.

(257) Sun, L.; Yin, Y.; Ren, B.; Qin, Y.; Wen, G.; Chen, Z. ZIF-derived ternary Pt-Co-Ni alloy as the superior active and durable catalyst for PEMFC. *Nano Energy* 2024, *120*, No. 109154.

(258) Huang, J.; Peng, B.; Stracensky, T.; Liu, Z.; Zhang, A.; Xu, M.; Liu, Y.; Zhao, Z.; Duan, X.; Jia, Q.; Huang, Y. 1D PtCo nanowires as catalysts for PEMFCs with low Pt loading. *Sci. China Mater.* 2022, *65* (3), 704−711.

(259) Hu, B.; Yuan, J.; Zhang, J.; Shu, Q.; Guan, D.; Yang, G.; Zhou, W.; Shao, Z. High activity and durability of a Pt−Cu−Co ternary alloy

electrocatalyst and its large-scale preparation for practical proton exchange membrane fuel cells. *Composites, Part B* **2021**, *222*, No. 109082.

(260) Chang, Y.-F.; Wu, C.-Y.; Chang, M.-H. Fabrication of platinum-cobalt nanowires by centrifugal electrospinning as oxygen reduction catalyst for PEMFC. *Int. J. Hydrogen Energy* **2024**, *54*, 437−445.

(261) Zhou, N.; Li, Y. PtFe and Fe3C nanoparticles encapsulated in Fe−N-doped carbon bowl toward the oxygen reduction reaction. *Int. J. Hydrogen Energy* **2023**, *48* (36), 13591−13602.

(262) Wang, X.; Zhou, Y.; Chang, C.; Qiao, Y.; Jiang, Y.; Gao, M.; Hou, L. Optimization and regulation of catalytic activity and stability: Pt−Ni diamond-shaped pearl nanochains with core-shell structure as high-efficient oxygen reduction reaction catalysts. *Mater. Chem. Phys.* **2024**, *316*, No. 129127.

(263) Do, V.-H.; Lee, J.-M. Surface engineering for stable electrocatalysis. *Chem. Soc. Rev.* **2024**, *53*, 2693−2737, DOI: 10.1039/D3CS00292F.

(264) Cruz-Martínez, H.; Rojas-Chávez, H.; Matadamas-Ortiz, P. T.; Ortiz-Herrera, J. C.; López-Chávez, E.; Solorza-Feria, O.; Medina, D. I. Current progress of Pt-based ORR electrocatalysts for PEMFCs: An integrated view combining theory and experiment. *Mater. Today Phys.* **2021**, *19*, No. 100406.

(265) Wang, X. X.; Sokolowski, J.; Liu, H.; Wu, G. Pt alloy oxygen-reduction electrocatalysts: Synthesis, structure, and property. *Chin. J. Catal.* **2020**, *41* (5), 739−755.

(266) Tian, S.-Y.; Hu, S.-N.; Shen, J.-F.; Tian, N.; Xu, W.-C.; Yang, S.-L.; Li, M.-Y.; Jin, Y.-Q.; Chen, S.-M.; Chen, M.-S.; Zhou, Z.-Y.; Sun, S.-G. P and O Co-Doped Pt−Co Octahedral Nanocrystals as Highly Active and Stable Electrocatalysts for Oxygen Reduction Reaction. *ChemCatChem* **2024**, *116* (16), No. e202400260.

(267) Wang, J.; Xue, Q.; Li, B.; Yang, D.; Lv, H.; Xiao, Q.; Ming, P.; Wei, X.; Zhang, C. Preparation of a Graphitized-Carbon-Supported PtNi Octahedral Catalyst and Application in a Proton-Exchange Membrane Fuel Cell. *ACS Appl. Mater. Interfaces* **2020**, *12* (6), 7047−7056.

(268) Cai, X.; Hua, S.; Lin, R.; Chen, L.; Wang, H.; Liu, S. An effective method of applying octahedral Pt-Ni/C to membrane electrode assembly and related in-situ X-ray absorption fine structures study. *Appl. Surf. Sci.* **2022**, *598*, No. 153789.

(269) Pan, L.; Parnière, A.; Dunseath, O.; Fongalland, D.; Nicolau, G.; Weber, C. C.; Lu, J.; Klingenhof, M.; Arinchtein, A.; Oh, H.-S.; Blanchard, P.-Y.; Cavaliere, S.; Heggen, M.; Dunin-Borkowski, R. E.; Bonastre, A. M.; Dionigi, F.; Sharman, J.; Jones, D.; Strasser, P. Enhancing the Performance of Shape-Controlled Octahedral Rhodium-Doped PtNi Nanoalloys inside Hydrogen−Air Fuel Cell Cathodes Using a Rational Design of Catalysts, Supports, and Layering. *ACS Catal.* **2024**, *14* (1), 10−20.

(270) Danisman, B.; Zhang, G.-R.; Baumunk, A. F.; Yang, J.; Brummel, O.; Darge, P.; Dworschak, D.; Mayrhofer, K. J. J.; Libuda, J.; Zhou, X.; Wu, M.; Spiecker, E.; Ledendecker, M.; Etzold, B. J. M. Increasing Activity of Trimetallic Oxygen Reduction PtNiMo/C Catalysts Through Initial Conditioning. *ChemElectroChem* **2024**, *11* (9), No. e202400070.

(271) Hornberger, E.; Klingenhof, M.; Polani, S.; Paciok, P.; Kormányos, A.; Chattot, R.; MacArthur, K. E.; Wang, X.; Pan, L.; Drnec, J.; Cherevko, S.; Heggen, M.; Dunin-Borkowski, R. E.; Strasser, P. On the electrocatalytical oxygen reduction reaction activity and stability of quaternary RhMo-doped PtNi/C octahedral nanocrystals. *Chem. Sci.* **2022**, *13* (32), 9295−9304.

(272) Shi, W.; Park, A.-H.; Kwon, Y.-U. Scalable synthesis of (Pd,Cu)@Pt core-shell catalyst with high ORR activity and durability. *J. Electroanal. Chem.* **2022**, *918*, No. 116451.

(273) Xie, M.; Lyu, Z.; Chen, R.; Shen, M.; Cao, Z.; Xia, Y. Pt−Co@ Pt Octahedral Nanocrystals: Enhancing Their Activity and Durability toward Oxygen Reduction with an Intermetallic Core and an Ultrathin Shell. *J. Am. Chem. Soc.* **2021**, *143* (22), 8509−8518.

(274) Lu, L.; Deng, H.; Zhao, Z.; Xu, B.; Sun, X. N-doped carbon nanotubes supported Pt nanowire catalysts for proton exchange membrane fuel cells. *J. Power Sources* **2022**, *529*, No. 231229.

(275) Peng, X.; Zhao, S.; Omasta, T. J.; Roller, J. M.; Mustain, W. E. Activity and durability of Pt-Ni nanocage electocatalysts in proton exchange membrane fuel cells. *Appl. Catal., B* **2017**, *203*, 927−935.

(276) Liu, X.; Tian, J.; Zhou, C.; Jiang, J.; Cheng, X.; Yang, L.; Wu, Q.; Wang, X.; Hu, Z. Constructing membrane electrodes of low Pt areal loading with the new support of N-doped carbon nanocages for PEMFC. *FlatChem* **2023**, *40*, No. 100515.

(277) Gong, M.; Xiao, D.; Deng, Z.; Zhang, R.; Xia, W.; Zhao, T.; Liu, X.; Shen, T.; Hu, Y.; Lu, Y.; Zhao, X.; Xin, H.; Wang, D. Structure evolution of PtCu nanoframes from disordered to ordered for the oxygen reduction reaction. *Appl. Catal., B* **2021**, *282*, No. 119617.

(278) Malheiro, A. R.; Perez, J.; Santiago, E. I.; Villullas, H. M. The Extent on the Nanoscale of Pt-Skin Effects on Oxygen Reduction and Its Influence on Fuel Cell Power. *J. Phys. Chem. C* **2010**, *114* (47), 20267−20271.

(279) Sugawara, Y.; Konno, M.; Muto, I.; Hara, N. Formation of Pt Skin Layer on Ordered and Disordered Pt-Co Alloys and Corrosion Resistance in Sulfuric Acid. *Electrocatalysis* **2018**, *9* (5), 539−549.

(280) Sasaki, K.; Kuttiyiel, K. A.; Adzic, R. R. Designing high performance Pt monolayer core−shell electrocatalysts for fuel cells. *Curr. Opin. Electrochem.* **2020**, *21*, 368−375.

(281) Wang, C.; Fang, J. Octahedral Noble-Metal Nanoparticles and Their Electrocatalytic Properties. *ChemSusChem* **2013**, *6* (10), 1848−1857.

(282) Zhao, X.; Chen, S.; Fang, Z.; Ding, J.; Sang, W.; Wang, Y.; Zhao, J.; Peng, Z.; Zeng, J. Octahedral Pd@Pt1.8Ni Core−Shell Nanocrystals with Ultrathin PtNi Alloy Shells as Active Catalysts for Oxygen Reduction Reaction. *J. Am. Chem. Soc.* **2015**, *137* (8), 2804−2807.

(283) Comini, E. Metal oxides nanowires chemical/gas sensors: recent advances. *Mater. Today Adv.* **2020**, *7*, No. 100099.

(284) Grandi, M.; Rohde, S.; Liu, D. J.; Gollas, B.; Hacker, V. Recent advancements in high performance polymer electrolyte fuel cell electrode fabrication − Novel materials and manufacturing processes. *J. Power Sources* **2023**, *562*, No. 232734.

(285) Caldwell, K. M.; Ramaker, D. E.; Jia, Q.; Mukerjee, S.; Ziegelbauer, J. M.; Kukreja, R. S.; Kongkanand, A. Spectroscopic in situ Measurements of the Relative Pt Skin Thicknesses and Porosities of Dealloyed PtM n (Ni, Co) Electrocatalysts. *J. Phys. Chem. C* **2015**, *119* (1), 757−765.

(286) Zhang, Q.; Wang, B. Development and Challenges of Electrode Ionomers Used in the Catalyst Layer of Proton-Exchange Membrane Fuel Cells: A Review. *Trans. Tianjin Univ.* **2023**, *29* (5), 360−386.

(287) Paul, D. K.; Fraser, A.; Karan, K. Towards the understanding of proton conduction mechanism in PEMFC catalyst layer: Conductivity of adsorbed Nafion films. *Electrochem. Commun.* **2011**, *13* (8), 774−777.

(288) Iden, H.; Ohma, A.; Shinohara, K. Analysis of Proton Transport in Pseudo Catalyst Layers. *J. Electrochem. Soc.* **2009**, *156* (9), B1078.

(289) Farzin, S.; Sarella, A.; Yandrasits, M. A.; Dishari, S. K. Fluorocarbon-Based Ionomers with Single Acid and Multiacid Side Chains at Nanothin Interfaces. *J. Phys. Chem. C* **2019**, *123* (51), 30871−30884.

(290) Chatterjee, S.; Obewhere, O. A.; Zamani, E.; Keloth, R.; Farzin, S.; Morton, M. D.; Sarella, A.; Dishari, S. K. Advancing ionomer design to boost interfacial and thin-film proton conductivity via styrene-calix[4]arene-based ionomers. *Cell Rep. Phys. Sci.* **2023**, *4* (2), No. 101282.

(291) Woo, S.; Lee, S.; Taning, A. Z.; Yang, T.-H.; Park, S.-H.; Yim, S.-D. Current understanding of catalyst/ionomer interfacial structure and phenomena affecting the oxygen reduction reaction in cathode catalyst layers of proton exchange membrane fuel cells. *Curr. Opin. Electrochem.* **2020**, *21*, 289−296.

(292) Schuler, T.; Chowdhury, A.; Freiberg, A. T.; Sneed, B.; Spingler, F. B.; Tucker, M. C.; More, K. L.; Radke, C. J.; Weber, A. Z. Fuel-Cell Catalyst-Layer Resistance via Hydrogen Limiting-Current Measurements. *J. Electrochem. Soc.* **2019**, *166* (7), F3020.

(293) Subbaraman, R.; Strmcnik, D.; Paulikas, A. P.; Stamenkovic, V. R.; Markovic, N. M. Oxygen Reduction Reaction at Three-Phase Interfaces. *ChemPhysChem* **2010**, *11* (13), 2825−2833.

(294) Gao, W.; Yin, Q.; Chen, J.; Liu, Z.; Zhang, Z.; Lu, J.; Lei, Y.; Xu, H.; Ouyang, H.; Yin, Y.; Wang, C. Mechanism study of the improved catalytic activity of PEMFC catalyst layer by short-side-chain ionomer: Focusing on the ionomer/Pt interface. *Chem. Eng. J.* **2024**, *479*, No. 147787.

(295) Sakai, K.; Tokumasu, T. Molecular Dynamics Study of Oxygen Permeation in PFSA Ionomer on the Pt Catalyst Surface. *ECS Trans.* **2011**, *41* (1), 2105.

(296) Cheng, X.; Shen, S.; Wei, G.; Wang, C.; Luo, L.; Zhang, J. Perspectives on Challenges and Achievements in Local Oxygen Transport of Low Pt Proton Exchange Membrane Fuel Cells. *Adv. Mater. Technol.* **2022**, *7* (8), No. 2200228.

(297) Sun, F.; Di, Q.; Chen, M.; Liu, H.; Wang, H. Exploring local oxygen transport in low-Pt loading proton exchange membrane fuel cells: A comprehensive review. *eTransportation* **2024**, *20*, No. 100327.

(298) Kurihara, Y.; Mabuchi, T.; Tokumasu, T. Molecular Simulation of Oxygen Permeation through Ionomer in Catalyst Layer. *ECS Trans.* **2014**, *64* (3), 559.

(299) Kurihara, Y.; Mabuchi, T.; Tokumasu, T. Molecular Analysis of Structural Effect of Ionomer on Oxygen Permeation Properties in PEFC. *J. Electrochem. Soc.* **2017**, *164* (6), F628.

(300) Kang, B. G.; Kwon, Y. R.; Hong, K. W.; Kwon, S. K.; Lee, H. M.; Song, D. K.; Jeon, J. W.; Jung, D. Y.; Go, D.; Cho, G. Y. Performance Improvement of Proton Exchange Membrane Fuel Cells with a TiO2 Sputtered Gas Diffusion Layer Under Low-Humidity Conditions. *Energies* **2025**, *18* (6), 1525.

(301) Yusaf, T.; Faisal Mahamude, A. S.; Kadirgama, K.; Ramasamy, D.; Farhana, K.; A Dhahad, H.; Abu Talib, A. B. D. R. Sustainable hydrogen energy in aviation − A narrative review. *Int. J. Hydrogen Energy* **2024**, *52*, 1026−1045.

(302) Yan, Q.; Toghiani, H.; Lee, Y.-W.; Liang, K.; Causey, H. Effect of sub-freezing temperatures on a PEM fuel cell performance, startup and fuel cell components. *J. Power Sources* **2006**, *160* (2), 1242−1250.

(303) Liepold, H.; Bird, A.; Heizmann, P. A.; Fadlullah, H.; Nguyen, H.; Klose, C.; Holdcroft, S.; Kusoglu, A.; Vierrath, S.; Münchinger, A. High protonic resistance of hydrocarbon-based cathodes in PEM fuel cells under low humidity conditions: Origin, implication, and mitigation. *J. Power Sources* **2024**, *624*, No. 235537.

(304) Fan, L.; Wang, Y.; Du, Q.; Ni, M.; Jiao, K. Linking the ionomer film morphology and nanoscale oxygen transport properties in fuel cells. *Appl. Energy Combust. Sci.* **2024**, *17*, No. 100243.

(305) Maier, M.; Abbas, D.; Komma, M.; Mu'min, M. S.; Thiele, S.; Böhm, T. A comprehensive study on the ionomer properties of PFSA membranes with confocal Raman microscopy. *J. Membr. Sci.* **2023**, *669*, No. 121244.

(306) Kreuer, K. D.; Schuster, M.; Obliers, B.; Diat, O.; Traub, U.; Fuchs, A.; Klock, U.; Paddison, S. J.; Maier, J. Short-side-chain proton conducting perfluorosulfonic acid ionomers: Why they perform better in PEM fuel cells. *J. Power Sources* **2008**, *178* (2), 499−509.

(307) Ous, T.; Arcoumanis, C. Degradation aspects of water formation and transport in PEMFC: A review.

(308) Jiang, S.; Xiang, Q.; Xie, Z.; Yang, N.; Liu, J.; Li, L.; Wei, Z. Influence of the Pt/ionomer/water interface on the oxygen reduction reaction: insights into the micro-three-phase interface. *Chem. Sci.* **2024**, *15* (46), 19290−19298.

(309) Huang, S.; Zhao, Y.; Wang, X.; Shi, J.; Yao, S. A Comprehensive Review of Passive Water and Thermal Management of Air-Breathing Proton Exchange Membrane Fuel Cell. *Int. J. Energy Res.* **2025**, *2025* (1), No. 5554089.

(310) Eren, E. O.; Özkan, N.; Devrim, Y. Polybenzimidazole-modified carbon nanotubes as a support material for platinum-based high-temperature proton exchange membrane fuel cell electro-catalysts. *Int. J. Hydrogen Energy* **2021**, *46* (57), 29556−29567.

(311) Li, Y.; Jiang, G.; Yang, Y.; Song, W.; Yu, H.; Hao, J.; Shao, Z. PtIr/CNT as anode catalyst with high reversal tolerance in PEMFC. *Int. J. Hydrogen Energy* **2023**, *48* (93), 36500−36511.

(312) Huda, M.; Kawahara, T.; Park, J.-H.; Kawasumi, M.; Matsuo, Y. Single-Walled Carbon Nanotubes Supported Pt Electrocatalyst as a Cathode Catalyst of a Single Fuel Cell with High Durability against Start-up/Shut-down Potential Cycling. *ACS Appl. Energy Mater.* **2023**, *6* (24), 12226−12236.

(313) Chung, S.; Ham, K.; Kang, S.; Ju, H.; Lee, J. Enhanced corrosion tolerance and highly durable ORR activity by low Pt electrocatalyst on unique pore structured CNF in PEM fuel cell. *Electrochim. Acta* **2020**, *348*, No. 136346.

(314) Zhuang, Y.; Yang, J.; Meng, L.; Ma, C.; Peng, L.; Chen, D.; Chen, Q. Polyaniline-derived carbon nanofibers with a high graphitization degree loading ordered PtNi intermetallic nanoparticles for oxygen reduction reaction. *Ind. Chem. Mater.* **2023**, *1* (3), 458−464.

(315) Yarar Kaplan, B.; Haghmoradi, N.; Jamil, E.; Merino, C.; Alkan Gürsel, S. Platinum nanoparticles decorated carbon nanofiber hybrids as highly active electrocatalysts for polymer electrolyte membrane fuel cells. *Int. J. Energy Res.* **2020**, *44* (13), 10251−10261.

(316) Ponnusamy, P.; Panthalingal, M. K.; Badhirappan, G. P.; Pullithadathil, B. Durable Electrocatalyst Support Materials Based on N-Doped Mesoporous Carbon Nanofibers with Titanium Nitride Overlay Coating for High-Performance Proton Exchange Membrane Fuel Cells. *ACS Appl. Nano Mater.* **2024**, *7* (5), 4676−4691.

(317) Manna, N.; Singh, M.; Kurungot, S. Microporous 3D-Structured Hierarchically Entangled Graphene-Supported Pt3Co Alloy Catalyst for PEMFC Application with Process-Friendly Features. *ACS Appl. Mater. Interfaces* **2023**, *15* (23), 28023−28035.

(318) Marinoiu, A.; Carcadea, E.; Sacca, A.; Carbone, A.; Sisu, C.; Dogaru, A.; Raceanu, M.; Varlam, M. One-step synthesis of graphene supported platinum nanoparticles as electrocatalyst for PEM fuel cells. *Int. J. Hydrogen Energy* **2021**, *46* (22), 12242−12253.

(319) Pushkareva, I. V.; Pushkarev, A. S.; Kalinichenko, V. N.; Chumakov, R. G.; Soloviev, M. A.; Liang, Y.; Millet, P.; Grigoriev, S. A. Reduced Graphene Oxide-Supported Pt-Based Catalysts for PEM Fuel Cells with Enhanced Activity and Stability. *Catalysts* **2021**, *11* (2), 256 DOI: 10.3390/catal11020256.

(320) Bhaskaran, R.; Chetty, R. One-Pot Room Temperature Synthesis of Nitrogen-Doped Graphene and Its Application as Catalyst Support for ORR in PEMFCs. *ACS Appl. Energy Mater.* **2024**, *7* (2), 390−402.

(321) Yang, Y.; Zhao, C.; Wang, Z.; Fan, X.; Yan, C. Synergistic effects of N-doping and mesoporous structures in block copolymer-derived three-dimensional ordered mesoporous carbon for PEMFC. *Int. J. Hydrogen Energy* **2024**, *51*, 747−757.

(322) Yarlagadda, V.; Ramaswamy, N.; Kukreja, R. S.; Kumaraguru, S. Ordered mesoporous carbon supported fuel cell cathode catalyst for improved oxygen transport. *J. Power Sources* **2022**, *532*, No. 231349.

(323) Yang, Y.; Wang, Z.; Mai, Y.; Guo, C.; Shi, Y.; Tan, H.; Lu, Z.; Shen, L.; Yan, C. Highly active PtCo nanoparticles on hierarchically ordered mesoporous carbon support for polymer electrolyte membrane fuel cells. *J. Mater. Sci.* **2021**, *56* (23), 13083−13095.

(324) Ramaswamy, N.; Zulevi, B.; McCool, G.; Shi, Z.; Chavez, A.; Muller, D. A.; Kongkanand, A.; Kumaraguru, S. Graphitized Mesoporous Engineered Carbon Support for Fuel Cell Applications. *ACS Appl. Eng. Mater.* **2023**, *1* (10), 2543−2554.

(325) Öner, E.; Öztürk, A.; Yurtcan, A. B. Utilization of the graphene aerogel as PEM fuel cell catalyst support: Effect of polypyrrole (PPy) and polydimethylsiloxane (PDMS) addition. *Int. J. Hydrogen Energy* **2020**, *45* (60), 34818−34836.

(326) Gu, K.; Kim, E. J.; Sharma, S. K.; Sharma, P. R.; Bliznakov, S.; Hsiao, B. S.; Rafailovich, M. H. Mesoporous carbon aerogel with tunable porosity as the catalyst support for enhanced proton-exchange

membrane fuel cell performance. *Mater. Today Energy* **2021**, *19*, No. 100560.

(327) Luo, Y.; Feng, J.; Jiang, Y.; Li, L.; Feng, J. Accessible mesoporous carbon aerogel preparation and its application as ultra-low pt support for oxygen reduction reaction with high catalytic activity. *J. Porous Mater.* **2021**, *28* (3), 661−672.

(328) Shahgaldi, S.; Hamelin, J. Improved carbon nanostructures as a novel catalyst support in the cathode side of PEMFC: a critical review. *Carbon* **2015**, *94*, 705−728.

(329) Xie, M.; Chu, T.; Wang, X.; Li, B.; Yang, D.; Ming, P.; Zhang, C. Effect of mesoporous carbon on oxygen reduction reaction activity as cathode catalyst support for proton exchange membrane fuel cell. *Int. J. Hydrogen Energy* **2022**, *47* (65), 28074−28085.

(330) Ouattara-Brigaudet, M.; Berthon-Fabry, S.; Beauger, C.; Chatenet, M.; Job, N.; Sennour, M.; Achard, P. Influence of the carbon texture of platinum/carbon aerogel electrocatalysts on their behavior in a proton exchange membrane fuel cell cathode. *Int. J. Hydrogen Energy* **2012**, *37* (12), 9742−9757.

(331) Xu, J. B.; Zhao, T. S. Mesoporous carbon with uniquely combined electrochemical and mass transport characteristics for polymer electrolyte membrane fuel cells. *RSC Adv.* **2013**, *3* (1), 16−24.

(332) Wang, T.; Chen, Z.-X.; Chen, Y.-G.; Yang, L.-J.; Yang, X.-D.; Ye, J.-Y.; Xia, H.-P.; Zhou, Z.-Y.; Sun, S.-G. Identifying the Active Site of N-Doped Graphene for Oxygen Reduction by Selective Chemical Modification. *ACS Energy Lett.* **2018**, *3* (4), 986−991.

(333) Takeyasu, K.; Furukawa, M.; Shimoyama, Y.; Singh, S. K.; Nakamura, J. Role of Pyridinic Nitrogen in the Mechanism of the Oxygen Reduction Reaction on Carbon Electrocatalysts. *Angew. Chem., Int. Ed.* **2021**, *60* (10), 5121−5124.

(334) Roudbari, M. N.; Ojani, R.; Raoof, J. B. Nitrogen functionalized carbon nanotubes as a support of platinum electro-catalysts for performance improvement of ORR using fuel cell cathodic half-cell. *Renewable Energy* **2020**, *159*, 1015−1028.

(335) Li, Y.; Gui, F.; Wang, F.; Liu, J.; Zhu, H. Synthesis of modified, ordered mesoporous carbon-supported Pt3Cu catalyst for enhancing the oxygen reduction activity and durability. *Int. J. Hydrogen Energy* **2021**, *46* (76), 37802−37813.

(336) Yao, R.; Gu, J.; He, H.; Yu, T. Improved Electrocatalytic Activity and Durability of Pt Nanoparticles Supported on Boron-Doped Carbon Black. *Catalysts* **2020**, *10* (8), 862 DOI: 10.3390/catal10080862.

(337) Han, C.; Chen, Z. Study on the synergism of thermal transport and electrochemical of PEMFC based on N, P co-doped graphene substrate electrode. *Energy* **2021**, *214*, No. 118808.

(338) Long, Y.; Ye, F.; Shi, L.; Lin, X.; Paul, R.; Liu, D.; Hu, C. N, P, and S tri-doped holey carbon as an efficient electrocatalyst for oxygen reduction in whole pH range for fuel cell and zinc-air batteries. *Carbon* **2021**, *179*, 365−376.

(339) Krawczyk, J. M.; Mazur, A. M.; Sasin, T.; Stokłosa, A. Fuel cells as alternative power for unmanned aircraft systems—current situation and development trends. *Prace Instytutu Lotnictwa* **2014**, *4* (237), 49−62.

(340) Lori, O.; Gonen, S.; Kapon, O.; Elbaz, L. Durable Tungsten Carbide Support for Pt-Based Fuel Cells Cathodes. *ACS Appl. Mater. Interfaces* **2021**, *13* (7), 8315−8323.

(341) Hamo, E. R.; Saporta, R.; Rosen, B. A. Active and Stable Oxygen Reduction Catalysts Prepared by Electrodeposition of Platinum on Mo2C at Low Overpotential. *ACS Appl. Energy Mater.* **2021**, *4* (3), 2130−2137.

(342) Prithi, J. A.; Shanmugam, R.; Sahoo, M. K.; Rajalakshmi, N.; Rao, G. R. Evaluation of the durability of ZrC as support material for Pt electrocatalysts in PEMFCs: Experimental and computational studies. *Int. J. Hydrogen Energy* **2022**, *47* (85), 36232−36247.

(343) Kumar, S.; Yoyakki, A.; Kurungot, S. Surface-Anchored PtNi Alloy Network over SiO2 (PtNi/SiO2): A Versatile Carbon-Free Cathode for Proton Exchange Membrane Fuel Cells (PEMFCs). *ACS Appl. Eng. Mater.* **2024**, *2* (4), 1110−1121.

(344) Hung, Y.-Y.; Liu, W.-S.; Chen, Y.-C.; Wang, K.-W.; Perng, T.-P. On the mesoporous TiN catalyst support for proton exchange membrane fuel cell. *Int. J. Hydrogen Energy* **2020**, *45* (27), 14083−14092.

(345) Ahmad Junaidi, N. H.; Wong, W. Y.; Loh, K. S.; Rahman, S.; Daud, W. R. W. A comprehensive review of MXenes as catalyst supports for the oxygen reduction reaction in fuel cells. *Int. J. Energy Res.* **2021**, *45* (11), 15760−15782.

(346) Xu, C.; Fan, C.; Zhang, X.; Chen, H.; Liu, X.; Fu, Z.; Wang, R.; Hong, T.; Cheng, J. MXene (Ti3C2Tx) and Carbon Nanotube Hybrid-Supported Platinum Catalysts for the High-Performance Oxygen Reduction Reaction in PEMFC. *ACS Appl. Mater. Interfaces* **2020**, *12* (17), 19539−19546.

(347) Wang, R.; Chang, Z.; Fang, Z.; Xiao, T.; Zhu, Z.; Ye, B.; Xu, C.; Cheng, J. Pt nanowire/Ti3C2Tx-CNT hybrids catalysts for the high performance oxygen reduction reaction for high temperature PEMFC. *Int. J. Hydrogen Energy* **2020**, *45* (52), 28190−28195.

(348) Ahmad Junaidi, N. H.; Wong, W. Y.; Loh, K. S.; Rahman, S.; Choo, T. F.; Wu, B. Enhanced oxygen reduction reaction catalyst stability and durability of MXene-supported Fe-N-C catalyst for proton exchange membrane fuel cell application. *J. Alloys Compd.* **2023**, *968*, No. 171898.

(349) Chang, Z.; Ren, W.; Wang, Y.; Zhang, J.; Liu, X.; Xu, C. A Highly CO-Tolerant Anode Pt/Ti3C2Tx-CNT Hybrid Catalysts for PEMFC. *Electrocatalysis* **2023**, *14* (1), 1−8.

(350) Yang, X.; Zhang, Y.; Fu, Z.; Lu, Z.; Zhang, X.; Wang, Y.; Yang, Z.; Wu, R. Tailoring the Electronic Structure of Transition Metals by the V2C MXene Support: Excellent Oxygen Reduction Performance Triggered by Metal−Support Interactions. *ACS Appl. Mater. Interfaces* **2020**, *12* (25), 28206−28216.

(351) Zhang, S.; Zhang, R.; Zhang, Z.; Shi, K.; Sun, G. Scalable Synthesis of Accordion-Like Multilayered Titanium Nitride in Air with Enhanced Performance as Catalytic Support for Oxygen Reduction. *ChemRxiv*, 2024. DOI: 10.26434/chemrxiv-2024-8j81v.

(352) Guan, S.; Zhou, F.; Tan, J.; Pan, M. Influence of pore size optimization in catalyst layer on the mechanism of oxygen transport resistance in PEMFCs. *Prog. Nat. Sci.: Mater. Int.* **2020**, *30* (6), 839−845.

(353) Garsany, Y.; Atkinson, R. W.; Gould, B. D.; Martin, R.; Dubau, L.; Chatenet, M.; Swider-Lyons, K. E. Dual-layer catalyst layers for increased proton exchange membrane fuel cell performance. *J. Power Sources* **2021**, *514*, No. 230574.

(354) Lin, R.; Wang, H.; Zhu, Y. Optimizing the structural design of cathode catalyst layer for PEM fuel cells for improving mass-specific power density. *Energy* **2021**, *221*, No. 119909.

(355) Wan, Y.; Qiu, D.; Yi, P.; Peng, L.; Lai, X. Design and optimization of gradient wettability pore structure of adaptive PEM fuel cell cathode catalyst layer. *Appl. Energy* **2022**, *312*, No. 118723.

(356) Zheng, Z.; Yang, F.; Lin, C.; Zhu, F.; Shen, S.; Wei, G.; Zhang, J. Design of gradient cathode catalyst layer (CCL) structure for mitigating Pt degradation in proton exchange membrane fuel cells (PEMFCs) using mathematical method. *J. Power Sources* **2020**, *451*, No. 227729.

(357) Wang, Y.; Liu, T.; Sun, H.; He, W.; Fan, Y.; Wang, S. Investigation of dry ionomer volume fraction in cathode catalyst layer under different relative humilities and nonuniform ionomer-gradient distributions for PEM fuel cells. *Electrochim. Acta* **2020**, *353*, No. 136491.

(358) Mu, Y.-T.; Yang, S.-R.; He, P.; Tao, W.-Q. Mesoscopic modeling impacts of liquid water saturation, and platinum distribution on gas transport resistances in a PEMFC catalyst layer. *Electrochim. Acta* **2021**, *388*, No. 138659.

(359) Dong, E.; Zhao, H.; Zhang, R.; Chen, L.; Tao, W.-Q. Effects of gradient structures of cathode catalyst layers on performance and durability of proton exchange membrane fuel cells. *Electrochim. Acta* **2024**, *477*, No. 143772.

(360) Fan, R.; Chang, G.; Xu, Y.; Xu, J. Multi-objective optimization of graded catalyst layer to improve performance and current density uniformity of a PEMFC. *Energy* **2023**, *262*, No. 125580.

(361) Liu, J.; Yin, Y.; Zhang, J.; Zhang, T.; Zhang, X.; Chen, H. Mechanical degradation of catalyst layer under accelerated relative humidity cycling in a polymer electrolyte membrane fuel cell. *J. Power Sources* **2021**, *512*, No. 230487.

(362) Uchimura, M.; Sugawara, S.; Suzuki, Y.; Zhang, J.; Kocha, S. S. Electrocatalyst durability under simulated automotive drive cycles. *ECS Trans.* **2008**, *16* (2), 225.

(363) Drugeot, T.; Micoud, F.; Pinton, E.; Rosini, S.; Poirot-Crouvezier, J.-P.; Poupin, L.; Bultel, Y. Experimental assessment of proton exchange membrane fuel cell performance degradations during emulated start-up/shut-down phases. *Int. J. Hydrogen Energy* **2023**, *48* (14), 5630−5642.

(364) Laghryb, I.; Malki, M.; Yousfi Steiner, N.; Barrett, C. D.; El Kadiri, H. Catalyst degradation in proton exchange membrane fuel cells: Mechanisms, investigation techniques, and predictive modelling. *Int. J. Hydrogen Energy* **2025**, *145*, 496−507.

(365) Zhao, J.; Tu, Z.; Chan, S. H. Carbon corrosion mechanism and mitigation strategies in a proton exchange membrane fuel cell (PEMFC): A review. *J. Power Sources* **2021**, *488*, No. 229434.

(366) Li, C.; Wang, W.; Zhu, S.; Pan, H.; Xu, Q.; Shi, P.; Min, Y. Electrocatalyst with fluorinated protective layer for efficient oxygen reduction in the operating temperature of PEMFCs. *Chem. Eng. J.* **2023**, *466*, No. 143105.

(367) Seselj, N.; Alfaro, S. M.; Bompolaki, E.; Cleemann, L. N.; Torres, T.; Azizi, K. Catalyst development for high-temperature polymer electrolyte membrane fuel cell (HT-PEMFC) applications. *Adv. Mater.* **2023**, *35* (40), No. 2302207.

(368) Eidinejad, H.; Rivola, A.; Troncossi, M.; Martini, A. Vibration Analysis of Lithium-Ion Batteries and Proton Exchange Membrane Fuel Cells in Electric Vehicles: A Comprehensive Survey. *IEEE Access* **2025**, *13*, 104565−104613, DOI: 10.1109/ACCESS.2025.3578818.

(369) Ramaswamy, N.; Jiang, R.; Kumaraguru, S.; Kongkanand, A.; Gittleman, C.; Lindell, M.; Zulevi, B.; McCool, G.; Kim, C.; Kuo, M.-C. *Durable fuel cell MEA through immobilization of catalyst particle and membrane chemical stabilizer*; General Motors Company, Pontiac, MI (United States), 2023.

(370) Malkow, T.; Pilenga, A. EU harmonised accelerated stress testing protocols for low-temperature water electrolyser. 2024.

(371) Pan, M.; Pan, C.; Li, C.; Zhao, J. A review of membranes in proton exchange membrane fuel cells: Transport phenomena, performance and durability. *Renewable Sustainable Energy Rev.* **2021**, *141*, No. 110771.

(372) Rafei, T. A.; Steiner, N. Y.; Pahon, E.; Hissel, D. Polymer electrolyte membrane fuel cell for medium- and heavy-duty vehicles: An opportunity for commercialization. *Energy Convers. Manage.: X* **2025**, *27*, No. 101070.

(373) Zhu, L.-Y.; Li, Y.-C.; Liu, J.; He, J.; Wang, L.-Y.; Lei, J.-D. Recent developments in high-performance Nafion membranes for hydrogen fuel cells applications. *Petroleum Sci.* **2022**, *19* (3), 1371−1381.

(374) Foniok, K.; Drozdova, L.; Prokop, L.; Krupa, F.; Kedron, P.; Blazek, V. Mechanisms and Modelling of Effects on the Degradation Processes of a Proton Exchange Membrane (PEM) Fuel Cell: A Comprehensive Review. *Energies* **2025**, *18* (8), No. 19961073.

(375) Maiti, T. K.; Singh, J.; Dixit, P.; Majhi, J.; Bhushan, S.; Bandyopadhyay, A.; Chattopadhyay, S. Advances in perfluorosulfonic acid-based proton exchange membranes for fuel cell applications: A review. *Chem. Eng. J. Adv.* **2022**, *12*, No. 100372.

(376) Arun, M.; Giddey, S.; Joseph, P.; Dhawale, D. S. Challenges and mitigation strategies for general failure and degradation in polymer electrolyte membrane-based fuel cells and electrolysers. *J. Mater. Chem. A* **2025**, *13* (16), 11236−11263.

(377) Mhaske, S.; Mohanty, J.; Chugh, K. Fluoropolymers: brief history, fundamental chemistry, processing, structure, properties, and applications. In *Advanced Fluoropolymer Nanocomposites*; Elsevier, 2023; pp 1−27.

(378) Dallaev, R.; Pisarenko, T.; Sobola, D.; Orudzhev, F.; Ramazanov, S.; Trčka, T. Brief review of PVDF properties and applications potential. *Polymers* **2022**, *14* (22), 4793.

(379) Esmaeili, N.; Gray, E. M.; Webb, C. J. Non-fluorinated polymer composite proton exchange membranes for fuel cell applications—A review. *ChemPhysChem* **2019**, *20* (16), 2016−2053.

(380) Ogungbemi, E.; Ijaodola, O.; Khatib, F. N.; Wilberforce, T.; El Hassan, Z.; Thompson, J.; Ramadan, M.; Olabi, A. G. Fuel cell membranes − Pros and cons. *Energy* **2019**, *172*, 155−172.

(381) Sood, R.; Cavaliere, S.; Jones, D. J.; Rozière, J. Electrospun nanofibre composite polymer electrolyte fuel cell and electrolysis membranes. *Nano Energy* **2016**, *26*, 729−745.

(382) Tang, H.; Wang, X.; Pan, M.; Wang, F. Fabrication and characterization of improved PFSA/ePTFE composite polymer electrolyte membranes. *J. Membr. Sci.* **2007**, *306* (1), 298−306.

(383) Ryu, S.; Lee, B.; Kim, J.-H.; Pak, C.; Moon, S.-H. High-temperature operation of PEMFC using pore-filling PTFE/Nafion composite membrane treated with electric field. *Int. J. Energy Res.* **2021**, *45* (13), 19136−19146.

(384) Zhang, X.; Trieu, D.; Zheng, D.; Ji, W.; Qu, H.; Ding, T.; Qiu, D.; Qu, D. Nafion/PTFE Composite Membranes for a High Temperature PEM Fuel Cell Application. *Ind. Eng. Chem. Res.* **2021**, *60* (30), 11086−11094.

(385) Hwang, C.-K.; Lee, K. A.; Lee, J.; Kim, Y.; Ahn, H.; Hwang, W.; Ju, B.-K.; Kim, J. Y.; Yeo, S. Y.; Choi, J.; Sung, Y.-E.; Kim, I.-D.; Yoon, K. R. Perpendicularly stacked array of PTFE nanofibers as a reinforcement for highly durable composite membrane in proton exchange membrane fuel cells. *Nano Energy* **2022**, *101*, No. 107581.

(386) He, Y.; Wang, D.; Li, Q.; Huang, L.; Bao, H. Composite Polymer Electrolyte Membranes based on Nafion and Modified PVDF Electrospun Nanofiber Mats. *J. Wuhan Univ. Technol.-Mater. Sci. Ed.* **2020**, *35* (4), 677−681.

(387) Safronova, E. Y.; Lysova, A. A.; Voropaeva, D. Y.; Yaroslavtsev, A. B. Approaches to the modification of perfluorosulfonic acid membranes. *Membranes* **2023**, *13* (8), 721.

(388) Awang, N.; Ismail, A.; Jaafar, J.; Matsuura, T.; Junoh, H.; Othman, M.; Rahman, M. Functionalization of polymeric materials as a high performance membrane for direct methanol fuel cell: A review. *React. Funct. Polym.* **2015**, *86*, 248−258.

(389) Rozière, J.; Jones, D. J. Non-fluorinated polymer materials for proton exchange membrane fuel cells. *Annu. Rev. Mater. Res.* **2003**, *33* (1), 503−555.

(390) Babu, A.; Aazem, I.; Walden, R.; Bairagi, S.; Mulvihill, D. M.; Pillai, S. C. Electrospun nanofiber based TENGs for wearable electronics and self-powered sensing. *Chem. Eng. J.* **2023**, *452*, No. 139060.

(391) Cali, A.; Yağızatlı, Y.; Sahin, A.; Ar, İ. Highly durable phosphonated graphene oxide doped polyvinylidene fluoride (PVDF) composite membranes. *Int. J. Hydrogen Energy* **2020**, *45* (60), 35171−35179.

(392) Rajabalizadeh Mojarrad, N.; Iskandarani, B.; Taşdemir, A.; Yürüm, A.; Alkan Gürsel, S.; Yarar Kaplan, B. Nanofiber based hybrid sulfonated silica/P(VDF-TrFE) membranes for PEM fuel cells. *Int. J. Hydrogen Energy* **2021**, *46* (25), 13583−13593.

(393) Thmaini, N.; Charradi, K.; Ahmed, Z.; Aranda, P.; Chtourou, R. Nafion/SiO2@TiO2-palygorskite membranes with improved proton conductivity. *J. Appl. Polym. Sci.* **2022**, *139* (21), No. 52208.

(394) Bisht, S.; Balaguru, S.; Ramachandran, S. K.; Gangasalam, A.; Kweon, J. Proton exchange composite membranes comprising SiO2, sulfonated SiO2, and metal−organic frameworks loaded in SPEEK polymer for fuel cell applications. *J. Appl. Polym. Sci.* **2021**, *138* (22), No. 50530.

(395) Vázquez-Fernández, I.; Raghibi, M.; Bouzina, A.; Timperman, L.; Bigarré, J.; Anouti, M. Protic ionic liquids/poly(vinylidene fluoride) composite membranes for fuel cell application. *J. Energy Chem.* **2021**, *53*, 197−207.

(396) Zheng, C.; Xie, N.; Liu, X.; Wang, L.; Zhu, W.; Pei, Y.; Yue, R.; Liu, H.; Yin, S.; Yao, J.; Zhang, J.; Yin, Y.; Guiver, M. D. Durability improvement of proton exchange membrane fuel cells by doping silica−ferrocyanide antioxidant. *J. Membr. Sci.* **2024**, *690*, No. 122195.

(397) Xu, Y.; Liang, X.; Shen, X.; Yu, W.; Yang, X.; Li, Q.; Ge, X.; Wu, L.; Xu, T. In situ construction of ultra-thin PANI/CeOx layer on

proton exchange membrane for enhanced oxidation resistance in PEMFC. *J. Membr. Sci.* **2024**, *689*, No. 122167.

(398) Kang, Y. S.; Jang, S.; Choi, E.; Jo, S.; Kim, S. M.; Yoo, S. J. Sandwich-like Nafion composite membrane with ultrathin ceria barriers for durable fuel cells. *Int. J. Energy Res.* **2022**, *46* (5), 6457−6470.

(399) Jiao, K.; Xuan, J.; Du, Q.; Bao, Z.; Xie, B.; Wang, B.; Zhao, Y.; Fan, L.; Wang, H.; Hou, Z.; et al. Designing the next generation of proton-exchange membrane fuel cells. *Nature* **2021**, *595* (7867), 361−369.

(400) Zhang, G.; Qu, Z.; Tao, W.-Q.; Mu, Y.; Jiao, K.; Xu, H.; Wang, Y. Advancing next-generation proton-exchange membrane fuel cell development in multi-physics transfer. *Joule* **2024**, *8* (1), 45−63.

(401) Li, J.; Singh, J. P.; Neklyudov, V.; Stolov, M.; Yuan, Z.; Schilt, Y.; Raviv, U.; Dekel, D. R.; Freger, V. Anisotropic membrane with high proton conductivity sustaining upon dehydration. *Sci. Adv.* **2024**, *10* (43), No. eadp1450.

(402) Sun, X.; Simonsen, S. C.; Norby, T.; Chatzitakis, A. Composite membranes for high temperature PEM fuel cells and electrolysers: a critical review. *Membranes* **2019**, *9* (7), 83.

(403) Sarkar, A.; Bidu, J. M.; Panda, J.; Kwon, Y. J.; Bak, S.; Cho, K. Y.; Byun, S.; Cheong, J. Y. Applications of electrospinning for fuel cell and electrolysis cell applications in hydrogen technologies. *Energy Rev.* **2025**, *4* (1), No. 100119.

(404) Yusoff, Y. N.; Shaari, N. An overview on the development of nanofiber-based as polymer electrolyte membrane and electrocatalyst in fuel cell application. *Int. J. Energy Res.* **2021**, *45* (13), 18441− 18472.

(405) Raja Rafidah, R. S.; Rashmi, W.; Khalid, M.; Wong, W.; Priyanka, J. Recent progress in the development of aromatic polymer-based proton exchange membranes for fuel cell applications. *Polymers* **2020**, *12* (5), 1061.

(406) Zhang, F.; Maddy, J. Investigation of the challenges and issues of hydrogen and hydrogen fuel cell applications in aviation *Authorea Preprints* 2021 DOI: 10.36227/techrxiv.14958057.v1.

(407) Gagliardi, G. G.; Palone, O.; Paris, E.; Borello, D. An efficient composite membrane to improve the performance of PEM reversible fuel cells. *Fuel* **2024**, *357*, No. 129993.

(408) Wang, Y.; Seo, B.; Wang, B.; Zamel, N.; Jiao, K.; Adroher, X. C. Fundamentals, materials, and machine learning of polymer electrolyte membrane fuel cell technology. *Energy AI* **2020**, *1*, No. 100014.

(409) Wu, Q.; Dong, Z.; Zhang, X.; Zhang, C.; Iqbal, A.; Chen, J. Towards More Efficient PEM Fuel Cells Through Advanced Thermal Management: From Mechanisms to Applications. *Sustainability* **2025**, *17* (3), 943.

(410) Li, H.; Yazdi, M.; Adumene, S.; Goleiji, E. Integrating safety management systems in hydrogen production facilities. *Int. J. Hydrogen Energy* **2025**, *128*, 345−358.

(411) Wu, X.; Xing, S.; Luo, J.; Wang, H.; Huang, F.; Zhao, C. Progress and challenges on air-cooled open-cathode proton exchange membrane fuel cells: Materials, structures, and systems. *Energy Rev.* **2025**, *4* (2), No. 100130.

(412) Al-Anazi, A.; Wilberforce, T.; Khatib, F. N.; Vichare, P.; Olabi, A. G. Performance evaluation of an air breathing polymer electrolyte membrane (PEM) fuel cell in harsh environments − A case study under Saudi Arabia's ambient condition. *Int. J. Hydrogen Energy* **2021**, *46* (45), 23463−23479.

(413) Liao, Y.; Zhao, S.; Liu, G.; Li, H.; Shuai, J.; Wang, L.; Liu, B.; Tang, H. Proton exchange membranes with functionalized sulfoni-mide and phosphonic acid groups for next-generation fuel cells operating at 120 °C. *Chem. Eng. J.* **2024**, *488*, No. 150971.

(414) Tan, H.; Zhao, S.; Ali, S. E.; Zheng, S.; Alanazi, A. K.; Wang, R.; Zhang, H.; Abo-Dief, H. M.; Xu, B. B.; Algadi, H.; et al. Perfluorosulfonic acid proton exchange membrane with double proton site side chain for high-performance fuel cells at low humidity. *J. Mater. Sci. Technol.* **2023**, *166*, 155−163.

(415) Lou, J.; Lu, Y.; Yang, D.; Pan, X.; Li, B.; Ming, P. Experimental and model refinement of water content and membrane conductivity in reinforced composite proton exchange membranes. *Int. J. Hydrogen Energy* **2024**, *94*, 756−764.

(416) Baik, K. D.; Hong, B. K.; Kim, M. S. Effects of operating parameters on hydrogen crossover rate through Nafion membranes in polymer electrolyte membrane fuel cells. *Renewable Energy* **2013**, *57*, 234−239.

(417) Omrani, R.; Shabani, B. Hydrogen crossover in proton exchange membrane electrolysers: The effect of current density, pressure, temperature, and compression. *Electrochim. Acta* **2021**, *377*, No. 138085.

(418) Schalenbach, M.; Stolten, D. High-pressure water electrolysis: Electrochemical mitigation of product gas crossover. *Electrochim. Acta* **2015**, *156*, 321−327.

(419) Ouerghemmi, M.; Carral, C.; Mele, P. Understanding the influence of MEA interfaces properties on PEMFC mechanical behavior through numerical analysis. *Int. J. Hydrogen Energy* **2024**, *69*, 242−251.

(420) Niu, H.; Ji, C.; Wang, S.; Liang, C. Research on PEMFC resistance relaxation characteristics and degradation under thermal cycles with different residual water locations. *Int. J. Hydrogen Energy* **2022**, *47* (4), 2662−2672.

(421) Zou, Y.; Yang, M.; Liu, G.; Xu, C. Sulfonated poly (fluorenyl ether ketone nitrile) membranes used for high temperature PEM fuel cell. *Heliyon* **2020**, *6* (9), No. e04855, DOI: 10.1016/j.heli-yon.2020.e04855.

(422) Liu, N.; Bi, S.; Zhang, Y.; Ou, Y.; Gong, C.; Ran, J.; Chen, Y.; Yang, Y. Nanofiber-based polymer electrolyte membranes for fuel cells. *Carbon Energy* **2025**, *7* (4), No. e677.

(423) Kim, J.-H.; Noh, M. S.; Shin, E. J.; Lee, S. Y.; Kim, Y.; Jung, H. J.; Lee, H. J.; Lee, H. I.; Lim, D.-H.; Lee, Y. S.; et al. Improved Mechanical Stability and Proton Conductivity of Reinforced Membranes for Proton Exchange Membrane Fuel Cells (PEMFCs). *ACS Phys. Chem. Au* **2025**, *5* (5), 425−434, DOI: 10.1021/acsphyschemau.5c00009.

(424) Choi, H. J.; Choi, Hj.; Kim, J.; Choi, H.; Chu, C.; La, I.; Ahn, C.-Y.; Shim, H.; Kim, O.-H.; Cho, Y.-H. Comparison on the impact of membrane thickness on the performance of proton exchange membrane-based electrochemical devices. *Int. J. Hydrogen Energy* **2025**, *119*, 161−172.

(425) Sharma, T.; Adhikari, U.; Nandimath, A.; Pandey, J. Investigating degradation & mitigation strategies for proton conducting membrane in proton exchange membrane fuel cell: An approach to develop an active & stable membrane. *Mater. Today Sustainability* **2025**, *30*, No. 101103.

(426) Abedin, T.; Pasupuleti, J.; Paw, J. K. S.; Tak, Y. C.; Mahmud, M.; Abdullah, M. P.; Nur-E-Alam, M. Proton exchange membrane fuel cells in electric vehicles: Innovations, challenges, and pathways to sustainability. *J. Power Sources* **2025**, *640*, No. 236769.

(427) Bayat, A.; Das, P. K.; Saha, G.; Saha, S. C. Optimizing proton exchange membrane electrolyzer cells: A comprehensive parametric analysis of flow, electrochemical, and geometrical factors. *Int. J. Thermofluids* **2025**, *27*, No. 101177.

(428) d'Adamo, A.; Martoccia, L.; Croci, F.; Marra, C. CFD simulation of the effect of membrane thickness and reactants flow rate on water management in PEM fuel cells. *Int. J. Heat Mass Transfer* **2025**, *249*, No. 127207.

(429) Tsampas, M. N.; Pikos, A.; Brosda, S.; Katsaounis, A.; Vayenas, C. G. The effect of membrane thickness on the conductivity of Nafion. *Electrochim. Acta* **2006**, *51* (13), 2743−2755.

(430) Varyukhin, A.; Zakharchenko, V.; Vlasov, A.; Gordin, M.; Ovdienko, M. *Roadmap for the technological development of hybrid electric and full-electric propulsion systems of aircrafts*, 2019 international conference on electrotechnical complexes and systems (ICOECS), IEEE, 2019; pp 1−7.

(431) Pan, Z.; An, L.; Wen, C. Recent advances in fuel cells based propulsion systems for unmanned aerial vehicles. *Appl. Energy* **2019**, *240*, 473−485.

(432) Navabpour, P.; Cooper, L.; Yang, S.; Yin, J.; Zhang, K.; El-Kharouf, A.; Sun, H. PVD Coatings for Lightweight Bipolar Plates. *Surfaces* 2024, 7 (4), 812−823.

(433) Hung, Y.; El-Khatib, K.; Tawfik, H. Corrosion-resistant lightweight metallic bipolar plates for PEM fuel cells. *J. Appl. Electrochem.* 2005, 35, 445−447.

(434) Husby, H.; Kongstein, O. E.; Oedegaard, A.; Seland, F. Carbon-polymer composite coatings for PEM fuel cell bipolar plates. *Int. J. Hydrogen Energy* 2014, 39 (2), 951−957.

(435) Pedapati, P. R.; Dhanushkodi, S. R.; Chidambaram, R. K.; Taler, D.; Sobota, T.; Taler, J. Design and manufacturing challenges in PEMFC flow fields—a review. *Energies* 2024, 17 (14), 3499.

(436) Wang, H.; Wang, R.; Sui, S.; Sun, T.; Yan, Y.; Du, S. Cathode design for proton exchange membrane fuel cells in automotive applications. *Automot. Innov.* 2021, 4, 144−164.

(437) Salah, I. M. *Modelling, simulation and performance evaluation: PEM fuel cells for high altitude UAS*; Sheffield Hallam University: United Kingdom, 2015.

(438) Alam Rimon, S. T.; Mourshed, M.; Kibria, M. G. Proton exchange membrane fuel cells: advances in materials development, performance optimization, and future outlook. *Energy Convers. Manage.: X* 2025, 27, No. 101102.

(439) Huang, L.; Qi, R. A comprehensive review on assembly design strategies on proton exchange membrane applications. *Int. J. Hydrogen Energy* 2022, 47 (80), 33903−33918.

(440) Bhatti, W. *Mechanical integration of a PEM fuel cell for a multifunctional aerospace structure*; Loughborough University, 2016.

(441) Srinath, A. N.; Pena López, Á.; Miran Fashandi, S. A.; Lechat, S.; di Legge, G.; Nabavi, S. A.; Nikolaidis, T.; Jafari, S. Thermal management system architecture for hydrogen-powered propulsion technologies: Practices, thematic clusters, system architectures, future challenges, and opportunities. *Energies* 2022, 15 (1), 304.

(442) Chiche, A.; Lindbergh, G.; Stenius, I.; Lagergren, C. Design of experiment to predict the time between hydrogen purges for an air-breathing PEM fuel cell in dead-end mode in a closed environment. *Int. J. Hydrogen Energy* 2021, 46 (26), 13806−13817.

(443) Peng, Y.; Choi, J.-Y.; Bai, K.; Tian, L.; Pei, K.; Zhang, Y.; Banham, D. Pitfalls of a commonly used accelerated stress test for reversal tolerance testing of proton exchange membrane fuel cell anode layers. *J. Power Sources* 2024, 596, No. 234087.

(444) Nørgaard, C. F.; Stamatin, S. N.; Skou, E. M. Redeposition of electrochemically dissolved platinum as nanoparticles on carbon. *Int. J. Hydrogen Energy* 2014, 39 (30), 17322−17326.

(445) Hart, D.; Jones, S.; Lewis, J. The fuel cell industry review 2020. 2020.

(446) Hrytsyk, N. I. Safety aspects of electrical systems in modern commercial aircraft. 2024.

(447) Kongkanand, A.; Gu, W.; Mathias, M. F. Proton-exchange membrane fuel cells with low-Pt content. In *Fuel Cells and Hydrogen Production*; Springer, 2019; pp 323−342.

(448) Kongkanand, A.; Mathias, M. F. The priority and challenge of high-power performance of low-platinum proton-exchange membrane fuel cells. *J. Phys. Chem. Lett.* 2016, 7 (7), 1127−1137.

(449) Mori, M.; Iribarren, D.; Cren, J.; Cor, E.; Lotrič, A.; Gramc, J.; Drobnič, B.; Rey, L.; Campos-Carriedo, F.; Puig-Samper, G.; Bargiacchi, E.; Dufour, J.; Stropnik, R. Life cycle sustainability assessment of a proton exchange membrane fuel cell technology for ecodesign purposes. *Int. J. Hydrogen Energy* 2023, 48 (99), 39673−39689.

(450) Scibioh, M. A.; Viswanathan, B. The status of catalysts in PEMFC technology. In *Catalysis for alternative energy generation*; Springer, 2012; pp 329−368.

(451) Chu, Y.; Cheng, Y.; Wang, P.; Bai, J.; Guan, X.; Wang, S.; Lan, C.; Wu, H.; Shi, Z.; Zhu, S.; et al. Unraveling the potential-dependent degradation mechanism in Fe-NC catalysts for oxygen reduction reaction. *Sci. China Chem.* 2025, 68 (4), 1541−1549.

(452) Li, J.-C.; Xu, H.; Zhou, K.; Li, J.-Q. A review on the research progress and application of compressed hydrogen in the marine hydrogen fuel cell power system. *Heliyon* 2024, 10 (3), No. e25304, DOI: 10.1016/j.heliyon.2024.e25304.

(453) Zatoń, M.; Rozière, J.; Jones, D. Current understanding of chemical degradation mechanisms of perfluorosulfonic acid membranes and their mitigation strategies: a review. *Sustainable Energy Fuels* 2017, 1 (3), 409−438.

(454) Disalvo, E. A.; Lairion, F.; Martini, F.; Tymczyszyn, E.; Frías, M.; Almaleck, H.; Gordillo, G. J. Structural and functional properties of hydration and confined water in membrane interfaces. *Biochim. Biophys. Acta, Biomembr.* 2008, 1778 (12), 2655−2670.

(455) Xu, G.; Dong, X.; Xue, B.; Huang, J.; Wu, J.; Cai, W. Recent approaches to achieve high temperature operation of nafion membranes. *Energies* 2023, 16 (4), 1565.

(456) Woo, S. H.; Otazaghine, B.; Cavaliere, S.; An, B.-S.; Kim, H. S.; Kim, J.-H.; Yoon, Y.-G.; Lee, S. Y.; Rigacci, A.; Beauger, C. Less sensitive proton-exchange membrane to a relative humidity below 30%. *J. Membr. Sci.* 2024, 698, No. 122574.

(457) Shi, S.; Si, Y.; Han, Y.; Wu, T.; Iqbal, M. I.; Fei, B.; Li, R. K.; Hu, J.; Qu, J. Recent progress in protective membranes fabricated via electrospinning: advanced materials, biomimetic structures, and functional applications. *Adv. Mater.* 2022, 34 (17), No. 2107938.

(458) Singh, A. K.; Prakash, S.; Kulshrestha, V.; Shahi, V. K. Cross-linked hybrid nanofiltration membrane with antibiofouling properties and self-assembled layered morphology. *ACS Appl. Mater. Interfaces* 2012, 4 (3), 1683−1692.

(459) Donateo, T. Simulation Approaches and Validation Issues for Open-Cathode Fuel Cell Systems in Manned and Unmanned Aerial Vehicles. *Energies* 2024, 17 (4), 900.

(460) ÖZEL, M. A.; Sumer, O. Enhancing Performance and Energy Efficiency in Air Compressor Systems for Hydrogen Electric Vehicles: A Comprehensive Study of Pressurized Air Cabin with Open Cathode Pem Fuel Cell. *Available at SSRN 4841665.*.

(461) Li, J.; Wu, T.; Cheng, C.; Li, J.; Zhou, K. A review of the research progress and application of key components in the hydrogen fuel cell system. *Processes* 2024, 12 (2), 249.

(462) Moon, J. W.; Kim, S. K.; Jung, S. Y. In-situ visualization of cathode flow channel in polymer electrolyte membrane fuel cell: Effect of GDL degradation. *Int. J. Hydrogen Energy* 2024, 51, 1255−1263.

(463) Kocha, S. S.; Deliang Yang, J.; Yi, J. S. Characterization of gas crossover and its implications in PEM fuel cells. *AIChE J.* 2006, 52 (5), 1916−1925.

(464) Afshari, E.; Khodabakhsh, S.; Jahantigh, N.; Toghyani, S. Performance assessment of gas crossover phenomenon and water transport mechanism in high pressure PEM electrolyzer. *Int. J. Hydrogen Energy* 2021, 46 (19), 11029−11040.

(465) Choi, Y.; Platzek, P.; Coole, J.; Buche, S.; Fortin, P. The Influence of Membrane Thickness and Catalyst Loading on Performance of Proton Exchange Membrane Fuel Cells. *J. Electrochem. Soc.* 2024, 171 (10), No. 104507.

(466) Athanasaki, G.; Jayakumar, A.; Kannan, A. Gas diffusion layers for PEM fuel cells: Materials, properties and manufacturing−A review. *Int. J. Hydrogen Energy* 2023, 48 (6), 2294−2313.

(467) Hosseini, S. S.; Bringas, E.; Tan, N. R.; Ortiz, I.; Ghahramani, M.; Shahmirzadi, M. A. A. Recent progress in development of high performance polymeric membranes and materials for metal plating wastewater treatment: A review. *J. Water Process Eng.* 2016, 9, 78−110.

(468) Okonkwo, P. C.; Otor, C. A review of gas diffusion layer properties and water management in proton exchange membrane fuel cell system. *Int. J. Energy Res.* 2021, 45 (3), 3780−3800.

(469) Mao, J.; Li, Z.; Xuan, J.; Du, X.; Ni, M.; Xing, L. A review of control strategies for proton exchange membrane (PEM) fuel cells and water electrolyser: From automation to autonomy. *Energy AI* 2024, 17, No. 100406.

(470) Singh, R.; Oberoi, A. S.; Singh, T. Factors influencing the performance of PEM fuel cells: A review on performance parameters, water management, and cooling techniques. *Int. J. Energy Res.* 2022, 46 (4), 3810−3842.

(471) Wu, D.; Peng, C.; Yin, C.; Tang, H. Review of system integration and control of proton exchange membrane fuel cells. *Electrochem. Energy Rev.* **2020**, *3*, 466−505.

(472) Rouss, V.; Lesage, P.; Bégot, S.; Candusso, D.; Charon, W.; Harel, F.; François, X.; Selinger, V.; Schilo, C.; Yde-Andersen, S. Mechanical behaviour of a fuel cell stack under vibrating conditions linked to aircraft applications part I: Experimental. *Int. J. Hydrogen Energy* **2008**, *33* (22), 6755−6765.

(473) BLOOM, I.; Basco, J.; Walker, L.; MALKOW, T.; DE, M. G.; SATURNIO, A.; TSOTRIDIS, G. Fuel cell testing protocols: an international perspective. 2013.

(474) Haji Hosseinloo, A.; Ehteshami, M. M. Shock and vibration effects on performance reliability and mechanical integrity of proton exchange membrane fuel cells: A critical review and discussion. *J. Power Sources* **2017**, *364*, 367−373.

(475) Hou, Y.; Hao, D.; Shen, J.; Li, P.; Zhang, T.; Wang, H. Effect of strengthened road vibration on performance degradation of PEM fuel cell stack. *Int. J. Hydrogen Energy* **2016**, *41* (9), 5123−5134.

(476) Dhimish, M.; Lazarov, V. Assessing durability in automotive fuel cells: Understanding the degradation patterns of PEM fuel cells under variable loads, temperature, humidity, and defective stack conditions. *IEEE Trans. Transport. Electrif.* **2024**, *11* (1), 3091−3101, DOI: 10.1109/tte.2024.3434609.

(477) Murschenhofer, D.; Settele, J.; Stengele, S.; Bänsch, C. In *Optimization Potential for Operating PEMFC Systems Under High-Altitude Conditions*, Electrochemical Society Meeting Abstracts prime2024, 2024 ; The Electrochemical Society, Inc., 2024; pp 3256.

(478) Saleh, I. M.; Ali, R.; Zhang, H. Environmental impact of high altitudes on the operation of PEM fuel cell based UAS. *J. Energy Power Eng.* **2018**, *10* (3), 87−105.

(479) Bvumbe, T. J.; Bujlo, P.; Tolj, I; Mouton, K.; Swart, G.; Pasupathi, S.; Pollet, B. G. Review on management, mechanisms and modelling of thermal processes in PEMFC. *Hydrogen Fuel Cells* **2016**, *1* (1), 1−20.

(480) Sun, Z.; Li, Y.; Liao, G.; Luo, X.; Liang, Y.; Chen, J.; Yang, Z.; Chen, Y. Experimental study on temperature characteristics and output performance of PEMFCs based on HFE-7100 boiling cooling. *Energy Convers. Manage.* **2025**, *334*, No. 119838.

(481) Renau, J.; García, V.; Domenech, L.; Verdejo, P.; Real, A.; Giménez, A.; Sánchez, F.; Lozano, A.; Barreras, F. Novel use of green hydrogen fuel cell-based combined heat and power systems to reduce primary energy intake and greenhouse emissions in the building sector. *Sustainability* **2021**, *13* (4), 1776.

(482) Liu, P.; Xu, S.*Experimental analysis of-30° C cold start process for an automotive PEM fuel cell system*; 0148-7191; SAE Technical Paper, 2022.

(483) Dyantyi, N.; Parsons, A.; Bujlo, P.; Pasupathi, S. Behavioural study of PEMFC during start-up/shutdown cycling for aeronautic applications. *Mater. Renewable Sustainable Energy* **2019**, *8* (1), No. 4.

(484) Dyantyi, N.; Parsons, A.; Barron, O.; Pasupathi, S. State of health of proton exchange membrane fuel cell in aeronautic applications. *J. Power Sources* **2020**, *451*, No. 227779.

(485) Chaurasia, P. B. L.; Panja, N.; Kendall, K. Performance study of power density in PEMFC for power generation from solar energy. *Renewable Energy* **2011**, *36* (12), 3305−3312.

(486) Thiele, P.; Gouveia, L.; Ulrich, O.; Yang, Y.; Liu, Y.; Wick, M.; Pischinger, S. Realistic accelerated stress tests for PEM fuel cells: Operation condition dependent load profile optimization. *J. Power Sources* **2024**, *617*, No. 234959.

(487) Birkner, L.; Foreta, M.; Rinaldi, A.; Orekhov, A.; Willinger, M.-G.; Eichelbaum, M. Dynamic accelerated stress test and coupled on-line analysis program to elucidate aging processes in proton exchange membrane fuel cells. *Sci. Rep.* **2024**, *14* (1), No. 3999.

(488) Tsotridis, G.; Pilenga, A.; De Marco, G.; Malkow, T. *EU harmonised test protocols for PEMFC MEA testing in single cell configuration for automotive applications*; Publications Office of the European Union Luxembourg, 2015.

(489) Rajalakshmi, N.; Pandian, S.; Dhathathreyan, K. S. Vibration tests on a PEM fuel cell stack usable in transportation application. *Int. J. Hydrogen Energy* **2009**, *34* (9), 3833−3837.

(490) Zhang, Z.; Chen, Z.; Li, K.; Zhang, X.; Zhang, C.; Zhang, T. A multi-field coupled PEMFC model with force-temperature-humidity and experimental validation for high electrochemical performance design. *Sustainability* **2023**, *15* (16), 12436.

(491) Mølmen, L.; Fast, L.; Lundblad, A.; Eriksson, P.; Leisner, P. Contact resistance measurement methods for PEM fuel cell bipolar plates and power terminals. *J. Power Sources* **2023**, *555*, No. 232341.

(492) Pahon, E.; Hissel, D.; Yousfi-Steiner, N. A review of accelerated stress tests dedicated to proton exchange membrane fuel cells − Part I: Fuel cell component level. *J. Power Sources* **2022**, *546*, No. 231895.

(493) St-Pierre, J.; Zhai, Y.; Angelo, M. Quantitative ranking criteria for PEMFC contaminants. *Int. J. Hydrogen Energy* **2012**, *37* (8), 6784−6789.

(494) Zhao, Y.; Luo, M.; Yang, J.; Chen, B.; Sui, P.-C.; Zhou, W. Experimental Study of PEMFC Stack Performance Degradation Considering the Shutdown and Rest Processes. *Int. J. Energy Res.* **2025**, *2025* (1), No. 3246950.

(495) Shen, C.; Xu, S.; Gao, Y. Analysis of fuel cell stack performance attenuation and individual cell voltage uniformity based on the durability cycle condition. *Polymers* **2021**, *13* (8), 1199.

(496) Spencer, R. Certification considerations for the configuration of a hydrogen-fuelled aeroplane. *Aeronaut. J.* **2023**, *127* (1308), 213−231.

(497) O'sullivan, G.; Horvat, A. B.; Jézégou, J.; Carrasco, B. J.; André, R. Hydrogen Aircraft, Technologies and Operations Towards Certification Readiness Level 1. *Aerospace* **2025**, *12* (6), 490.

(498) Jézégou, J.; André, R.; Gourinat, Y. *Hydrogen Aircraft Certification: Determination of Regulatory Gaps*, Proceedings of the International Conference on More Electric Aircraft, Towards Greener Aviation, Toulouse, France, 2024; pp 7−8.

(499) FAA. *Hydrogen-Fueled Aircraft Safety and Certification Roadmap*; Federal Aviation Administration: USA, 2024; pp 1−26.

(500) Jézégou, J.; Almeida-Marino, A. M.; O'sullivan, G.; Carrasco, B. J.; André, R.; Gourinat, Y. Certification Gap Analysis for Normal-Category and Large Hydrogen-Powered Airplanes. *Aerospace* **2025**, *12* (3), 239.

(501) Ding, F.; Zou, T.; Wei, T.; Chen, L.; Qin, X.; Shao, Z.; Yang, J. The pinhole effect on proton exchange membrane fuel cell (PEMFC) current density distribution and temperature distribution. *Appl. Energy* **2023**, *342*, No. 121136.

(502) Chen, Z.; Xing, Y.; Cao, J.; Yang, F.; Zhang, X. Leakage analysis of PEMFC sealing system considering temperature cycling. *Energies* **2023**, *16* (14), 5475.

(503) Dijoux, E.; Steiner, N. Y.; Benne, M.; Péra, M.-C.; Pérez, B. G. A review of fault tolerant control strategies applied to proton exchange membrane fuel cell systems. *J. Power Sources* **2017**, *359*, 119−133.

(504) Yakubu, A. U.; Qingsheng, L.; Kai, M.; Jinwei, C.; Mohammed, O. A. A.; Zhao, J.; Jiang, Q.; Ye, X.; Liu, J.; Yu, Q.; Aurangzeb, M.; Xiong, S. Modeling, optimization, and thermal management strategies of hydrogen fuel cell systems. *Results Eng.* **2025**, *27*, No. 105924.

(505) Giri, M.; Zhang, C.; Timalsina, S.; Hada, S.; Holubnyak, E. A Comparative Study of Regulatory and Policy Framework in Hydrogen Pipeline Development. *J. Legal Affairs Dispute Resol. Eng. Constr.* **2025**, *17* (4), No. 04525063.

(506) Flamberg, S.; Rose, S.; Stephens, D. *Analysis of Published Hydrogen Vehicle Safety Research*; National Highway Traffic Safety Administration. United States: 2010.

(507) Guo, M.; Qiu, D.; Yi, P.; Peng, L. Study on the insulation resistance of proton exchange membrane fuel cell stacks. *Renewable Energy* **2025**, *241*, No. 122318.

(508) Khan, N.; Al-Sagheer, Y.; Steinberger-Wilckens, R. PEFC System Reactant Gas Supply Management and Anode Purging Strategy: An Experimental Approach. *Energies* **2022**, *15* (1), 288.

(509) ISO14687:2025 — Hydrogen fuel quality — Product specification. In *International Organization for Standardization*; ISO, 2025; pp 1−27.

(510) *SAE International Technical Standard, Standard for Fuel Systems in Fuel Cell and Other HydrogenVehicles*, SAE20181-108.

(511) Szpakowska-Peas, E.; Filipowicz, M. Selected aspects of electronic hardware development and testing for the flight reconfiguration system in accordance with the RTCA DO-160G standard. *Aircraft Engineering and Aerospace Technology* **2025**, 97 (1), 28−36.

(512) Lele, S.; Menacho, R. G. Energy storage system safety and compliance. In *The Sustainable Power Grid*; Elsevier, 2025; pp 139−164.